REPORT DOCUMENTATION PAGE

Form Approved
OMB No. 0704-0188

AFRL-SR-BL-TR-98-

0265

1. AGENCY USE ONLY (Leave blank)	2. REPORT DATE	3

4. TITLE AND SUBTITLE

Transport Processes in Pulsed Plasma Thruaters

96-1-0200

6. AUTHOR(S)

PROFESSOR P. J. TURCHI

7. PERFORMING ORGANIZATION NAME(S) AND ADDRESS(ES)

The Ohio State University Research Foundation
1960 Kenny Road
Columbus, Ohio 43210

8. PERFORMING ORGANIZATION REPORT NUMBER

9. SPONSORING/MONITORING AGENCY NAME(S) AND ADDRESS(ES)

AFOSR/NA
Bolling AFB DC 20332-6448

N A

10. SPONSORING/MONITORING AGENCY REPORT NUMBER

11. SUPPLEMENTARY NOTES

12a. DISTRIBUTION/AVAILABILITY STATEMENT

Approved for public release,
distribution unlimited

19980331 033

13. ABSTRACT (Maximum 200 words)

The simplicity of the pulsed plasma microthruster (PPT) allowed its selection for space flight application, even with low efficiency relative to other concepts. Improvements to PPT thrust efficiency and specific impulse represent today's challenges for research and development. Self-consistent modeling of PPT behavior requires a description of the flow composition as it changes from complex molecular forms to highly-ionized, constituent atoms. Heat flux from the plasma discharge to the solid propellant, (traditionally, Teflon), depends on transport coefficients for electrical and thermal conductivity in the partially ionized flow. Numerical simulations now use an existing, single-temperature equation of state for Teflon (from the SESAME tables) along with classical transport formulas based on Coulomb collisions. The principal effort under the present grant has been to develop a two-temperature, LTE model for Teflon in the regime of interest for PPTs. This model includes 25 species (atoms, molecules, ions and electrons) and allows separate heavy-particle and electron temperatures. An idealized analysis, limited to one-dimensional, quasi-steady MHD flow, but incorporating resistive heating and thermal diffusion, has also been developed and provides useful guidance on PPT operation and propellant behavior.

14. SUBJECT TERMS	15. NUMBER OF PAGES
PULSED PLASMA MICROTHRUSTER	139
	16. PRICE CODE

17. SECURITY CLASSIFICATION

CONTENTS

INTRODUCTION

Electric propulsion provides higher exhaust speeds than chemical techniques, thereby offering considerable economic advantage for several applications in space. Today, these applications include on-board propulsion for satellites that already require significant electrical power to accomplish their missions (e.g., communication). Such propulsion presently serves station-keeping needs, but may also extend to re-positioning geosynchronous satellites, drag compensation and orbit-raising. While electric propulsion no longer waits for dedicated power sources and primary propulsion missions, flight experience gained in near earth missions may soon encourage application of electric propulsion for planetary and deep space exploration.

Basic research can contribute to the application of electric propulsion by providing the tools and insights needed for improvements in specific impulse, thrust efficiency and lifetime. The present research recognizes that transport processes play a major role in determining the behavior of plasma thrusters. Modern computational techniques make it possible to simulate complex plasma and electromagnetic interactions within plasma thrusters, but depend for accurate results on the properties of the propellant material. For devices such as the pulsed plasma microthruster (PPT), Teflon has been the propellant of choice. Self-consistent modeling of PPT behavior requires a description of the composition of Teflon as it changes from complex molecular forms to highly-ionized, constituent atoms. Knowledge of this composition allows calculation of thermodynamic and transport properties. This report describes the development of a model for the composition of Teflon plasma in which separate electron and heavy-particle temperatures exist.

During the period of the grant, the Principal Investigator had additional duties as visiting Chief Scientist for Advanced Weapons and Survivability, Phillips Laboratory, Kirtland AFB, NM. Part of these duties included examination of diffusive processes in plasma devices, such as high-power microwave sources. The particular problem of impedance collapse in high-voltage, electron-beam diodes involves plasma layers in close contact with electrodes. Modeling such layers with the MACH2 code, a subject related to numerical simulation of plasma thrusters, led to a technical paper included as an appendix to this report. Technical discussions at Phillips Laboratory, as part of the work on plasma closure, resulted in improvements to the treatment of both resistive transport and non-neutral plasma regions in the MACH2 code. These improvements assist the use of MACH2 for modeling various kinds of electric thrusters.

BACKGROUND

Over the past several decades, research and development of electric propulsion has embraced a great variety of candidate techniques. Standard texts provide the taxonomy of these techniques. The three main categories of electrothermal, electromagnetic and electrostatic propulsion comprise dozens of concepts. Plasma thrusters often combine aspects from more than one category of electric propulsion.

They tend to share characteristics of simplicity and robustness of construction, and typically have electrical impedance values in the range of 1 – 100 mΩ. Plasma thrusters operate in steady state and pulses of duration down to sub-microsecond. The inherent physics of plasma thruster operation may remain the same over this wide range of time scales. If all conditions stay approximately constant for times much longer than the time for flow transit through the thruster, operation is often termed 'quasi-steady'. Propellant supply, by gas injection vs ablation offers an additional distinction for plasma thrusters. Furthermore, the magnetic field in the thruster may originate with plasma currents or by application of external magnets.

The present research focuses on a form of plasma propulsion embodied by the pulsed plasma microthruster, generally abbreviated as PPT. In its traditional, rectangular form, driven by an LRC-circuit, a Teflon propellant bar separates two electrodes connected to a charged capacitor in vacuum. A spark plug provides a small amount of initial plasma, triggering an electrical discharge across the exposed surface of the Teflon. Heat transfer from this discharge causes evaporation of propellant material, which then accelerates through the discharge due to electromagnetic and pressure forces. As propellant evaporates with each discharge, a simple spring mechanism advances the propellant bar into the thrust chamber. Two limiting modes of operation can occur depending on the details of the heat transfer and acceleration process. For sufficient heat transfer, the surface provides new electrically conducting material, so the discharge path can remain adjacent to the propellant surface in an 'ablation arc' mode. Otherwise, the discharge must follow the material it accelerates, so the PPT operates in the 'propagating' mode.

Choice of the PPT for a research focus follows from its special status within electric propulsion. For many years, of all the various electric thruster concepts, only the PPT had achieved acceptance for application on actual space missions. Recently, with the continuing success of the kilowatt-level arcjets on Telstar IV, electric propulsion should see representation as well by xenon ion engines and Hall thrusters, such as the SPT-100. In contrast with the PPT, these other devices have all attained a high degree of refinement by decades of development in the laboratory, achieving perhaps their optimum levels of performance. For example, the thrust efficiencies of xenon ion engines and the SPT-100 can exceed 70%, while flight models of the PPT have efficiencies of less than 10%. The simplicity of the PPT allowed its selection for space flight application, even with such low efficiency relative to other concepts. Improvements to PPT thrust efficiency and specific impulse represent today's challenges for research and development. Only the PPT combines decades of flight use with considerable opportunity for increasing thrust efficiency and specific impulse.

APPROACH

The experimental simplicity of the PPT has permitted empirical studies to provide sufficient data and experience to allow development of space-qualified hardware used in actual missions without the benefit of a complete theoretical understanding.

Unfortunately, these studies have failed to improve PPT efficiency (with notable exceptions at high energy) above several percent. Furthermore, little insight has been forthcoming to guide the choice of candidate propellants that might offer higher specific impulse or better plume characteristics than the traditional use of Teflon. Instead, graphs summarize empirical results for impulse-bit and mass loss per shot vs stored energy in the PPT capacitor. From these data, empirical constants permit closure of simple models for PPT performance, thereby allowing design of ablation-fed, MPD thrusters . Minor manipulation of system equations, along with data on masses and lifetimes of components (e.g., capacitors), can indicate optimum parameters for PPT application to particular missions. The renewed attention to the PPT for small satellites, has created a need for theoretical tools that can predict directions for improving PPT performance in terms of mass utilization, efficiency and component reliability.

The problem of associating the mass evolved from the propellant surface with the impulse developed during the operating pulse represents the principal difficulty in establishing the performance of the PPT in terms of its specific impulse or (average) exhaust speed. Empirically, measurement of the total mass lost by the surface over many discharges provides the mass loss per shot. This value divided into the impulse per shot offers the average exhaust speed. Experimental data suggest that the mass loss is proportional to the stored energy. This intuitively pleasant result implies a constant value for the average exhaust speed, and a reasonable way to scale new designs from existing data. At this level of discussion, however, there is no further insight to provide a firm basis for improving PPT performance.

It is necessary to develop theoretical modeling that can incorporate physical processes not captured by lumped-circuit representations and empirical scaling laws. For example, the discharge current must have the opportunity to flow both through paths propagating along the accelerator electrodes and through a path remaining on the propellant surface. This requires a formulation at least at the level of magnetohydrodynamics in order to obtain the distribution of current density within the thruster. An effort to extend PPT operation to the millipound level first attempted such an approach. At the time, however, computational simulation of plasma acceleration was too difficult to achieve within a program largely devoted to experimental exploration and development. Over the past decade, modern calculational techniques, created to support experiments with powerful plasma-guns, have been applied to plasma thruster problems. These applications included quasi-steady MPD arcjets and steady state, applied-field, MPD thrusters, and more recently PPTs.

The need for self-consistent addition of mass during the discharge pulse makes numerical simulation much more difficult for the PPT than for a gas-fed, plasma thruster. Presumably, heat transfer from the plasma discharge to the exposed surface of the propellant results in evaporation of material through which the discharge current flows. Electromagnetic forces accelerate this material, while resistive heating contributes to the overall flow enthalpy. Typically, pulsed plasma discharges propagate with the accelerated plasma, in order to follow the electrically conducting material, unless

discharge processes create new conducting material closer to the source of electromagnetic power.

The PPT traditionally ignites when a spark plug generates an initial plasma between the accelerator electrodes. If new material does not evaporate quickly enough from the propellant surface, the discharge will accelerate this initial plasma, travelling with it along the electrodes. The increased separation of the discharge from the propellant surface reduces the opportunity for heat transfer and thus encourages a propagating mode for discharge operation. Similar behavior would occur if the discharge current waveform resulted in rapid acceleration of an initial amount of material evaporated from the propellant surface before heat transfer was sufficient to maintain further mass addition. On the other hand, adequate heat transfer to the surface can provide a continual source of electrically conducting material, allowing the discharge to remain adjacent to the surface, thereby sustaining heat transfer.

To determine the actual mode of operation of the PPT for various possible values of parameters and arrangements requires time-dependent calculations combining electrical circuitry, MHD flow and heat transfer in the propellant. The MACH2 code, modified to include the features needed for simulating the PPT, was first used to model the LES-6 thruster. Modifications included the development of a separate numerical model for two-dimensional, unsteady heat-flow in the solid propellant, based on the net heat flux to the exposed surface. This heat flux comprised heat conduction and radiation from the plasma discharge, and convection due to evaporation or condensation of the propellant material. (Earlier models for ablation of solids assumed a thermal diffusion depth that increased with the square root of elapsed time. Such an approach might succeed for monotonically increasing temperatures, but cannot service the variations possible in the PPT.) The initial calculations for LES-6 captured both the magnitude and variation of the impulse-bit for the available values of experimental data. Such agreement must be considered somewhat fortuitous, the result of compensating errors, because of several limitations. These include the use of a two-dimensional calculation (in the plane of the current flow) for a three-dimensional problem, and approximate formulations for plasma composition and transport coefficients.

Heat flux from the plasma discharge depends on the distribution of current density near the propellant surface and the transport coefficients for electrical and thermal conductivity in the partially ionized flow. Present calculations use an existing, single-temperature equation of state for Teflon (from the SESAME tables) along with classical transport formulas based on Coulomb collisions. The principal effort under the present grant has been to develop a two-temperature, LTE model for Teflon in the regime of interest for PPTs. This model includes 25 species (atoms, molecules, ions and electrons) and allows separate heavy-particle and electron temperatures.

An idealized analysis, limited to one-dimensional, quasi-steady MHD flow, but incorporating resistive heating and thermal diffusion, has also been developed to provide some guidance on PPT operation and propellant behavior. In particular, application of a magneto-sonic choking condition at the downstream edge of the

discharge determines the mass flow rate needed by the MHD flow for given values of total current and size. This mass flow rate in turn specifies the surface temperature of the propellant and the associated equilibrium vapor pressure. The heat delivered to the propellant to achieve these conditions then depends on the given current waveform and duration.

PROGRESS

The five quarters of sponsorship under the present grant saw accomplishment of the first portions of the proposed two-year effort. Appendix I displays much of this work in the form of a presentation given at the AFOSR workshop in San Diego, 28 – 31 July 1997. Appendices II and III provide copies of technical papers on the directions for PPT improvement (based on the idealized model) and the two-temperature, LTE model for Teflon. The 25th International Electric Propulsion Conference, Cleveland, OH, 24 – 28 August 1997, served as the forum for these papers, which will appear in the conference proceedings. Appendix IV provides an updated version of the paper on transport properties of nitrogen, which led to the concern with severely non-monotonic variations of thermal conductivity with temperature and pressure in molecular gases. This concern resulted in attention (Appendix V) to capturing such variations in numerical simulations by means of computational grids that adapt to thermal conductivity, rather than simply geometry or flow density. Appendix VI presents the latest form of the two-temperature, LTE model for Teflon, including more accurate calculation of the effects of rotation and vibration of polyatomic species. The new model also allows for variation of coupling of vibrational states to electrons vs heavy-particles.

Appendix VII provides a paper, presented at the 11th IEEE International Pulsed Power Conference, Baltimore, MD, 30 June – 3 July 1997, on impedance collapse in high-voltage, electron-beam diodes. It summarizes the work on diffusive processes near electrodes, performed by the Principal Investigator while at Phillips Laboratory, Kirtland AFB.

CONCLUDING REMARKS

The most recent theoretical activity at Ohio State in support of PPT development has been under NASA sponsorship and comprises continuation of MACH2 calculations applied to the benchmark PPT, and extension of such calculations to coaxial configurations. The latter effort draws on earlier success in using MACH2 to model quasi-steady MPD thrusters. Simulations of coaxial PPTs have already included the use of plug nozzles to provide improved flow expansion. Modification of MACH2 to couple the PPT to other circuits, such as PFNs and the inductively-driven circuit has also begun.

Under AFOSR sponsorship, transport coefficients based on the two-temperature LTE model for Teflon are now developing. Extension of such modeling to other

candidate materials could guide propellant selection. Decomposition of solid propellants exposed to high current discharges remains a critical area of concern for both propellant choice and theoretical modeling. The idealized model has already suggested a connection between discharge operation and material properties. At sufficiently high currents, the temperature needed to supply the mass flow to the discharge will exceed values at which the solid propellant decomposes in some manner. For example, the surface may liquefy. A thin liquid film pressed by vapor against the still solid interior of the propellant can splash laterally on the electrode and insulator surfaces of the thrust chamber, resulting in mass ejection at low speed. If such a mechanism exists in present PPTs, it can provide a significant limitation on PPT performance. Proper choice of propellant and operating magnetic field to avoid pulsed liquid films would avoid this difficulty. The results of the idealized model depend on transport properties, such as the thermal conductivity. Decomposition of solid propellants involves particular values of temperature (e.g., melting point). Combination of plasma transport and solid decomposition will require self-consistent calculations based on accurate plasma properties and careful numerical modeling.

APPENDIX I

Transport Processes in Pulsed Plasma Thrusters

TRANSPORT PROCESSES IN PULSED PLASMA THRUSTERS

Prof. P.J. TURCHI
Principal Investigator

Department of Aerospace Engineering,
Applied Mechanics, and Aviation

The Ohio State University
Columbus, OH

Presented at AFOSR Space Propulsion and Power Contractor Meeting
28 - 31 July 1997, San Diego, CA

THE PULSED PLASMA MICROTHRUSTER (PPT) ACHIEVED EARLY ACCEPTANCE FOR SPACEFLIGHT USE LARGELY BECAUSE OF ITS SIMPLICITY, (e.g., PROPELLANT HANDLING, BASED ON SPRING-LOADED ADVANCE OF A TEFLON BAR ABLATED BY AN ARC)

---- How can we retain such simplicity in scaling to smaller satellites ?

---- What are the processes that determine scaling of ablated-mass and exhaust speed with circuit current, pulsetime, and thruster geometry ?

---- How do ablated-mass and exhaust speed depend on the properties of complex, molecular plasmas created from solid propellants ?

THE PRINCIPAL SCIENTIFIC DEFICIENCY IN SCALING THE PPT IS AN INABILITY TO CALCULATE THE MASS ABLATED PER SHOT WITHOUT RECOURSE TO EMPIRICAL TRENDS DEVELOPED FOR A FEW, GEOMETRIES AND CIRCUIT OPERATIONS

---- Such calculation requires self-consistent computation of the discharge flow field, including circuit behavior, ablation of the solid-propellant surface and transport processes in the plasma and solid.

[This is part of our program at Ohio State for NASA LeRC]

---- Calculation of heat transfer from complex, molecular plasmas to solid surfaces, as in the PPT and other Air Force systems, requires detailed knowledge of transport coefficients (e.g., thermal conductivity, electrical resistivity, radiation opacity) over a wide range of plasma conditions, including non-equilibria of various kinds.

[This is our program for AFOSR]

OUR PRINCIPAL TOOL FOR CALCULATING THE PPT DISCHARGE FLOW FIELD, INCLUDING PROPELLANT ABLATION IS THE MACH2 CODE. TODAY'S PRESENTATION COVERS OTHER TOPICS

Non-dimensional analysis of the PPT discharge, including heat conduction in an MHD formulation

- -- This work provides scaling relations for the discharge flow field (e.g., characteristic lengths, dependence of exhaust speed on propellant, electrical behavior)

Two-temperature LTE calculation of composition of a Teflon plasma

- -- Equilibrium between free and bound electrons, but separate heavy-particle temperature
- -- Includes 25 constituents from molecules through multiply-ionized carbon and fluorine
- -- Basis for generating transport coefficients

ONE-DIMENSIONAL, MHD EQUATIONS CAN BE USED TO DETERMINE STRUCTURE OF A PPT DISCHARGE

Mass-flow :

$$\rho u = \text{constant} = w \qquad (1)$$

ρ = local mass density, u = local flow speed, $w = \rho^* u^*$

Momentum :

$$\rho u \frac{du}{dx} + \frac{d}{dx}\left(B^2/2\mu + p \right) = 0 \qquad (2)$$

so,
$$wu + B^2/2\mu + p = \rho^* u^{*2} + B^{*2}/2\mu + p^* \qquad (3)$$

or,
$$wu + B^2/2\mu + wRT/u = \rho^* u^{*2} + B^{*2}/2\mu + \rho^* R^* T^* \qquad (4)$$

T = temperature, R = gas constant, B = magnetic induction

Energy :

$$w \frac{dU}{dx} = \frac{d}{dx} \kappa \frac{dT}{dx} + \eta j^2 - p \frac{du}{dx} \qquad (5)$$

U = energy per unit mass, κ = thermal conductivity, η = electrical resistivity, and j = current density.

FOR THE ONE-DIMENSIONAL, STEADY-STATE PROBLEM, THE ELECTRIC FIELD IS UNIFORM ACROSS THE CHANNEL

Electric Field:

$$E = \eta j - u \times B + (j \times B - \text{grad } p_e) / n_e e \qquad (6)$$

$$= \text{constant} = E^* \qquad (7)$$

Energy Equation:

$$w\frac{dU}{dx} = \frac{d}{dx}\kappa\frac{dT}{dx} + \frac{(E^* - uB)^2}{\eta} - p\frac{du}{dx} \qquad (8)$$

Transport Coefficients:

Thermal conductivity $\kappa = K_h T^{5/2}$ (9)

and

Electrical resistivity $\eta = K_r / T^{3/2}$ (10)

NON-DIMENSIONALIZING THE EQUATIONS PROVIDES DIMENSIONLESS PARAMETERS OF FLOW STRUCTURE

Temperature Equation:

$$w c_p \frac{dT}{dx} = \{ [\frac{d}{dx} K_h T^{5/2} \frac{dT}{dx} + \frac{(E^* - uB)^2 T^{3/2}}{K_r}](\gamma M^2 - 1) - ujB \} / (M^2 - 1) \qquad (11)$$

where $M^2 = u^2 / \gamma RT$, is the square of the local (thermal) Mach number

Nondimensional Variables and Parameters:

$$\theta = T / T^* , \qquad \omega = u / u^* , \qquad f = B / B^* , \qquad \alpha = x / x_c$$

$$\beta^* = p^* / (B^{*2} / 2\mu) , \qquad R_m^* = u^* B^* / \eta^* j^* , \qquad P = w c_p x_c / K_h T^{*5/2} \qquad (12)$$

Dimensionless Temperature Equation:

$$(\omega^2 M^{*2}/\theta - 1) P \frac{d\theta}{d\alpha} = (\gamma \omega M^{*2}/\theta - 1) [\frac{d}{d\alpha} \theta^{5/2} \frac{d\theta}{d\alpha} + (1 + 1/R_m^* - \omega f)^2 \theta^{3/2}] - \omega f (1 + 1/R_m^* - \omega f) \qquad (13)$$

A CHARACTERISTIC SCALE LENGTH FOR THE DISCHARGE FLOW IS BASED ON THE BALANCE OF HEAT CONDUCTION AND RESISTIVE DISSIPATION

Characteristic Distance:

$$x_c = (K_r K_h)^{1/2} T^* / u^* B^* \qquad (14)$$

Magnetic Field Variation:

$$\frac{dB}{dx} = -\mu j = -\mu (E^* - uB) / \eta \qquad (15)$$

Dimensionless Form:

$$\frac{df}{d\alpha} = -\Lambda (1 + 1/R_m^* - \omega f)\, \theta^{3/2} \qquad (16)$$

Dimensionless parameter :

$$\Lambda = \mu (K_h / K_r)^{1/2} T^{*5/2} / B^* = x_c / (\eta^* / \mu u^*) \qquad (17)$$

THE NON-DIMENSIONALIZED EQUATIONS MAY BE INTEGRATED UPSTREAM STARTING AT THE MAGNETO/THERMAL SONIC POINT

Magneto/thermal Sonic Condition ($Rm^* >>1$):

$$u^{*2} = \gamma RT^* + B^{*2} / \rho^* \mu = (B^{*2} / \rho^* \mu) [\, 1 + \gamma \beta^* / 2 \,] \qquad (18)$$

Non-dimensional speed, ω:

$$\omega + f^2 / (2 + \gamma\beta^*) + \beta^* \theta / \omega(2 + \gamma\beta^*) = 1 + (1 + \beta^*) / (2 + \gamma\beta^*) \qquad (19)$$

Non-dimensionalized Equations:

$$\frac{df}{db} = \Lambda (1 + 1/Rm^* - \omega f)\, \theta^{3/2} , \qquad \frac{d\theta}{db} = - \Gamma \qquad (20a,b)$$

$$\frac{d\Gamma}{db} = \{ (1 + 1/Rm^* - \omega f)^2 + 5\Gamma^2 / 2] - \omega f (1 + 1/Rm^* - \omega f) / (\gamma\omega M^{*2}/\theta - 1)\} / \theta$$
$$- P\Gamma (\omega^2 M^{*2}/\theta - 1) / (\gamma\omega M^{*2}/\theta - 1)\theta^{5/2} \qquad (20c)$$

Increment of integration is $db = - d\alpha$. Initial conditions are $f(0) = 1$, $\theta(0) = 1$, and $\Gamma(0) = 0$

THE LOCATION OF THE UPSTREAM BOUNDARY IS BASED ON ADEQUATE HEAT FLUX TO RAISE THE ENTHALPY OF THE PROPELLANT INPUT FLOW

Heat Flux for Normalized Value Γ at Inlet ($b = b_1$):

$$q = (K_h T^{*7/2} / x_c)\, \theta^{5/2}\, \Gamma \qquad (21)$$

Necessary heat flux for propellant mass flux, w:

$$q_1 = w\,(Q + c_p T_1 + u_1^2 / 2) \qquad (22)$$

where Q = energy per unit mass for evaporation, dissociation, ionization, etc.
Subscript '1' referrs to the inlet location $b = b_1$.

Temperature at Sonic Point:

$$T^* = (Q / c_p) / [\,(\theta^{5/2}\Gamma)_1 / P - \theta_1 - (\gamma - 1)(2 + \gamma\beta^*)\,\omega_1^2 / 2\gamma\beta^*\,] \qquad (23)$$

$$= \{\Lambda / \mu\,(K_h / K_r)^{1/2}\}^{2/5} (B_1 / f)^{2/5} \qquad (24)$$

where B_1 is the magnetic field at the inlet, due to the discharge current.
The inlet location is obtained from a consistent set of values for θ , Γ , ω , and f , all of which are functions of b.

WITH THE TEMPERATURE AT THE SONIC POINT, THE FLOW SPEED AND OTHER CONDITIONS ARE OBTAINED. THE FLOW SPEED IS PROPORTIONAL TO ALFVEN CRITICAL SPEED, AS EXPECTED.

Mass Density:

$$\rho^* = \beta^* (B^{*2} / 2\mu) / RT^* \quad (25)$$

Flow Speed:

Sonic condition $$u^{*2} = (B^{*2} / \rho^* \mu) [1 + \gamma\beta^* /2] \quad (26)$$

So,

$$u^* = Q^{1/2} \{ [1 + \gamma\beta^* /2] / [(\theta^{5/2} \Gamma)_1 / P - \theta_1 - (\gamma - 1)(2 + \gamma\beta^*) \omega_1^2 / 2\gamma\beta^*] P\Lambda \}^{1/2} \quad (27)$$

Alfven critical speed is $v_A = (2 Q)^{1/2}$.

NORMALIZED VARIABLES OF THE DISCHARGE FLOW FIELD vs DISTANCE UPSTREAM OF SONIC POINT

Temperature , θ

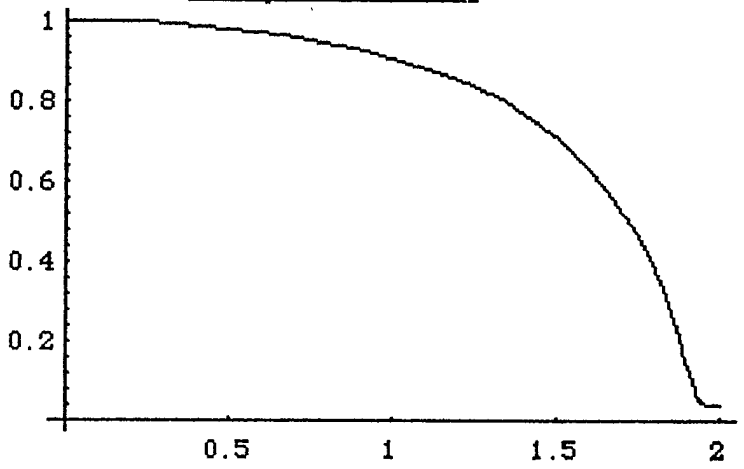

Magnetic Field, f

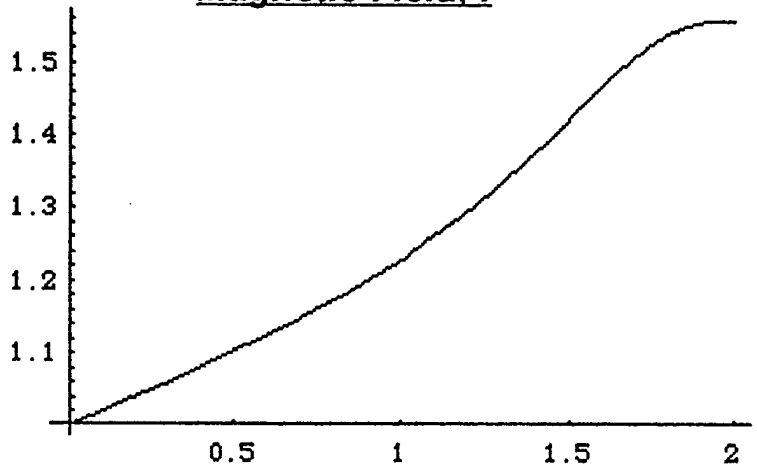

Flow Speed, ω

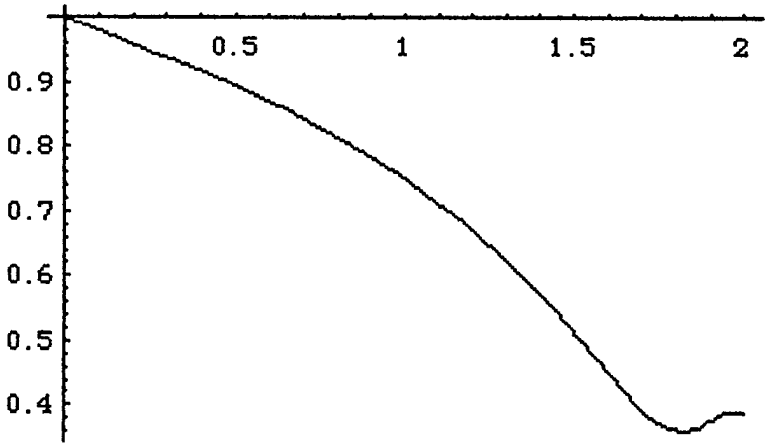

SAMPLE NUMERICAL RESULTS ARE COMPARABLE TO EXPERIMENTAL DATA FOR TYPICAL PULSED PLASMA MICROTHRUSTERS

For Inlet Magnetic Field $B_1 = 0.63$ T (10kA / 2 cm) :

Inlet location $b_1 = 1.88$

Magnetic field $B^* = 0.4$ T

Temperature $T^* = 7.8$ eV

Inlet temperature $T_1 = 0.9$ eV

Mass density $\rho^* = 8.3 \times 10^{-5}$ kg/m^3

Flow speed $u^* = 1.8 \times 10^4$ m/s

Mass flux $w = 1.5$ kg/m^2-s

Mass in 2 μs from 4 cm^2 = 1.2 μg

Voltage $E^*y = 158$ V (y = 2 cm)

Impedance $Z^* = 15.8$ mΩ

Characteristic Dimension x_C :

$$x_C = (K_r K_h)^{1/2} T^* / u^* B^* = 2.1 \text{ mm}$$

Location of inlet upstream of sonic point, $b_1 x_C = 4$ mm

PREVIOUS CALCULATIONS FOR NITROGEN HAVE SHOWN THAT THE TRANSPORT PROPERTIES CAN EXHIBIT SEVERELY NON-MONOTONIC VARIATIONS DUE TO CHEMICAL REACTIONS

Example: Thermal Conductivity of Nitrogen from 300 K - 30,000 K

(Ref. Master's Thesis , C. S. Schmahl, The Ohio State University, 1996)

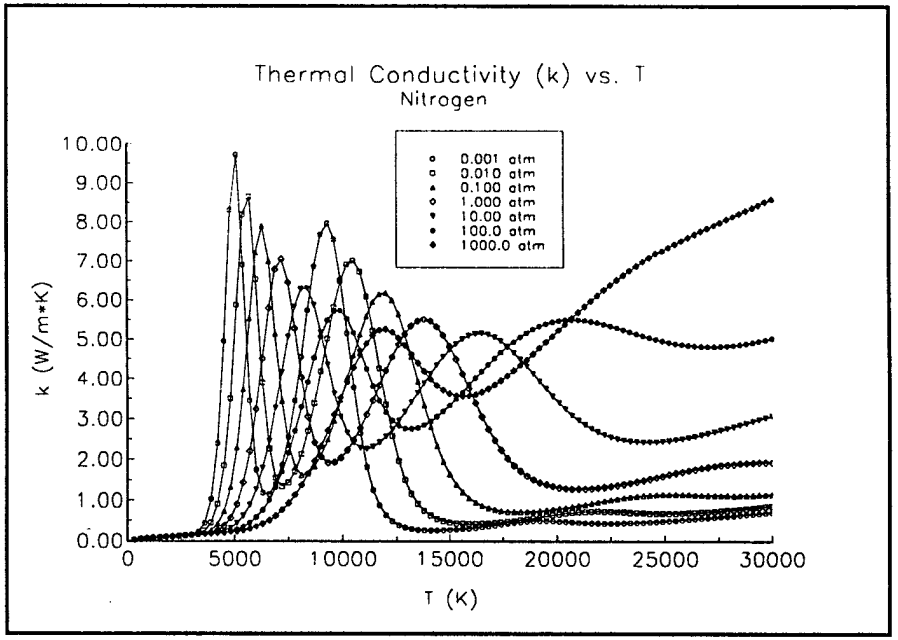

VARIATIONS OF THERMAL CONDUCTIVITY CAN AFFECT DISCHARGE FLOW STRUCTURE

Ersatz, non-monotonic thermal conductivity, $\kappa = K_h (1 + 0.5 \sin(\theta(b) / .05)) T^{*5/2} \theta^{5/2}$

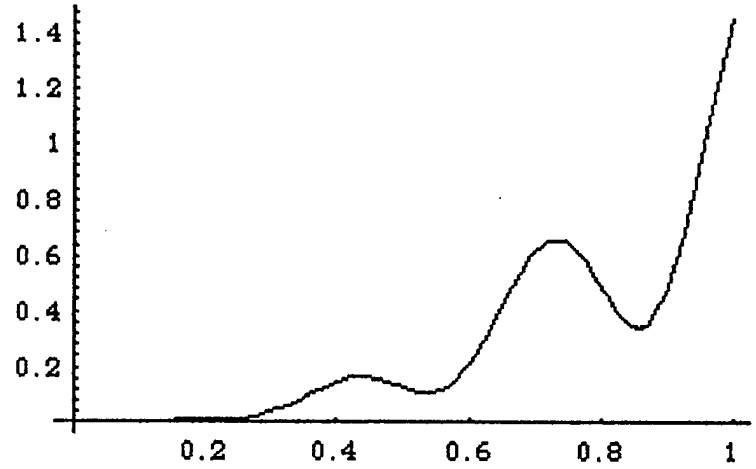

Normalized Heat Flux, monotonic:

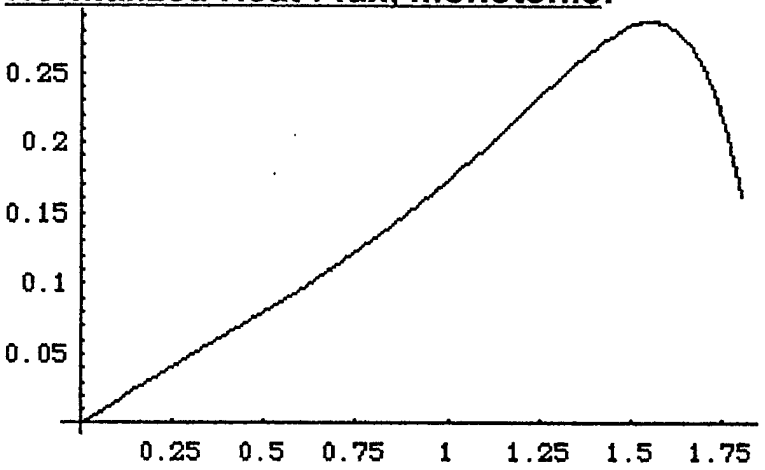

Normalized Heat Flux, non-monotonic:

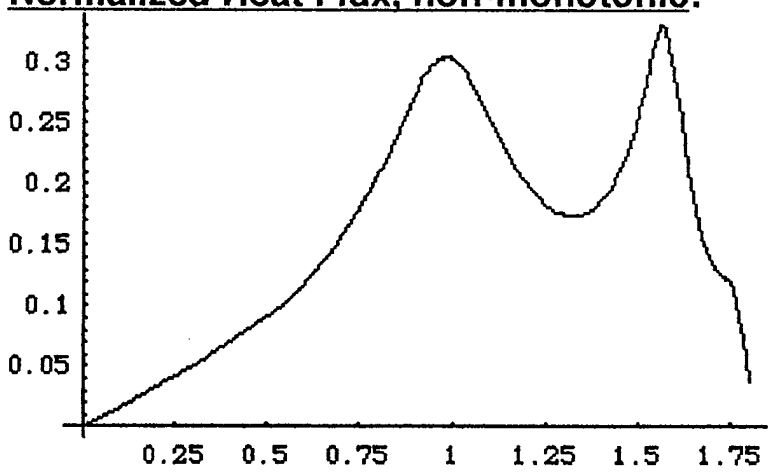

25 CHEMICAL SPECIES ARE INCLUDED IN THE TEFLON REACTION MODEL

Molecules	Molecular Ions	Atoms	Atomic Ions	Electrons
C_2F_4	CF_3^+	C	C^Z (Z=1,4)	e^-
C_2	CF_2^+	F	F^Z (Z=1,4)	
C_2F_2	F_2^+		F^-	
CF_3	CF^+		C^-	
CF_4				
CF_2				
CF				
F_2				

TWENTY-TWO INDEPENDANT CHEMICAL REACTIONS ARE CONSIDERED

Dissociation

$C_2F_4 <=> 2\ CF_2$
$C_2 <=> 2\ C$
$C_2F_4 <=> C_2F_2 + F_2$
$C_2F_4 <=> CF_3 + CF$
$C_2F_4 <=> CF_4 + C$
$CF_2 <=> CF + F$
$CF <=> C + F$
$F_2 <=> 2\ F$

Atomic Ionization

$C^{Z-1} <=> C^Z + e^-$ (Z=0,4)
$F^{Z-1} <=> F^Z + e^-$ (Z=0,4)

Molecular Ionization

$CF_2 <=> CF_2^+ + e^-$
$CF <=> CF^+ + e^-$
$F_2 <=> F_2 + e^-$
$CF_3 <=> CF_3^+ + e^-$

TO DETERMINE THE COMPOSITION FOR EACH THERMODYNAMIC STATE WE NEEDED TO SOLVE A NONLINEAR SET OF TWENTY-FIVE COUPLED ALGEBRAIC EQUATIONS

i) **Twenty-Two Mass Action Relations Of The Form**

$$K_{p_j} = (k)^{\sum \nu_I} \prod_i (T_i)^{\nu_I} K_{n_j} \Big|_{j=1,22}$$

$$K_{p_j} = \prod_i P_i^{\nu_I}$$

$$\text{where: } K_N = e^{\frac{-\Delta\epsilon_0}{kT}} \prod_i Q_i^{\nu_I}$$

ii) **Conservation of Fluorine and Carbon Nuclei**

iii) **Dalton's Law**

iv) **Charge Neutrality**

THE RESULTS OF THE TWO-TEMPERATURE CALCULATIONS SHOW THE COMPOSITION CHANGES CAN BE GREATLY ENHANCED UNDER CONDITIONS OF THERMAL NONEQUILIBRIUM

Sample Species Compositions For The 2-Temperature Calculations

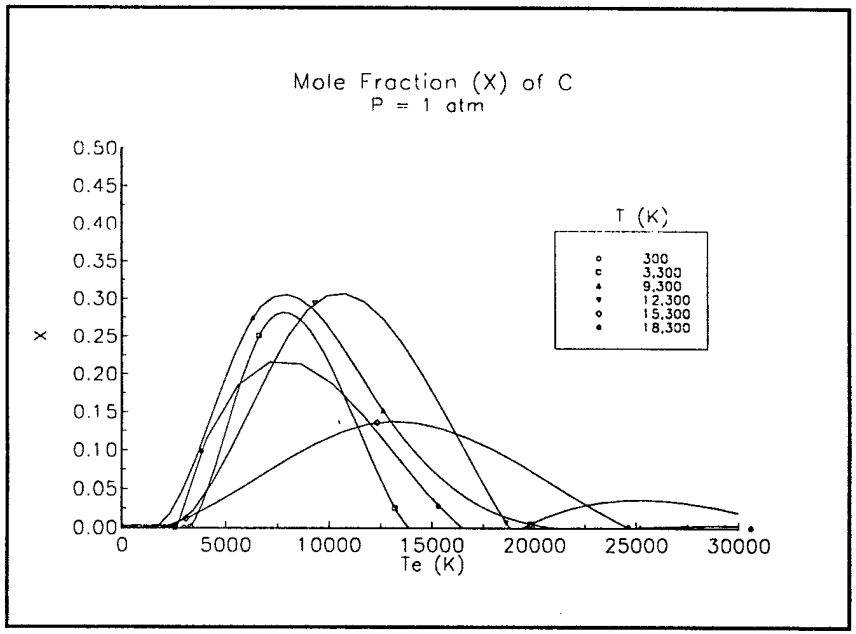

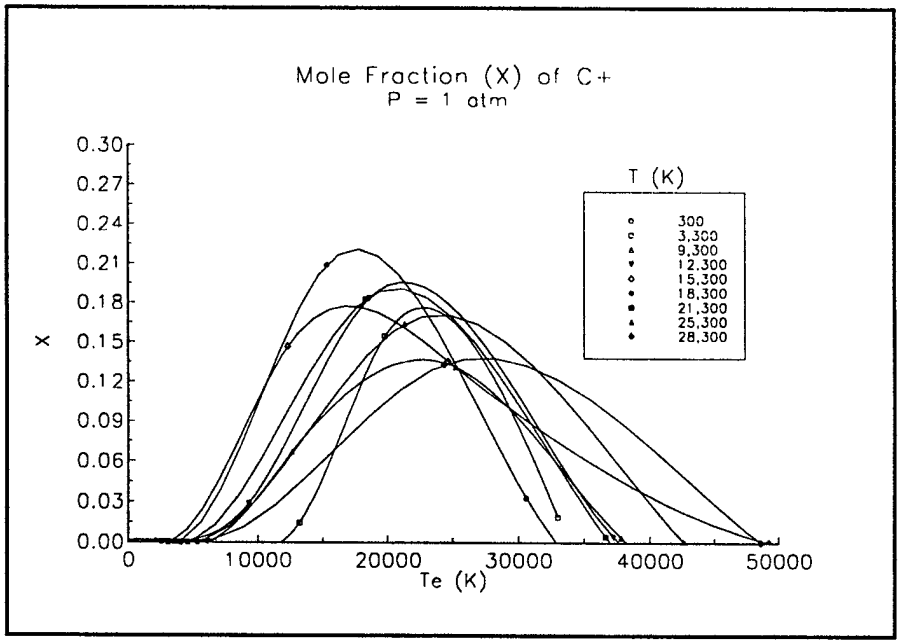

Sample Species Compositions For The 2-Temperature Calculations Continued

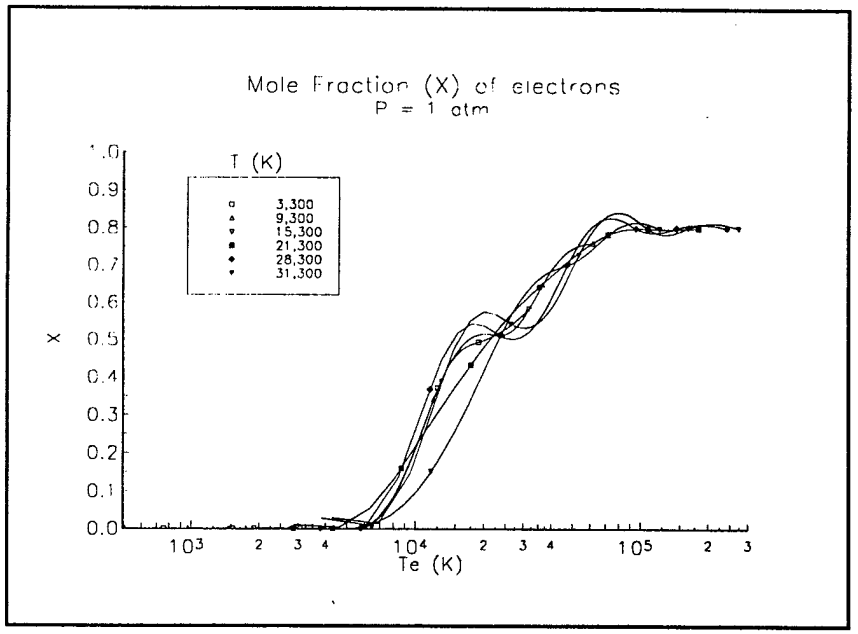

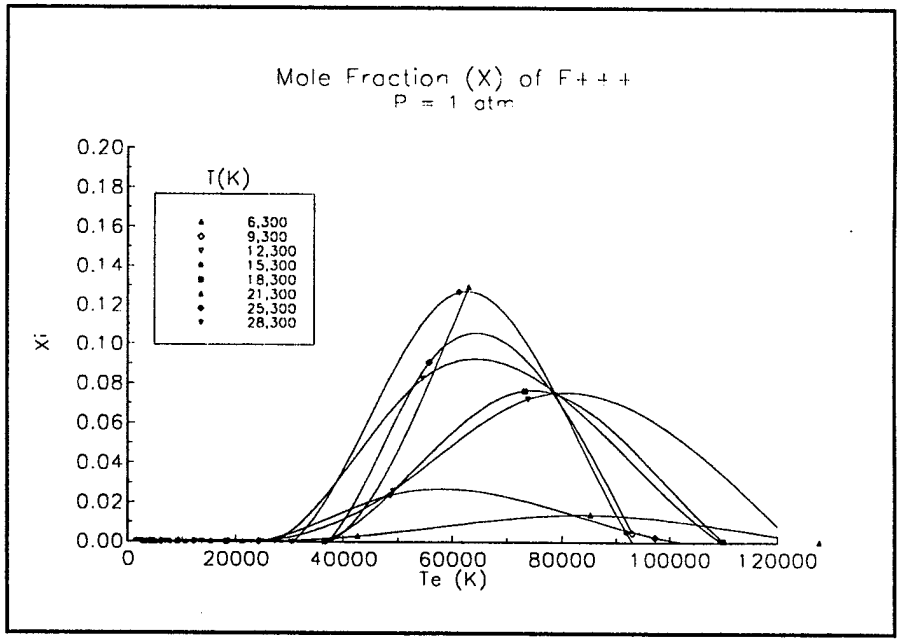

SUMMARY

Non-Dimensional MHD Analysis, with Heat Conduction:

---- Provides scaling relations for characteristic lengths, plasma and flow conditions

---- Provides numerical estimates that are in reasonable agreement with typical PPT properties

---- Provides indication of importance of accurate specification of plasma behavior (e.g., transport)

Composition of Teflon Plasma:

---- Two-temperature LTE formulation

---- Twenty-five constituents

---- Basis for tabular representations of thermodynamic properties and transport coefficients in MACH2

APPENDIX II

Directions for Improving PPT Performance

IEPC 97 - 038

DIRECTIONS FOR IMPROVING PPT PERFORMANCE

P.J. Turchi
The Ohio State University
Columbus, Ohio USA

25th International Electric Propulsion Conference
August 24-28, 1997, Cleveland, Ohio

DIRECTIONS FOR IMPROVING PPT PERFORMANCE

P.J. Turchi

The Ohio State University
Columbus, Ohio USA

ABSTRACT

Potential improvements in PPT performance are discussed from analytical considerations, and comprise the following sequence of conditions that need to be established. Presently, the exhaust of the PPT is allowed to expand without regard to extracting directed kinetic energy efficiently from the hot, highly-magnetized plasma in the thrust chamber. Analytically, it appears that improvements by a factor of 1.7 in specific impulse and three in thrust efficiency should be possible with proper expansion. A major area for improving PPT performance is the reduction of relative mass expelled that is not electromagnetically-accelerated to high speed. Analytical modeling indicates that mass evolved by post-discharge evaporation can exceed that during the discharge by a factor of more than five. An inductively-driven circuit, previously suggested, would maintain electromagnetic acceleration as the propellant surface cools. This circuit also improves PPT performance by eliminating losses and difficulties of present oscillatory waveforms.

INTRODUCTION

It is useful to consider directions for improving the pulsed plasma microthruster (PPT) so that it may be applied to a greater range of missions. In particular, higher thrust efficiency, and, for some uses, higher specific impulse are needed. It is critical that improvements to the PPT retain the simplicity that allowed its early operation in actual space missions, and maintain the connection to the PPTs extensive flight-experience. Of the four or five devices selected from dozens of concepts in electric propulsion, only the PPT has both a record of actual accomplishment in space, and the potential for significant improvement through further research. The other devices have already been taken to high levels of performance (probably their limiting values) by many years of sustained laboratory research and development.

BASIC OPERATION OF PRESENT PPT

The traditional pulsed plasma microthruster (PPT) operates with an unsteady, oscillatory discharge. This is a consequence of the relatively low energies used by PPTs for satellite station-keeping. With a stored-energy in the capacitor on the order of 20 J, at an initial voltage of 2 kV, the capacitance is only 10 μf.; circuit inductance values below 100 nh are difficult to obtain with commercially-available components. The impedance of an LRC-circuit for critical damping is $2(L/C)^{1/2}$ = 200 mΩ. The characteristic impedance of the electromagnetically-accelerated discharge flow, however, is (for a propagating discharge, with inductance gradient, L'):

$$Z_d = L' u / 2 \qquad (1)$$

so, at an exhaust speed of 40 km/s, and L' = 10^{-6} h/m, Z_d = 20 mΩ. Thus, the circuit is hardly loaded by the thruster, and can deposit much of its energy in the internal resistance of the capacitor. The losses associated with such resistance increases the operating temperature of the capcacitor. The combination of higher temperature with the severe and repeated reversals of the capacitor voltage reduces the reliable life of the capacitor, which must be compensated by a reduction in design voltage and energy per unit mass.

It is also typical of traditional PPT operation that the discharge flow simply exits abruptly from a constant area. For a magnetized-plasma flow, this fails to extract energy from the magnetic field (and any accessible thermal modes) into the directed kinetic energy of the exhaust. An additional source of inefficiency in traditional PPTs has recently been suggested after initial attempts at numerical simulation of the LES-6 device[1]. The numerical calculations, using the MACH2 code, agreed well with the impulse-bit per shot, but the mass ablated during the discharge pulse was about a factor of ten lower in the simulation vs the experimental data for mass loss per shot. Subsequent calculation indicated that evaporation of the Teflon propellant between firings might account for this mass discrepancy. If a major portion of the mass per shot is lost at relatively low speed, then the efficiency of the PPT is substantially reduced from ideal values.

In combination, the efficiency factors associated with external-circuit resistance (<60%), improper flow expansion (<33%) and mass loss at low speed (<50%) multiply to provide a total thruster efficiency of less than 10% . By addressing each of the inefficiencies in turn, it should be possible to improve the performance of the PPT substantially.

Consideration may be framed first in terms of quasi-analytical modeling, before invoking more powerful numerical tools and testing ideas experimentally. Idealized modeling may be applied to initial design of proper flow expansion, to the questions of mass loss and thermal management and, finally, to improved circuitry for the PPT.

IDEALIZED MODEL FOR PPT

The essential features of the ablation-fed discharge in the PPT include resistive heating near the entrance of a constant-area channel (where the back EMF is relatively low), heat transfer from the discharge back to the propellant surface to provide mass by ablation, and electromagnetic acceleration of the plasma by the Lorentz force. In pulsed operation, particularly with high-frequency, oscillatory waveforms, the preceding features are unsteady and require numerical modeling for accurate calculations in time and space. A first step in simplifying analysis of the PPT, while attempting to retain the fundamental interactions among resistive heating, heat transfer and flow, restricts examination to a steady state, and one-dimensional flow. (The details of such examination are briefly described in Appendix I.) The use of a steady analysis in discussing the PPT, however, means that comments can only be applied to situations in which there is enough time for the discharge flow to operate with a balance of heat conduction, resistive dissipation and flow acceleration. Convective times based on the discharge thickness divided by the flow speed must certainly be less than the time for variation of circuit current. Furthermore, the ablating surface must be able to supply new material in times shorter than the convective time. Thus, for example, discharges that lift off of refractory insulators may remain in an unsteady, propagating mode, rather than achieving the quasi-steady situation of the present analysis.

For a Teflon-based PPT, the analysis of Appendix I suggests that an ablation arc, with a thickness less than two millimeters, is formed adjacent to the propellant surface. In the numerical example, the speed of the flow through the arc increases by a factor of about three to an exit velocity of 41 km/s. The characteristic convective time for the flow structure is therefore about 0.1 μsec. Heat conduction to the colder upstream boundary automatically supplies the power needed to dissociate and ionize the flow, and also the relatively minor, additional power level required to provide mass flow by ablation. The calculated size and timescale suggest that the analysis is consistent with PPT operation at frequencies (within the discharge pulse) less than a MHz, and dimensions greater than a cm.

SPECIFIC IMPULSE

As previously noted in a simpler analysis (without heat conduction)[2], the proportionality of resistive heating and electromagnetic work, in the context of a flow in which heat is largely absorbed by the ionization of the propellant, leads to an exhaust speed that scales closely with Alfven critical speed. Thus, the specific impulse of self-field, plasma thrusters, operating with mass addition (vs constant mass, propagating discharges) will tend to values proportional to Alfven critical speed, if heating can supply additional conducting material. Improvements of PPT performance, in terms of higher specific impulse, therefore, would require propellants with lower average molecular-mass than the Teflon presently used. In the present example, the computed exit speed already corresponds to a specific impulse of 4180 s. Even moderate attention to proper expansion of this magnetosonic flow to magnetic field-free conditions will offer values of specific impulse that cover the range of any near term missions, (upwards of 7000 s). The earlier analysis[2] suggests improvements by up to $3^{1/2}$. The principal reason for the more modest values of specific impulse (~ 1000 s) is mass that is not accelerated electro-magnetically (e.g., post-discharge evaporation).

MASS ABLATED DURING DISCHARGE

By the analysis of Appendix I, the necessary mass-flow rate is actually controlled by a magnetosonic condition in the constant-area channel, rather than a separate condition on heat transfer to the propellant surface. The details of such heat transfer adjust to satisfy the mass flow constraints in the overall MHD flow. The mass loss during the discharge pulse may thus be estimated from the mass flow rate (per unit area):

$$w = \rho^* u^* \qquad (2)$$

where the speed at the sonic point is:

$$u^* = \{(B^{*2} / \rho^* \mu)[\, 1 + \gamma\beta^* / 2\,]\}^{1/2} \qquad (3)$$

and the mass density there is:

$$\rho^* = (\beta^* B^{*2} / 2\mu) / R^* T^* \qquad (4)$$

The temperature at the sonic point is obtained in terms of the magnetic field at the propellant surface, B_1:

$$T^* = \{\, \Lambda / f_1 \mu (K_h / K_r)^{1/2} \,\}^{2/5} \; B_1^{2/5} \qquad (5)$$

The mass flow rate is therefore proportional to $B_1^{9/5}$. For a constant current, the mass ablated during a pulsetime t_p is merely wAt_p, where A is the area of the ablating surface. In the case of an exponentially-decaying sinusoidal pulse, within the quasi-steady approximation, the mass flow rate may be integrated over the oscillatory waveform; if the ratio of risetime to decay time is 0.3, for example, the mass ablated is $0.933 w_o A t_r$, where t_r is the risetime and w_o is the mass flow rate per unit area based on the undamped amplitude of the current. Note that this represents a nearly linear dependence on stored energy, W_o, in the capacitor ($\Delta m \sim W_o^{9/10}$) for the mass ablated during the discharge.

THERMAL CONDITIONS AT SURFACE

The mass lost between discharges may be considered in terms of the temperature of the propellant surface. From the idealized analysis, it is possible to estimate the surface temperature of the propellant that is consistent with the flow conditions. In particular, the equibrium vapor pressure should equal the total pressure at the entrance to the ablation arc. A formula for the equilibrium vapor pressure for Teflon is:

$$p_{eq} = p_c \exp(-T_c / T) \qquad (6)$$

with $T_c = 20{,}815$ K and $p_c = 1.872 \times 10^{20}$ N/m^2.

The total pressure calculated from the one-dimensional, idealized model is:

$$p_t = p_1 + \rho_1 u_1^2 \qquad (7)$$

$$= (B_1^2 / 2\mu f_1^2)[\beta^* \theta_1/\omega_1 + (2 + \gamma\beta^*)\omega_1]$$

The necessary surface temperature is then:

$$T_s = T_c / \ln\{ p_c / (B_1^2 / 2\mu f_1^2)[\beta^* \theta_1/\omega_1 + (2 + \gamma\beta^*)\omega_1]\} \qquad (8)$$

For the numerical example of Appendix I, the surface temperature is 600 K. Note: this value is only weakly dependent on the operating magnetic field, but material transitions can be quite sensitive to exact values of temperature. This particular value is very close to the melting point of Teflon (~ 600 K). (Nonuniformities in arc distribution across the face of the propellant might cause local melting in any event.) The depth of propellant heated to this temperature during pulsetimes of several microseconds is less than a few microns. Growth of perturbations of a liquefied surface due to Rayleigh-Taylor instability would be suppressed for wavelengths approaching the depth of the layer, while the exponential growth of shorter wavelengths would not persist beyond amplitudes comparable to these wavelengths. Thus, micron-size droplets might be expected, especially from edges. Such droplets would be responsible for mass loss by surface disruption, as indicated in some experiments[3].

THERMAL MANAGEMENT

It has been suggested[1] that the loss of mass between shots depends critically on the overall thermal management of the PPT, both in the laboratory and in space. The estimated surface temperature is well above mean-values within the propellant measured in laboratory tests[4] at total power levels of 40 W (40 J at 1 Hz) which indicate a rise over several thousand shots from room temperature (300 K) to about 370 K. For the acknowledged low efficiency of present PPT operation, only a small fraction of the total power is delivered to the Teflon surface. The estimated surface temperature allows calculation of the heat deposited in the surface during the pulse, based on the thermal skin-depth , δ:

$$H = \rho c A \delta (T_s - T_i) \qquad (9)$$

where the thermal skin-depth is given in terms of the pulsetime t_p as:

$$\delta = (k t_p / \rho c)1/2 \qquad (10)$$

With $k = 0.305$ W/m-s-K, $\rho = 2.15 \times 10^3$ kg/m^3, and $c = 1171$ J/kg, a pulsetime of 10 μs would provide a skin-depth of 1.1 microns. At a surface temperature of 600 K, this contains 637 J/m^2 of heat added by the discharge pulse, which represents an average heat load to a 4 cm^2 surface of 0.25 W at a 1 Hz repetition rate. This exceeds the power required to evaporate Teflon from the surface by a factor of 5 (using the mass flow computed in Appendix I and a heat of vaporization and de-polymerization of 3.67 MJ/kg). The "extra" power delivered to the surface has consequences for both late-time pulsed and steady mass evolution.

After the discharge pulse ends, the heat deposited in the skin-layer will be shared with the rest of the solid propellant in a depth that continues to increase as the square-root of time. Without further heat addition (or significant cooling due to ablation), the surface temperature will decrease inversely with this depth:

$$(T_s - T_b) / (T_{si} - T_b) = (t_p / t)^{1/2} \qquad (11)$$

where T_{si} is the surface temperature at the end of the discharge pulse ($t = t_p$), and T_b is the base temperature of the propellant. The mass evaporated as the surface cools (for $t > t_p$) may be estimated using this time-dependence of the surface temperature in Eqn. 6.

By assuming one-dimensional expansion of the surface vapor to a (thermally) sonic condition, the mass flow per unit area is:

$$w = (\gamma / 2)[2/(\gamma + 1)]^{1/2} p_s / (\gamma RT_s)^{1/2} \qquad (12)$$

Integration of this mass flow rate provides a total evaporated mass (for $t > t_p$), Δm_e, that is proportional to the magnetic pressure and the pulsetime, allowing comparison with the mass ablated, Δm_d , during the discharge pulsetime:

$$\Delta m_e / \Delta m_d = K\{1 - \exp(-T_c / T_b) / \exp(-T_c / T_{si})\} \Big/ (T_c / T^*)^{1/2} (T_c / T_{si})^{1/2} (1 - T_b / T_{si})[\beta^*(1 + \gamma\beta^*/2)(\gamma + 1)/ 4\gamma]^{1/2} \qquad (13)$$

For the conditions of the previous numerical example, a base temperature T_b = 370 K, and the factor K = 1.26, the ratio of mass evaporated as the surface cools to that ablated during the discharge pulse is 5.1 . This ratio decreases to 4.3, if the base temperature of the propellant is kept at 300 K, indicating improved performance of PPTs with better cooling. The ratio increases largely as $B_1^{1/5}$, due to the variation of T^*, and thus is rather insensitive to the amplitude of the circuit current. Longer pulsetimes increase the mass ablated during the discharge, but also increase the heat deposited in the solid propellant, which maintains the surface temperature for a longer time after the pulse, allowing significant evaporation to continue longer. Major improvements will require either optimization of material properties or matching of the power circuit to the ablation process to avoid evolution of mass when electromagnetic forces are absent.

QUASI-STEADY, INDUCTIVE OPERATION

One approach to preventing such evolution would reduce the surface temperature needed to support the mass flow through the discharge as thermal conduction into the solid cools the surface. After an initial pulsetime due to the current rise, $t_p = t_r$, the surface temperature would then decline according to Eqn.11, if no significant additional heat deposition is required in order to supply mass flow to the discharge. Now, let the current decrease so that the required temperature follows the decreasing temperature of the surface:

$$J/J_o = B_1 / B_{1o} = \exp[-(T_c / T_b) / (1 + (T_{si} / T_b - 1)(t_p / t)^{1/2}] / \exp[-(Tc / Tb) / (1 + (Tsi / Tb - 1)] \qquad (14)$$

This is displayed in Fig. 1 with t in units of the risetime, $t_r = t_p$. (Temperature values are the same as in the earlier discussion.) Such a waveform may be compared with the experimental current behavior (Fig 2) obtained with an inductively-driven circuit[5] in which a plasma discharge (in this case a second PPT) is used to crowbar the capacitor shortly after peak current.

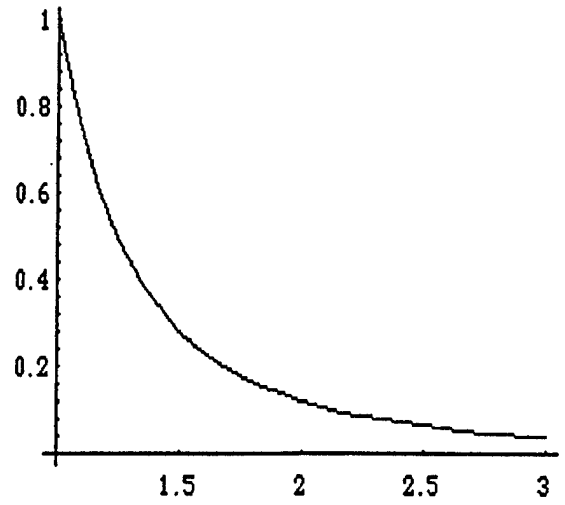

Figure 1: Normalized current waveform, J / J_o vs time in units of risetime, t / t_r

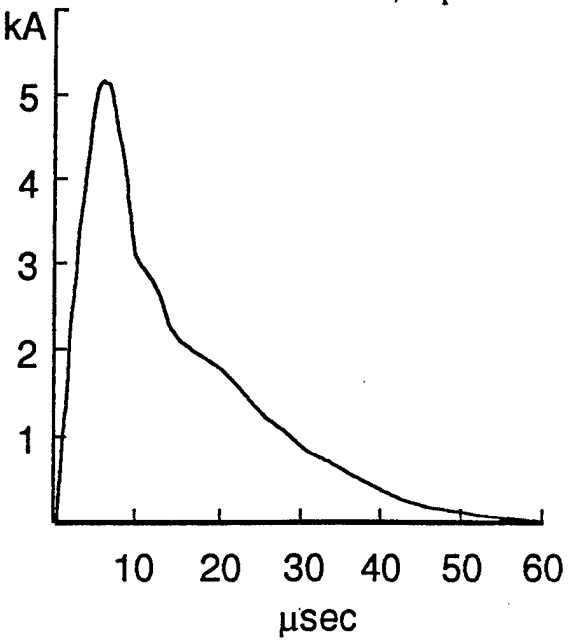

Figure 2: Experimental current waveform for inductively-driven circuit driving PPTs

The use of a inductively-driven circuit not only provides a current waveform that might alleviate mass evolution after the current pulse, but also avoids the severe voltage-reversals on the capacitor. With some attention to reducing the resistance of the external circuit to a small fraction of the PPT impedance, the electrical efficiency should greatly improve. From the idealized analysis, the impedance of the PPT is:

$$Z = u^*B^*h / J \qquad (15)$$

where h is the length of the discharge. For the values previously used, and h = 2 cm, Z = 33 mΩ. At J_O = 10 kA, and an initial circuit energy of 20 J, the inductance of the store could be 400 nh, for which the characteristic decay time of the waveform would be 12 μsec; the capacitance at an initial voltage of 2 kV is 10 μf, so the risetime is about 3.1 μsec.

CONCLUDING REMARKS

The idealized analysis has indicated that evolution of mass after the discharge pulse is a fundamental consequence of creating mass by ablation during the discharge. It is therefore useful to maintain electromagnetic forces while the surface cools. This can be accomplished simply by means of an inductively-driven circuit, which merely involves placing a low impedance across the energy-storage capacitor shortly after peak current. Such a circuit was originally suggested[5] to improve PPT design by allowing high energy per unit mass at low total energies (without the difficulties of parasitic inductance and internal resistance in the capacitor). In addition to reducing internal losses, reduction of the amplitude of voltage-reversal on the capacitor improves reliability at high energy density. Furthermore, the new circuit provides longer discharge times, so that proper flow expansion techniques can be used; nozzle sizes divided by flow speeds require quasi-steady currents for several μsec.

While the idealized analysis can guide general considerations, and may closely match experimental data in some cases, accurate analysis requires numerical tools, such as MACH2. This includes design of a properly expanded PPT flow, which has recently been successfully attempted with an annular PPT exiting to a plug nozzle.

ACKNOWLEDGEMENTS

This work is sponsored by NASA Lewis Research Center and AFOSR/NA, which is gratefully acknowledged by the author, who also expresses his appreciation for the hospitality extended while on sabbatical leave at USAF Phillips Laboratory, Kirtland AFB, NM.

REFERENCES

1. P.G. Mikellides and P.J. Turchi, "Modeling of Late-time Ablation in a PPT", AIAA 96-2733.

2. P.J. Turchi and P.G. Mikellides, "Modeling of Ablation-Fed Pulsed Plasma Thrusters", AIAA 95-2915.

3. G. Spanjers, et al, "Power Level Effects and Propellant Losses in a PPT", AIAA 97-2920.

4. H. Kamhawi and P.J. Turchi, "PPT Thermal Management", IEPC 97-125.

5. P.J. Turchi, et al, "Design of an Inductively-Driven Pulsed Plasma Thruster", AIAA 96-2731. Also, H. Kamhawi, for recent experimental data.

A1. L. Spitzer, Physics of Fully Ionized Gases, Wiley (1964). Chapter 5.

APPENDIX I

ONE-DIMENSIONAL, STEADY PLASMA THRUSTER FLOW WITH HEAT CONDUCTION

The conservation equations for a one-dimensional, steady plasma flow with resistive heating and heat conduction are written as:

Mass-flow :

$$\rho u = \text{constant} = w \qquad (A1)$$

where ρ is the local mass density and u is the local flow speed. The constant may be evaluated in terms of values at a particular location, $w = \rho^* u^*$.

Momentum :

$$\rho u \frac{du}{dx} + \frac{d}{dx}\left(B^2/2\mu + p \right) = 0 \qquad (A2)$$

so,

$$wu + B^2/2\mu + p = \text{constant}$$

$$= \rho^* u^{*2} + B^{*2}/2\mu + p^* \qquad (A3)$$

where B is the local magnetic field and p is the local pressure; starred quantities are evaluated at the same location. For simplicity, the pressure may be written as:

$$p = \rho R T \qquad (A4)$$

where T is the local temperature, and R is an appropriate gas constant. The momentum equation then becomes:

$$wu + B^2/2\mu + wRT/u$$

$$= \rho^* u^{*2} + B^{*2}/2\mu + \rho^* R^* T^* \qquad (A5)$$

The temperature distribution depends on the interplay of convection, heat conduction, resistive dissipation, and work, which may be written in terms of the third conservation equation:

Energy:

$$w \frac{dU}{dx} = \frac{d}{dx} k \frac{dT}{dx} + \eta j^2 - p \frac{du}{dx} \qquad (A6)$$

where U is the energy per unit mass, k is the thermal conductivity, η is the electrical resistivity, and j is the current density. In steady state, and one-dimension, the resistive dissipation may be written in terms of an electric field that is uniform:

$$E = \eta j - u \times B + (j \times B - \text{grad } p_e) / n_e e \qquad (A7)$$

$$= \text{constant} = E^* \qquad (A8)$$

where the electric field can be evaluated at the starred location for which $j = j^*$, so $E^* = \eta^* j^* + u^* B^*$. (Note that the gradient of the electron pressure, p_e, divided by the electron density, n_e, does not contribute to ηj^2 in the one-dimensional problem, nor does the Hall effect term.) The energy equation is then given by:

$$w\frac{dU}{dx} = \frac{d}{dx} k \frac{dT}{dx} + \frac{(E^* - uB)}{\eta} - p \frac{du}{dx} \qquad (A9)$$

In general, solution of this equation can be accomplished if the detailed behaviors of the energy and pressure functions, and the transport coefficients, k and η, are known in terms of temperature and density.

For ideal plasmas[A1], the thermal conductivity and electrical resistivity can be written in terms of formulas that only involve the temperature, if the plasma is sufficiently ionized (and does not change its degree of ionization) and magnetic fields do not suppress the electron heat conduction unduly. Thus,

$$k = K_h T^{5/2} \quad \text{and} \quad \eta = K_r / T^{3/2} \qquad (A10)$$

where K_h and K_r are constants. (We have also ignored the variation of the Coulomb logarithm here for continued simplicity.)

To delineate the flow structure, and avoid losing general results in consideration of particular plasma values, it is useful to non-dimensionalize variables in terms of conditions at the starred location (which might later be identified as a sonic point). Thus, let:

$$\theta = T / T^*, \ \omega = u / u^*, \ f = B / B^*,$$

$$\text{and } \alpha = x / x_c \qquad (A11)$$

where x_c is a characteristic distance determined later. Three dimensionless parameters are also obtained:

$$\beta^* = p^* / (B^{*2} / 2\mu), \ R_m{}^* = u^* B^* / \eta^* j^*$$

$$\text{and } P = w c_p x_c / K_h T^{*5/2} \qquad (A12)$$

where β^* and $R_m{}^*$ are the plasma-beta and local magnetic Reynolds number at the starred location, and P is essentially a Peclet number based on the characteristic length:

$$x_c = (K_r K_h)^{1/2} T^* / u^* B^* \qquad (A13)$$

which is found by inspection of the normalized equations. This characteristic length is the scale size for a temperature gradient supported by resistive dissipation.

There is an additional scale size for variation due to the change in magnetic field associated with the current density (that drives the dissipation):

$$\frac{dB}{dx} = -\mu j \qquad (A14)$$

$$= -\mu (E^* - uB) / \eta$$

In terms of dimensionless variables, this equation becomes:

$$\frac{df}{d\alpha} = -\Lambda (1 + 1/R_m{}^* - \omega f) \theta^{3/2} \qquad (A15)$$

where an additional dimensionless parameter is obtained:

$$\Lambda = \mu (K_h / K_r)^{1/2} T^{*5/2} / B^* \qquad (A16)$$

$$= x_c / (\eta^* / \mu u^*)$$

that relates the scale size for thermal conduction balancing resistive dissipation, x_c, to that for which convection balances diffusion of magnetic flux.

Solution of the set of normalized equation is obtained by integrating in the upstream direction from the starred location, where conditions are taken as $f(0) = 1$, $\theta(0) = 1$, and $\Gamma(0) = 0$, ($\Gamma = d\theta/d\alpha$, is a

dimensionless temperature gradient), to insure that uniform conditions are attained in the limit of high magnetic Reynolds number. The actual extent of the flow field is not prescribed, but is determined instead by requirements at the upstream boundary (e.g., necessary heat flux to establish conditions of the entering flow).

For the one-dimensional flow, it is useful to specify a sonic condition at the starred location, rather than providing values for the mass flow that might be inconsistent with such a condition. The necessary value of u^* is then given (in the limit of $R_m^* >> 1$) by:

$$u^{*2} = \gamma R T^* + B^{*2} / \rho^* \mu \qquad \text{(A17)}$$

The results of a sample calculation, performed using Mathematica, are displayed in Figures A-1 to A-3. Parameter values are $\Lambda = 2.0$, and $P = 0.1$, for which $\beta^* (= 2(\gamma - 1)P\Lambda / \gamma) = 0.114$. The local value of magnetic Reynolds number is (arbitrarily) $R_m^* = 10$, and the specific heat ratio is $\gamma = 1.4$. Distances are measured upstream of the sonic point by the dimensionless variable $b = x / x_c$.

To return to dimensional quantities, it is necessary to connect the results of the normalized calculation to the conditions of a particular thruster. For example, the heat flux is:

$$q = (K_h T^{*7/2} / x_c)\, \theta^{5/2}\, \Gamma \qquad \text{(A18)}$$

If the upstream boundary of the flow corresponds to the entry point of cold propellant, the heat flux from the discharge must be sufficient to raise the total enthalpy of this mass to the initial conditions of the discharge flow. For purposes of illustration here, the necessary heat flux may be written as:

$$q_1 = w\,(Q + c_p T_1 + u_1^2 / 2) \qquad \text{(A19)}$$

where Q is the chemical energy per unit mass (including the cost of vaporization, dissociation and ionization), and the subscript '1' refers to the entry station of the flow. The characteristic temperature T^* is then obtained in terms of the chemical energy per unit mass, Q:

$$T^* = (Q / c_p) / [\,(\theta^{5/2}\Gamma)_1 / P - \theta_1 - (\gamma - 1)(2 + \gamma\beta^*)\,\omega_1^2 / 2\gamma\beta^*\,] \qquad \text{(A20)}$$

In Fig. A-4, the denominator of Eqn. 21 is displayed for the same parameters previously used. Note that the minimum value of T^* corresponds to $b = 1.6$. For a Teflon plasma, fully dissociated into singly-ionized constituents, Q is about 62 eV/50 amu, while c_p would be 21 eV/50 amu-eV for the three heavy-particles and three electrons. Thus, $Q/c_p \simeq 3$, and the minimum value of T^* is 1.2 eV. Higher temperatures, however, are also possible and would be chosen in order to satisfy other conditions of the thruster, such as the operating value of magnetic field.

The driving source for the thruster can typically be characterized in terms of the current supplied. It is reasonable, therefore, to attempt to specify thruster operation by the magnetic field, B_1, at the entrance of the flow field. The magnetic field at the sonic point is then $B^* = B_1 / f(b_1)$. The temperature at the sonic point is related to the magnetic field by:

$$T^* = \{\Lambda / \mu (K_h / K_r)^{1/2}\}^{2/5}\, (B_1 / f(b_1))^{2/5} \qquad \text{(A21)}$$

Consistent solution requires agreement of Eqns. 21 and 22 for a specified magnetic field, B_1. In the present numerical example, this occurs at $b_1 = 1.88$. A total current of 10 kA over a 2 cm width provides a magnetic field of $B_1 = 0.63$ Tesla at the entrance implying (with $f_1 = 1.56$) a value of $B^* = 0.4$ T at the sonic point. For this value, the characteristic temperature may be found in terms of the transport properties of the plasma. (For an ideal, singly-ionized plasma, the values of K_r and K_h are[A1]:

$$K_r = 5.21 \times 10^{-5}\, \lambda \quad [\text{W-m-eV}^{3/2}]$$

and

$$K_h = 7.46 \times 10^{4} / \lambda \quad [\text{J / m-s-eV}^{7/2}]$$

where λ is the so-called Coulomb logarithm, and temperatures are measured in eV.) The characteristic temperature (with $\lambda = 10$) is then:

$$T^* = \{\Lambda B^* / \mu\, (K_h / K_r)^{1/2}\}^{2/5} \qquad \text{(A22)}$$

$$= 7.8 \text{ eV}$$

With the magnetic pressure, and plasma temperature, the mass density at the sonic point can be found in terms of the plasma-beta:

$$\rho^* = \beta^* (B^{*2} / 2\mu) / RT^* \qquad \text{(A23)}$$

$$= 8.3 \times 10^{-5} \text{ kg/m}^3$$

The flow speed can also be obtained from the sonic condition in the form:

$$u^{*2} = (B^{*2} / \rho^* \mu)\,[\,1 + \gamma\beta^* / 2\,] \qquad \text{(A24)}$$

For the numerical values previously used, $u^* = 41$ km/sec. The characteristic scale-size is 0.93 mm, so the discharge thickness is $d = b_1 x_c = 1.75$ mm.The mass flow per unit area is $\rho^* u^* = 3.4$ kg/m^2-sec. For a cross-sectional area of 4 cm^2, the mass ejected in 10 μs would be 13.6 μg.

Another relationship among parameters:

$$P\Lambda = \mu \rho^* c_p T^* / B^{*2} \qquad \text{(A25)}$$

provides the speed at the sonic point in the form:

$$u^* = Q^{1/2} \{ [\, 1 + \gamma\beta^*/2 \,] / [\, (\theta^{5/2}\Gamma)_1 / P - \theta_1 - (\gamma - 1)(2 + \gamma\beta^*)\, \omega_1^2 / 2\gamma\beta^* \,] P\Lambda \,\}^{1/2} \qquad \text{(A26)}$$

which displays the basic scaling with Alfven critical speed.

While the numerical results in the present example may be fortuitously close to values observed in various PPT experiments, accurate predictions require modeling based on the actual behavior of the propellant in the full two- (and three-) dimensional, unsteady environment of the thruster.

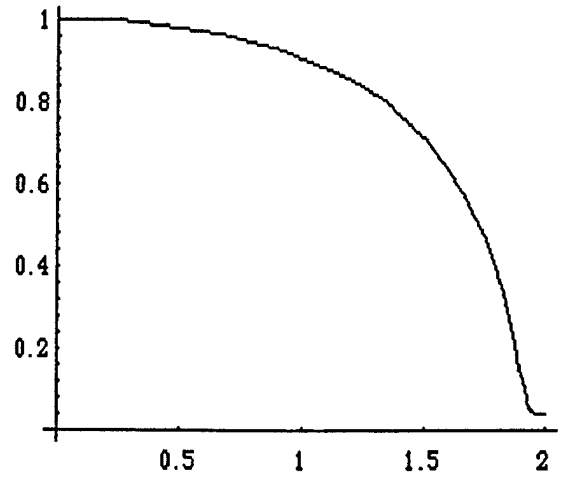

Fig. A-1 Normalized temperature, θ vs normalized distance, b, upstream of sonic point

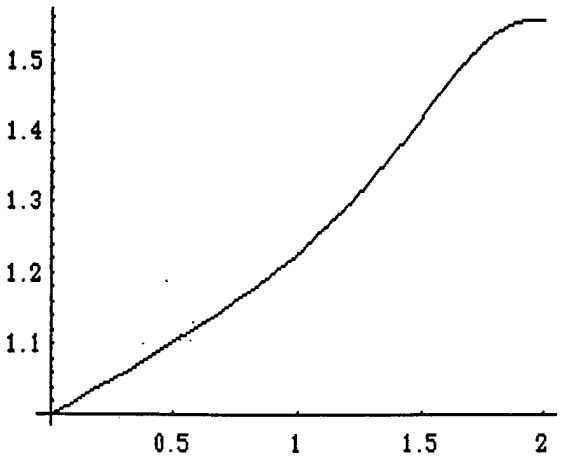

Fig. A-2 Normalized magnetic field, f vs normalized distance, b, upstream of sonic point

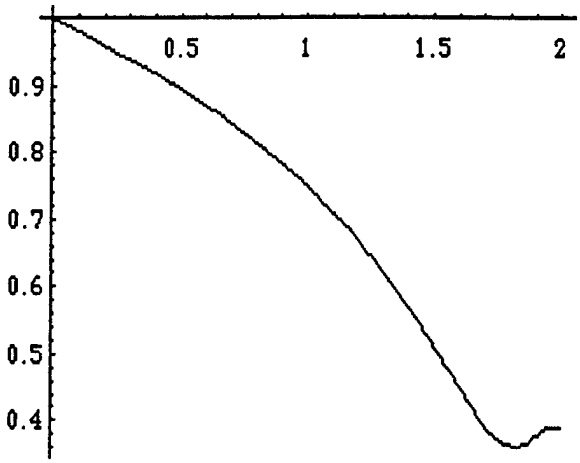

Fig. A-3 Normalized flow speed, ω vs normalized distance, b, upstream of sonic point

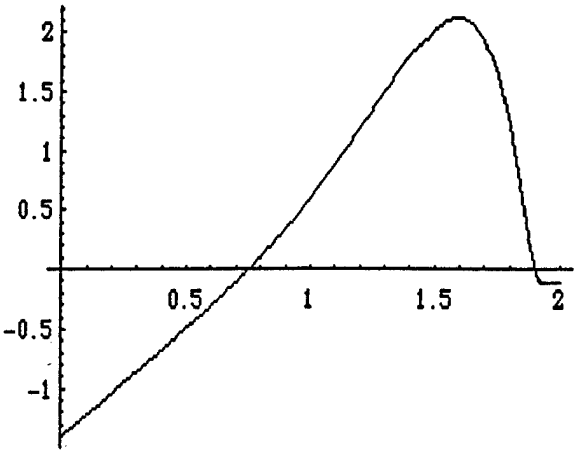

Fig. A-4: $[(\theta^{5/2}\Gamma)_1 / P - \theta_1 - (\gamma - 1)(2 + \gamma\beta^*)\, \omega_1^2 / 2\gamma\beta^*]$ of Eqn. 20 vs normalized distance, b, upstream of sonic point

APPENDIX III

Development of Equation-of-State and Transport Properties for Molecular Plasmas in Pulsed Plasma Thrusters, Part I: A Two-Temperature Equation-of-State for Teflon

IEPC-97-124

DEVELOPMENT OF EQUATION-OF-STATE AND TRANSPORT PROPERTIES FOR MOLECULAR PLASMAS IN PULSED PLASMA THRUSTERS PART I: A TWO-TEMPERATURE EQUATION-OF-STATE FOR TEFLON

C. S. Schmahl and P. J. Turchi
The Ohio State University
Columbus, Ohio
USA

25th International Electric Propulsion Conference
August 24-28, 1997, Cleveland, Ohio

DEVELOPMENT OF EQUATION-OF-STATE AND TRANSPORT PROPERTIES FOR MOLECULAR PLASMAS IN PULSED PLASMA THRUSTERS PART I: A TWO-TEMPERATURE EQUATION OF STATE FOR TEFLON

C. S. Schmahl and P. J. Turchi
The Ohio State University
Columbus, Ohio
USA

ABSTRACT

The chemical composition of tetrafluoroethylene (C_2F_4) is calculated with a two-temperature LTE formulation. Twenty-five chemical species are included in the analysis. The equilibrium constants are calculated using the most recent spectroscopic data available. Calculations are performed for pressures from 0.001 atm to 1.0 atm and for temperature ranges of 0.05 ev to 10 ev for both heavy particle and electron temperatures.

INTRODUCTION

Knowledge of the chemical, thermodynamic, and transport properties of a gas is required in almost any gasdynamic analysis. Accurate thermochemical and transport properties become particularly important in high-temperature applications such as the pulsed plasma thruster. In this paper, we shall concentrate on calculating the equilibrium composition of a gas mixture. This is the necessary first step for determining the thermodynamic and transport properties of a gas.

There are three primary thermochemical states possible for a gas. A calorically perfect gas has specific heats that are constant, and the enthalpy and internal energy are only functions of temperature. A thermally-perfect gas, in which variable vibrational and electronic excitation are taken into account, has specific heats, enthalpy, and internal energy that are all functions of temperature. If the conditions are right for chemical reactions to occur, then we can treat the gas as an equilibrium chemically-reacting gas for which properties area all functions of temperature and pressure. Even this can be generalized by stating that the reacting gas is in local thermodynamic equilibrium (LTE). This means that a local Boltzmann distribution exists at each point in the flow at the local temperature. We will extend this statement further for the case of a two temperature LTE gas modeled here. In this paper we calculate the chemical composition of the gaseous Teflon monomer (C_2F_4).

POSSIBLE SPECIES, REACTIONS, AND EQUILIBRIUM EQUATIONS

In this paper, we calculate the chemical composition of tetrafluoroethylene (C_2F_4). The analysis will include vibrational and electronic excitation, dissociation, first molecular ionization, and first through fourth monatomic ionization. Throughout of the analysis, we shall assume a perfect gas, where intermolecular forces are non-existent or negligible. This might seem a strange assumption when the gas is in the plasma state due to the presence of Coulomb collisions, but it is a widely used and accepted approximation.[1]

For a polyatomic base gas, C_2F_4 in our case, with the possibility of undergoing full dissociation, singular molecular ionization, and up to fourth monatomic ionization, we first assume there are twenty-five possible chemical species, which are C_2F_4, C_2F_2, CF_2, CF_2^+, CF_3, CF_3^+, CF_4, C_2, CF, CF^+, F_2, F_2^+, C^Z (Z=-1,4), F^Z (Z=-1,4), and e^-'s. For a gas containing twenty-five chemical species, which is composed of three elements (C, F, e^-), we are required to have twenty-two (25-3=22) independent chemical reaction equations (laws of mass action). The reactions considered here are

$$CF_2 \rightleftharpoons CF + F \qquad (1)$$

$$CF \rightleftharpoons C + F \qquad (2)$$

$$F_2 \rightleftharpoons 2F \qquad (3)$$

$$CF_2 \rightleftharpoons CF_2^+ + e^- \qquad (4)$$

$$CF \rightleftharpoons CF^+ + e^- \qquad (5)$$

$$C^{Z-1} \rightleftharpoons C^Z + e^- \quad \Big|_{Z=0}^{4} \qquad (6)$$

$$C_2F_4 \rightleftharpoons 2\,CF_2 \qquad (7)$$

$$F_2 \rightleftharpoons F_2^+ + e^- \qquad (8)$$

$$F^{Z-1} \rightleftharpoons F^Z + e^- \quad \Big|_{Z=0}^{4} \qquad (9)$$

$$C_2F_4 \rightleftharpoons C_2F_2 + F_2 \qquad (10)$$

$$C_2F_4 \rightleftharpoons CF_3 + CF \qquad (11)$$

$$C_2F_4 \rightleftharpoons CF_4 + C \qquad (12)$$

$$C_2 \rightleftharpoons 2C \qquad (13)$$

In actuality, there are other possible reactions that could yield the same chemical species. But, for an equilibrium calculation, the reactions chosen are arbitrary as long as they are linearly independent and account for all possible species.

Writing these reactions in terms of equilibrium relations for the partial pressures, we have

$$K_{p,j}(T) = \prod_i p_i^{\nu_i} \qquad (14)$$

where the $K_{p,j}$ are the equilibrium constants for the reaction (j) at the equilibrium temperature T, in terms of the partial pressures. Using the appropriate formulations, they may also be put in terms of concentrations, K_c, or number densities, K_n. It is important to note in the above equations that the equilibrium constants are written as functions of temperature only, as most authors point out. However, they may be functions of two or more state variables depending on whether such things as thermal non-equilibrium assumptions or electronic partition function cutoff is taken into account.[2]

In addition to twelve independent equations relating the twenty-five unknown partial pressures, we need three more equations to solve for the gas composition. The three chosen are; conservation of nuclei, Dalton's Law, and charge neutrality. The ideal thermal gas law for each species is written in the form

$$p_i = n_i k T_i \qquad (15)$$

where

$$p = \sum p_i \qquad (16)$$

For charge neutrality, we have

$$\sum_{i=1}^{25} Z n_{iz} = 0 \qquad (17)$$

In terms of partial pressures, this becomes (for ideal gases)

$$\sum_{i=1}^{25} Z\left(\frac{1}{T_i}\right) p_{iz} = 0 \qquad (18)$$

For conservation of nuclei, we write

$$\left(n_{C_2F_4}\right)_0 = \frac{1}{2}\left(n_C\right)_0 = \frac{1}{4}\left(n_F\right)_0 \qquad (19)$$

where

$$\left(n_C\right)_0 = \sum_{i=1}^{25} N n_{i_{C_N}} \qquad (20)$$

and

$$(n_F)_0 = \sum_{i=1}^{25} N n_{i_{F_N}} \qquad (21)$$

where $(n_{C2F4})_0$ is the total number of tetrafluoroethylene molecules available for dissociation and ionization (ie. the number of C_2F_4 molecules present if the gas was non-reacting at some initially low temperature). Dividing Eq. (20) by Eq. (21) and utilizing Eq. (19) gives us the nuclei conservation statement, where the number densities are related to the partial pressures by Eq. (15).

CALCULATION OF THE EQUILIBRIUM CONSTANT - PARTITION FUNCTIONS

To solve the system of equations, we only need values for the equilibrium constants which may be calculated from equilibrium statistical mechanics. In terms of partition functions Q_i, the law of mass action for a general system is

$$K_N(T) = \prod N_i^{\nu_i} = e^{\frac{-\Delta \varepsilon_0}{kT}} \prod Q_i^{\nu_i} \qquad (22)$$

or alternatively, substituting $n_i = N_i/V$ we have

$$K_n(T) = \prod n_i^{\nu_i} = \left(\frac{1}{V}\right)^{\Sigma \nu_i} e^{\frac{-\Delta \varepsilon_0}{kT}} \prod Q_i^{\nu_i} \qquad (23)$$

where ν_i is the stoichiometric mole number for species (i), that is, the coefficients in the balanced chemical equation, $\Delta\varepsilon_0$ is the reaction energy (change in zero-point energy) and Q_i is the total partition function for species (i). Thus, for a given reaction and thermodynamic state, the only unknowns in Eq. (23) are the Q_i's.

For a system in thermodynamic equilibrium, we have

$$N_j^* = N \frac{g_j e^{-\frac{\varepsilon_j}{kT}}}{\sum g_j e^{-\frac{\varepsilon_j}{kT}}} \qquad (24)$$

which gives the number of particles N_j^* in energy level ε_j with g_j degenerate states. We define the partition function, Q, as the sum in the denominator of Eq. (24) which is, in general, a function of T and

$$Q \equiv \sum g_j e^{-\frac{\varepsilon_j}{kT}} \qquad (25)$$

V. It is typical to express the total energy as the sum of translational and internal energies. Note that Eqs. (23) and (24) contain only one temperature. For the two temperature case considered in this research we make the assumption that the heavy-particle gas composed of neutrals and ions, has a Maxwellian distribution in velocities and a Boltzman distribution in energies at a heavy-particle temperature , T. The electron gas, composed of both free and bound electrons is in equilibrium with an electron temperature T_e defined by their Maxwellian velocity distribution. Note that, in this analysis, we are ignoring the interaction between electronic and vibrational states. Thus, we have defined a two-temperature LTE situation. For a molecule we have

$$\varepsilon = \varepsilon_{trans} + \varepsilon_{rot} + \varepsilon_{vib} + \varepsilon_{el} \qquad (26)$$

and for an atom

$$\varepsilon = \varepsilon_{trans} + \varepsilon_{el} \qquad (27)$$

where ε is the sensible energy, measured above the zero-point energy ε_0. Quantum mechanics gives us theoretical values for the quantized energies of a particle, at least for the translational, rotational, and vibrational modes.[3] Along with the assertion that particle energy is simply the sum of the modal energies, that is, the internal energies are uncoupled, which is a consequence of the more fundamental assumption of a separable Hamiltonian, the partition function is expressed as the product of the modal partitions Q_j, where

$$Q = \prod Q_j \qquad (28)$$

with j extending over all modes. Armed with the quantized values for the modal energies, and the associated degeneracies we can calculate the modal partition functions which are given here in reduced form, without proof as[4]

$$Q_{trans} = \left(\frac{2\pi mkT}{h^2} \right)^{\frac{3}{2}} \times V \qquad (29)$$

$$Q_{rot} = \frac{8\pi^2 IkT}{\sigma h^2} \qquad (30)$$

$$Q_{vib} = \frac{1}{1 - e^{-\frac{h\nu}{kT}}} \qquad (31)$$

where σ is a factor which arises from the symmetry requirements of the wave function in the exchange of an identical particle. It is equal to 1 for heteronuclear molecules (ex. CF), and equal to 2 for homonuclear molecules (ex. F_2). For electronic energy there is no closed form general expression for the quantized energy levels. Thus the electronic partition function must be left as an infinite series in the form

$$Q_{el} = \sum_{j=0}^{\infty} g_j e^{-\frac{\varepsilon_j}{kT}} \qquad (32)$$

Equation (32) is the true theoretical representation of the electronic partition function for an *isolated* particle. In theory there are in infinite number of electronic levels extending from the ground state energy ($\varepsilon_0 = 0$) to the ionization potential, which is the amount of energy needed to remove an electron from its ground state to infinity (bound-free transition). The electronic partition function is a diverging series because although the energy approaches a finite limit, the degeneracy increases as the square of the principal quantum number, so the series diverges.[5] For any general polyatomic molecule of N atoms, if we still assume a separable Hamiltonian then we can factor the partition function as in Eq. (28) with the product extending not only over all fundamental modes but also over all modal degrees of freedom.[6]

In actuality, the electronic series in not infinite because a particle in the real world is never truly isolated. Due to various interparticle interactions that arise in any finite density medium, the series will actually terminate at some principal quantum number, n^{cutoff}. The evaluation of n^{cutoff} and its associated effect of ionization potential lowering is the subject of some controversy and was explored in detail in a previous work.[2] Results from that work give the correct cutoff criterion as

$$n^{cutoff} = \sqrt{\frac{1 - \frac{1}{2}(\alpha_i)^{\frac{1}{2}}}{\tilde{a}}} \times n_p^{-\frac{1}{6}} \qquad (33)$$

where $\tilde{a} = Z_{eff} * e^2/2 * IP$. The lowered ionization potential is given by

$$\overline{IP} = IP\left(1 - \frac{1}{n_{cutoff}^2}\right) \qquad (34)$$

The K_n's are converted to K_p's using the relation

$$K_{p,j}(T) = (k)^{\Sigma\nu_i}\left(\prod_i T_i^{\nu_i}\right) K_{n,j}(T) \qquad (35)$$

The required molecular and atomic data, which are too numerous to give here, are taken from the works of Chase,[7] Moore,[8,9] Rosenstock,[10] Herzberg,[11] Buckely,[12] and Paulino and Squires.[13]

SOLUTION OF THE EQUILIBRIUM EQUATIONS

The equations given in the previous section to calculate the equilibrium composition in terms of partial pressures, given T , T_e and P, provide a closed set of twenty-five coupled nonlinear algebraic equations for which there is no analytic solution and numerical methods must be used. The numerical solution of systems of nonlinear equations is universally very difficult and is a topic of current research. As of yet, there are no appropriate numerical methods for solving coupled nonlinear systems of algebraic equations from arbitrary starting vectors.[14] One of the most commonly used methods and the one used previously for nitrogen research,[2] is the Newton-Raphson method. The Newton-Raphson method usually exhibits excellent convergence qualities when the starting vector (initial guesses for the roots) is near the actual root. For a homonuclear diatomic gas a good initial guess can usually be obtained through Saha-type statistical arguments using

weighted averages due to limited reactive simultaneity. In this case though, since we are dealing with a polyatomic heteronuclear gas, it was initially assumed that we could not get close enough to the root for Newton-Raphson to work properly. Many hybrid techniques have been proposed but most fail when the Jacobian becomes singular, or at stationary point.[15,16] The solution procedure initially chosen for this research is the one proposed by Powell.[17] Powell's technique exhibits almost guaranteed convergence even for poor initial guesses. It also has the ability to correctly handle stationary points. The price of this behavior is that the convergence is linear until very close to the root then it converges quadratically like the standard Newton-Raphson. Thus, the total number of iterations required is greatly increased resulting in much longer runtimes, up to 200 minutes per isobar on a Sun Supersparc . Thus, it was decided that the Newton-Raphson method would be used combined with a raster processing iteration procedure.

Given T, T_e, and P, an initial equilibrium composition is approximated using simple Saha-type arguments assuming totally uncoupled physical process, then partial pressures are backed out using weighted approximations or the initial guess was set equal to the previous converged root at the last temperature and pressure and stepped up in temperature on each isobar in small increments of from 0.1 to 10 K for heavy particle temperatures and 1 K to 100 K for electron temperatures. The completely closed system is solved at each point using the Newton-Raphson procedure, which iterates until the sum of the absolute values of the corrections is less than the chosen tolerance of

$$\frac{\epsilon P}{\left(\frac{T_e}{T} + \frac{T}{T_e}\right)} \qquad (36)$$

where $\epsilon = 10^{-4}$ or until 20,000 iterations are performed. Convergence to the tolerance is usually obtained quickly. An additional convergence check is performed after each completed iteration so that the total isobaric deviation is not allowed to exceed 5%. The correct composition is now known to within desired accuracy. The mixture molecular is was computed using the expression

$$MMG = \sum_{i=1}^{25} X_i MM_i \qquad (37)$$

where X_i is the mole fraction of species i, obtained using

$$X_i \equiv \frac{\eta_i}{\eta} = \frac{n_i}{n_{tot}} \qquad (38)$$

where n_{tot} is, of course, just the total number of particles.

RESULTS AND DISCUSSION

The chemical composition in terms of the mole fractions at 1 atm. and $T_e/T = 1.0$ from 300 to 30,000 K is shown in Fig. 1. We see the same rapid dissociation of C_2F_4 as observed by Paulino and Squires[13] due to the inherent weakness of the carbon double bond in this molecule. The results are consistent with those obtained by Kovitya.[18] Figure 2 shows a better view of the composition in the low temperature region where molecules dominate. In our case we see that at about 800 K C_2F_4 partially dissociates into C_2F_2 and CF_4, almost completely recombines as temperature increases, then dissociates into CF_2. Dissociation of CF_2 begins to at about 4,000 K and is almost completely dissociated by 7,500 K. The primary dissociation products are C and F which reach their maxima at about 7,500 K. Past this temperature ionization begins to occur and singly ionized C and F and electrons dominate the composition. Second ionization begins to occur between 22,500 and 25,000 K. Figures 3 through 8 show representative species compositions of C, C^+, F, F^+, e^- and CF_2 at two different pressures, 1 atm and .1 atm, for the case of thermal nonequilibrium.They are given for four heavy isotherms of .05, .1, 1, and 10 ev. Here we see drastically different behavior due to the highly energetic electrons at their elevated temperature. Dissociation of CF_2 happens rapidly, other molecules exhibited similar behavior. Single and multiple ionization of C and F follows the expected pattern of following the electron temperature, consistent with our original formulation. Figure 7, the electron partial pressure, shows we reach regions where dP_e/dT_e goes to zero. The composition is constant after this for we had assumed that the maximum ionic charge state was four. This suggests that for a correct chemical model at elevated electron temperatures we may need to extend the possible ionic species to a greater charge value. The molecular ionic and electronegative species were found to exist in only

very small amounts at all T_e/T values. In future work it is planned to include multi-phase species in like amorphous carbon. Molecular effects that are being evaluated for inclusion in future models include anharmonic vibrations and internal energy mode coupling. Also research is being performed to develop the complete reactive thermodynamic and transport models.

ACKNOWLEDGMENTS

The support of this work by AFOSR/NA is gratefully appreciated. The authors would also like to thank R.E. Peterkin Jr., USAF Phillips Laboratory, Kirtland AFB, NM for continued hospitality.

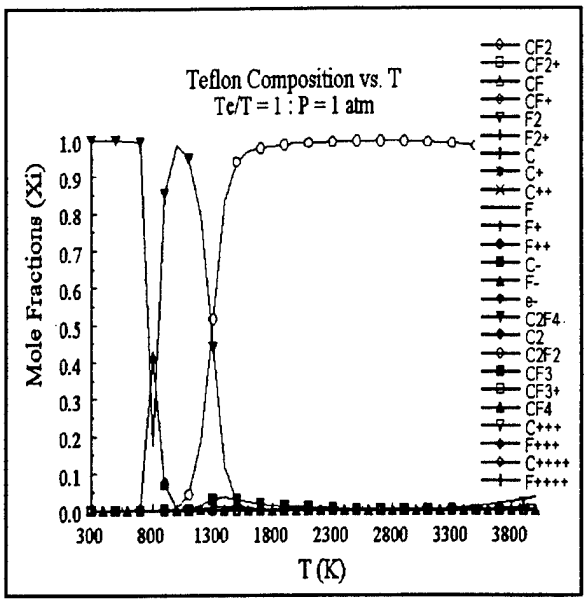

Figure 2. Composition of Teflon for Te/T = 1.0 at 1 atm. Lower temperature range.

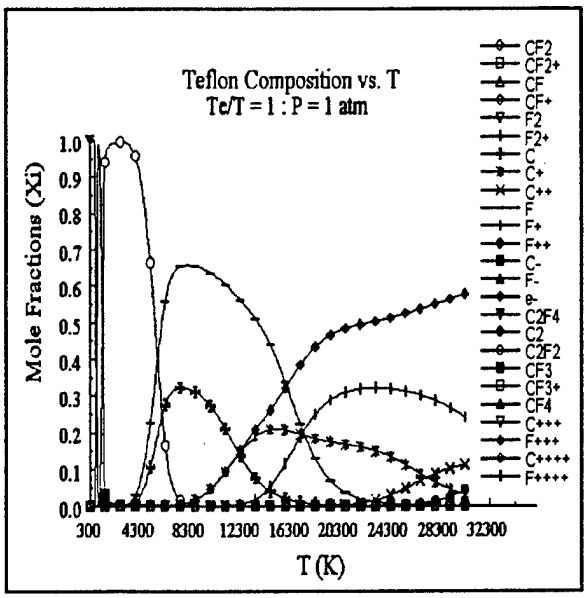

Figure 1. Composition of Teflon for Te/T = 1.0 at 1 atm.

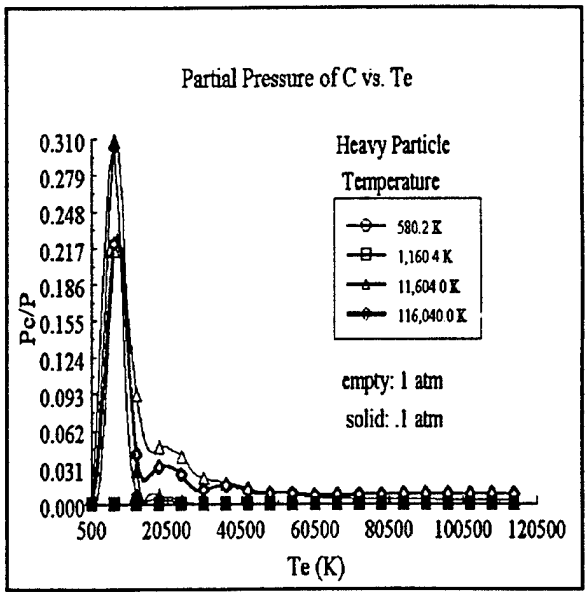

Figure 3. Partial Pressure of C vs. Te.

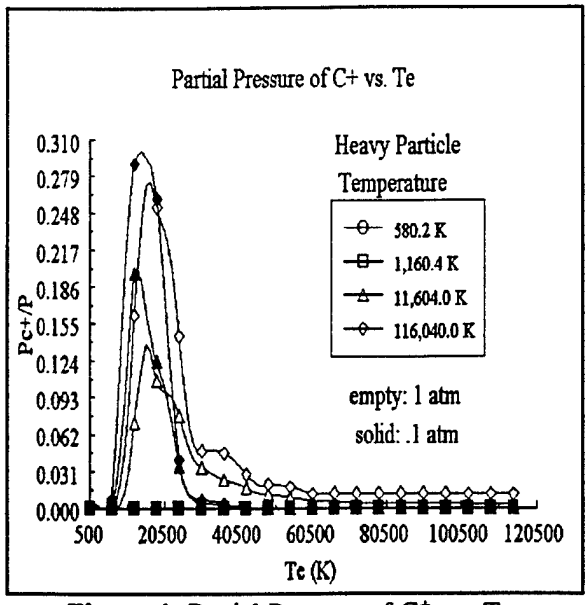

Figure 4. Partial Pressure of C^+ vs. Te.

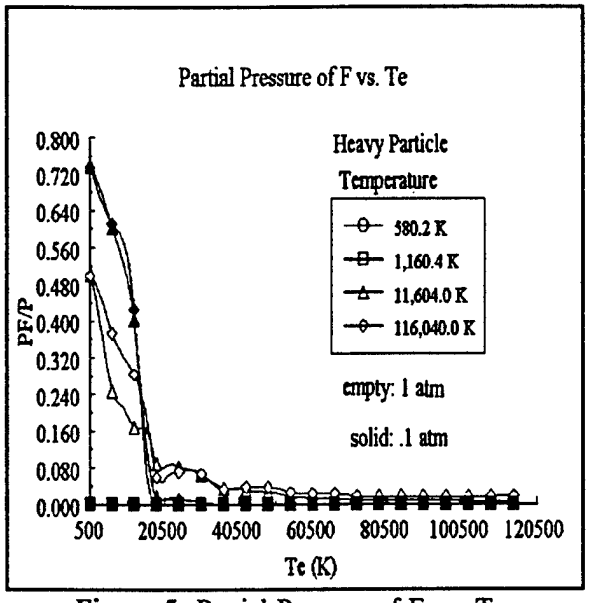

Figure 5. Partial Pressure of F vs. Te.

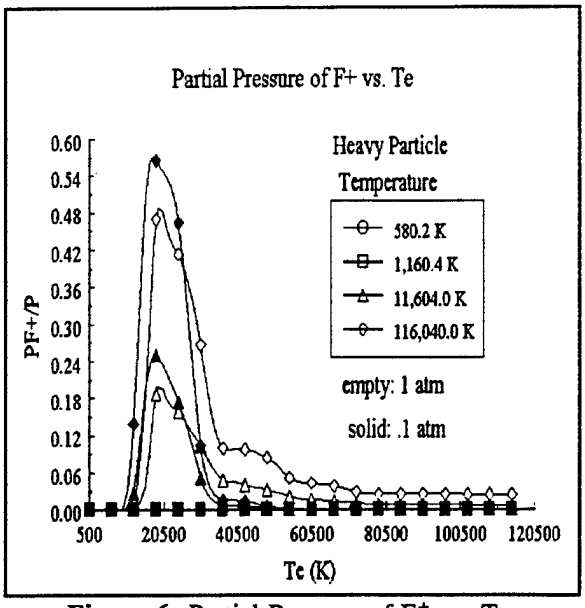

Figure 6. Partial Pressure of F^+ vs. Te.

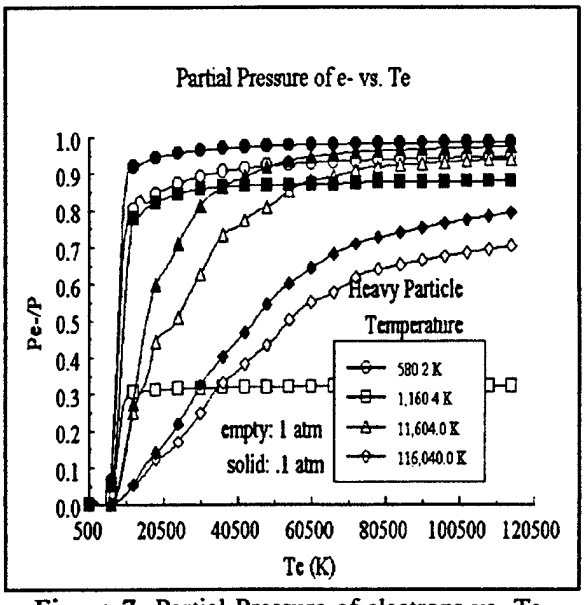

Figure 7. Partial Pressure of electrons vs. Te.

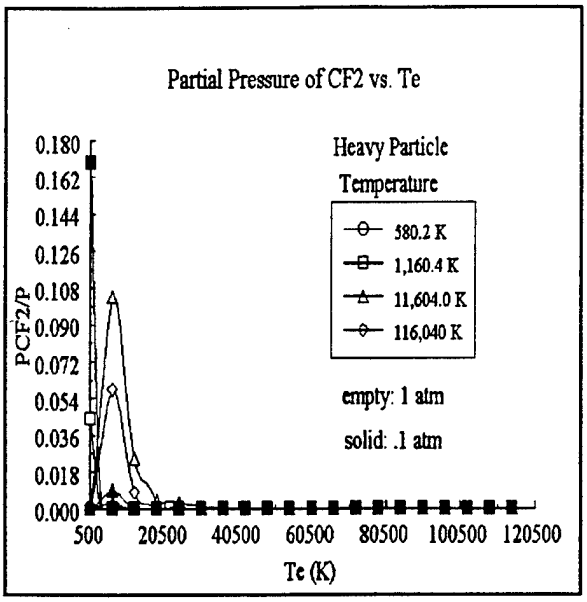

Figure 8. Partial Pressure of CF_2 vs. Te.

REFERENCES

[1]Duclos, D.P., D.P. Aeschliman, A.B. Cambel. 1963. " Approximate Equation for a Perfect Gas Plasma." ARS J.. April: 641-642.

[2]Schmahl, Christopher S. A Computational Study of Shocked Flow Heat Transfer with Improved Equation of State and Transport Properties - A Case Study for Nitrogen. Master's Thesis. The Ohio State University. 1996.

[3]Liboff, Richard L. 1992. Introductory Quantum Mechanics, 2nd ed. Addison-Wessley.

[4]Vincenti, Walter G., Charles H. Kruger Jr. 1965. Introduction to Physical Gas Dynamics. New York: Wiley.

[5]Drellishak, K.S., C.F. Knopp, A.B. Cambel. 1963. " Partition Functions and Thermodynamic Properties of Argon Plasma." Phys. Fluids. 6.6 Sept: 1280-1288.

[6]Mayer, Joseph E., M.G. Mayer. 1977. Statistical Mechanics, 2nd ed. New York: Wiley.

[7]Chase, M.W., et al. 1985. JANAF Thermochemical Tables. 3rd ed. J. Phys. and Chem. Ref. Data. 14.1.

[8]Moore, C.E. 1949. Atomic Energy Levels, v1. NBS Circular 467. Jan 15.

[9]Moore, C.E. 1993. Tables of Spectra of Hydrogen, Carbon, Nitrogen, Oxygen Atoms and Ions. ed. by J. Gallagher. Boca Ratan: CRC Press.

[10]Rosenstock, et al. 1977. Energetics of Gaseous Ions. J. Phys. and Chem. Ref. Data. 6.1

[11]Herzberg, G. 1966. Molecular Spectra and Molecular Structure v. 1. 2nd ed. Krieger: Florida.

[12]Buckely, et al. 1995. " Ionization Energies, Appearance Energies, and Thermochemistry of CF_2O and FCO." J. Phys. Chem. 99, pp 4879-4885.

[13]Paulino, Jose A., Robert R. Squires. 1991. " Carbene Thermochemistry from Collision-Induced Dissociation Threshold Energy Measurements. The Heats of Formation of $X^1A_1CF_2$ and $X^1A_1CCl_2$." J. Am. Chem. Soc. 113, 1573-1580

[14]Press, William H. et al. 1989. Numerical Recipes: The Art of Scientific Computing - FORTRAN version. Cambridge University Press.

[15]Broyden, C.G. " Recent Developments in the Solution of Nonlinear Algebraic Systems." Numerical Methods for Nonlinear Algebraic Equations. ed. by P. Rabinowitz. Ch. 4 pp 61-73. Gordon and Breach: New York.

[16]Powell[a], M.J.D. 1970. " A Hybrid Method for Nonlinear Equations." in Numerical Methods for Nonlinear Algebraic Equations. ed. by P. Rabinowitz. Ch.6. pp 87-114. Gordon and Breach: New York.

[17]Powell[b], M.J.D. 1970. " A FORTRAN Subroutine for Solving Systems of Nonlinear Algebraic Equations." in Numerical Methods for Nonlinear Algebraic Equations. ed. by P. Rabinowitz. Ch.7. pp 115-161. Gordon and Breach: New York.

[18]Kovitya, P. 1984." Thermodynamic and Transport Properties of Ablated Vapors of PTFE, Alumina, Perspex, and PVC in the Temperature Range 5000-30,000 K." IEEE Transactions on Plasma Science. PS-12.1 March: 38-42.

APPENDIX IV

Thermophysical Properties of Nitrogen

Thermophysical Properties of Nitrogen

C. S. Schmahl and P. J. Turchi
The Ohio State University
Columbus, Ohio
USA

ABSTRACT

The equilibrium chemical composition, thermodynamic, and transport properties of nitrogen is calculated over a wide range of thermodynamic state conditions. Six chemical species are included in the analysis. The equilibrium constants are calculated using the most recent spectroscopic data available. Calculations are performed for pressures from 0.001 atm to 1,000.0 atm and for temperature ranges of 300 K to 30,000 K.

INTRODUCTION

Knowledge of the chemical, thermodynamic, and transport properties of a gas is required in almost any gasdynamic analysis. Accurate thermochemical and transport properties become particularly important in high-temperature applications such as the pulsed plasma thruster and other high temperature devices. In this paper, we shall concentrate on calculating the equilibrium composition, thermodynamic, and transport properties of a gas mixture, in this case nitrogen.

There are three primary thermochemical states possible for a gas. A calorically perfect gas has specific heats that are constant, and the enthalpy and internal energy are only functions of temperature. A thermally-perfect gas, in which variable vibrational and electronic excitation are taken into account, has specific heats, enthalpy, and internal energy that are all functions of temperature. If the conditions are right for chemical reactions to occur, then we can treat the gas as an equilibrium chemically-reacting gas for which properties area all functions of temperature and pressure. Even this can be generalized by stating that the reacting gas is in local thermodynamic equilibrium (LTE). This means that a local Boltzmann distribution exists at each point in the flow at the local temperature. Recent research, both in the areas of advanced propulsion and high-temperature gas dynamics has demonstrated the need for accurate data on the chemical, thermodynamic, and transport properties of such reacting gases. In this paper we analyze the thermophysical properties of nitrogen with the inclusion of translational, rotational, vibrational, and electronic excitation.

POSSIBLE SPECIES, REACTIONS, AND EQUILIBRIUM EQUATIONS

In this section, we calculate the chemical composition of nitrogen. The analysis includes vibrational and electronic excitation, dissociation, first molecular ionization, and first through second monatomic ionization. Throughout of the analysis, we assume a perfect gas, where

intermolecular forces are non-existent or negligible. This might seem a strange assumption when the gas is in the plasma state due to the presence of Coulomb collisions, but it is a widely used and accepted approximation.[1]

For a diatomic base gas, N_2 in our case, with the possibility of undergoing full dissociation, singular molecular ionization, and up to second monatomic ionization, we first assume there are six possible chemical species, which are N_2, N_2^+, N^z (z=0,2) , and e^-'s. For a gas containing six chemical species, which is composed of two elements (N, e^-), we are required to have four (6-2=4) independent chemical reaction equations (laws of mass action). The reactions considered here are

$$N_2 + \epsilon_d^{N_2} \rightleftharpoons 2N \tag{1}$$

$$N_2 + \epsilon_i^{N_2} \rightleftharpoons N_2^+ + e^- \tag{2}$$

$$N + \epsilon_i^{N} \rightleftharpoons N^+ + e^- \tag{3}$$

$$N^+ + \epsilon_i^{N^+} \rightleftharpoons N^{++} + e^- \tag{4}$$

In actuality, there are other possible reactions that could yield the same chemical species. But, for an equilibrium calculation, the reactions chosen are arbitrary as long as they are linearly independent and account for all possible species.

Writing these reactions in terms of equilibrium relations for the partial pressures, we have

$$K_{p,j}(T) = \prod_i p_i^{\nu_i} \tag{5}$$

where the $K_{p,j}$ are the equilibrium constants for the reaction (j) at the equilibrium temperature T, in terms of the partial pressures. Using the appropriate formulations, they may also be put in terms of concentrations, K_c, or number densities, K_n.

In addition to four independent equations relating the six unknown partial pressures, we need two more equations to solve for the gas composition. The two chosen are Dalton's Law and charge neutrality. The ideal thermal gas law for each species is written in the form

$$p_i = n_i kT \tag{6}$$

where

$$p = \sum p_i \tag{7}$$

For charge neutrality, we have

$$\sum_{i=1}^{6} Z n_i z = 0 \tag{8}$$

In terms of partial pressures, this becomes (for ideal gases)

$$\sum_{i=1}^{6} Z p_i z = 0 \tag{9}$$

CALCULATION OF THE EQUILIBRIUM CONSTANT - PARTITION FUNCTIONS

To solve the system of equations, we only need values for the equilibrium constants which may be calculated from equilibrium statistical mechanics. In terms of partition functions Q_i, the law of mass action for a general system is

$$K_N(T) = \prod N_i^{\nu_i} = e^{\frac{-\Delta \varepsilon_0}{kT}} \prod Q_i^{\nu_i} \tag{10}$$

or alternatively, substituting $n_i = N_i/V$ we have

$$K_n(T) = \prod n_i^{\nu_i} = \left(\frac{1}{V}\right)^{\Sigma \nu_i} e^{\frac{-\Delta \varepsilon_0}{kT}} \prod Q_i^{\nu_i} \tag{11}$$

where ν_i is the stoichiometric mole number for species (i), that is, the coefficients in the balanced chemical equation, $\Delta\varepsilon_0$ is the reaction energy (change in zero-point energy) and Q_i is the total partition function for species (i). Thus, for a given reaction and thermodynamic state, the only unknowns in Eq. (11) are the Q_i's.

For a system in thermodynamic equilibrium, we have

$$N_j^* = N \frac{g_j e^{-\frac{\varepsilon_j}{kT}}}{\sum g_j e^{-\frac{\varepsilon_j}{kT}}} \tag{12}$$

which gives the number of particles N_j^* in energy level ε_j with g_j degenerate states. We define the partition function, Q, as the sum in the denominator of Eq. (12) which is, in general, a

$$Q \equiv \sum g_j e^{-\frac{\varepsilon_j}{kT}} \tag{13}$$

function of T and V. It is typical to express the total energy as the sum of translational and

internal energies. Note that, in this analysis, we are ignoring the interaction between electronic and vibrational states. Thus, we have defined a one-temperature LTE situation. For a molecule we have

$$\varepsilon = \varepsilon_{trans} + \varepsilon_{rot} + \varepsilon_{vib} + \varepsilon_{el} \tag{14}$$

and for an atom

$$\varepsilon = \varepsilon_{trans} + \varepsilon_{el} \tag{15}$$

where ε is the sensible energy, measured above the zero-point energy ε_0. Quantum mechanics gives us theoretical values for the quantized energies of a particle, at least for the translational, rotational, and vibrational modes.[2] Along with the assumption that particle energy is simply the sum of the modal energies, that is, the internal energies are uncoupled, which is a consequence of the more fundamental assumption of a separable Hamiltonian, the partition function is expressed as the product of the modal partitions Q_j, where

$$Q = \prod Q_j \tag{16}$$

with j extending over all modes. Armed with the quantized values for the modal energies, and the associated degeneracies we can calculate the modal partition functions which are given here in reduced form, without proof as[3]

$$Q_{trans} = \left(\frac{2\pi mkT}{h^2} \right)^{\frac{3}{2}} \times V \tag{17}$$

$$Q_{rot} = \frac{8\pi^2 IkT}{\sigma h^2} \tag{18}$$

$$Q_{vib} = \frac{1}{1 - e^{-\frac{h\nu}{kT}}} \tag{19}$$

where σ is a factor which arises from the symmetry requirements of the wave function in the exchange of an identical particle. It is equal to 1 for heteronuclear molecules (ex. NO), and equal to 2 for homonuclear molecules (ex. N_2). For electronic energy there is no closed form general expression for the quantized energy levels. Thus the electronic partition function must be left as an infinite series in the form

$$Q_{el} = \sum_{j=0}^{\infty} g_j e^{-\frac{\varepsilon_j}{kT}} \tag{20}$$

Eq. (20) is the true theoretical representation of the electronic partition function for an *isolated* particle. In theory there are in infinite number of electronic levels extending from the ground state energy ($\varepsilon_0 = 0$) to the ionization potential, which is the amount of energy needed to remove an electron from its ground state to infinity (bound-free transition). The electronic partition function is a diverging series because although the energy approaches a finite limit, the degeneracy increases as the square of the principal quantum number, so the series diverges.[4,5]

In actuality, the electronic series in not infinite because a particle in the real world is never truly isolated. Due to various interparticle interactions that arise in any finite density medium, the series will actually terminate at some principal quantum number, n^{cutoff}. The evaluation of n^{cutoff} and its associated effect of ionization potential lowering is the subject of some controversy and was explored in detail in a previous work.[6] Results from that work give the correct cutoff criterion as

$$n^{cutoff} = \sqrt{\frac{1 - \frac{1}{2}(\alpha_i)^{\frac{1}{2}}}{\tilde{a}}} \times n_p^{-\frac{1}{6}} \tag{21}$$

where $\tilde{a} = Z_{eff} * e^2/2 * IP$. The lowered ionization potential is given by

$$\overline{IP} = IP\left(1 - \frac{1}{n_{cutoff}^2}\right) \tag{22}$$

The K_n's are converted to K_p's using the relation

$$K_{p,j}(T) = (kT)^{\Sigma \nu_i} K_{n,j}(T) \tag{23}$$

The required molecular and atomic data, which are too numerous to give here, are taken from the works of Herzberg[7] and Moore[8].

SOLUTION OF THE EQUILIBRIUM EQUATIONS

The equations given in the previous section to calculate the equilibrium composition in terms of partial pressures, given T , T_e and P, provide a closed set of six coupled nonlinear algebraic equations for which there is no analytic solution and numerical methods must be used. The numerical solution of systems of nonlinear equations is universally very difficult and is a topic of current research. As of yet, there are no appropriate numerical methods for solving coupled nonlinear systems of algebraic equations from arbitrary starting vectors.[14] One of the most

commonly used methods is the Newton-Raphson method. The Newton-Raphson method usually exhibits excellent convergence qualities when the starting vector (initial guesses for the roots) is near the actual root. For a homonuclear diatomic gas a good initial guess can usually be obtained through Saha-type statistical arguments using weighted averages due to limited reactive simultaneity. Another technique, known as Powell's technique exhibits almost guaranteed convergence even for poor initial guesses.[10] It also has the ability to correctly handle stationary points. The price of this behavior is that the convergence is linear until very close to the root then it converges quadratically like the standard Newton-Raphson. Thus, the total number of iterations required is greatly increased resulting in much longer runtimes. Thus, it was decided that the Newton-Raphson method would be used combined with a raster processing iteration procedure.

Given T and P, an initial equilibrium composition is approximated using simple Saha-type arguments assuming totally uncoupled physical process, then partial pressures are backed out using weighted approximations or the initial guess was set equal to the previous converged root at the last temperature and pressure and stepped up in temperature on each isobar in small increments of from 100 to 300 K for heavy particle temperatures. The completely closed system is solved at each point using the Newton-Raphson procedure, which iterates until the sum of the absolute values of the corrections is less than the chosen tolerance of

$$\psi = \epsilon P \tag{24}$$

where $\epsilon = 10^{-4}$ or until 20,000 iterations are performed. Convergence to the tolerance is usually obtained quickly. An additional convergence check is performed after each completed iteration so that the total isobaric deviation is not allowed to exceed 5%. The correct composition is now known to within desired accuracy. The mixture molecular is was computed using the expression

$$MMG = \sum_{i=1}^{25} X_i MM_i \tag{25}$$

where X_i is the mole fraction of species i, obtained using

$$X_i \equiv \frac{\eta_i}{\eta} = \frac{n_i}{n_{tot}} \tag{26}$$

where n_{tot} is, of course, just the total number of particles.

CALCULATION OF THE THERMODYNAMIC PROPERTIES

For a given temperature and pressure, the complete gas composition can be calculated using the techniques in the previous section. Often, however, it is necessary to have the thermodynamic propertied of the gas. In this research, the calculated thermodynamic properties are specific enthalpy (h), specific internal energy (e), the specific heats (c_p and c_v), and consequently the ratio

of specific heats (γ).

a. Calculation of the specific internal energy (e) and specific enthalpy (h)

On a microscopic scale, a particle (atom or molecule) may possess energy due to its translational, rotational, vibrational, and electronic modes. This is expressed as

$$e_i = e_i^{trans} + e_i^{rot} + e_i^{vib} + e_i^{el} \tag{27}$$

where e is the total specific internal energy. Note that e is actually the total specific sensible internal energy and is measured above the zero point. In terms of partition functions the energy and enthalpy is expressed as[3]

$$e = RT^2\left(\frac{\partial \ln Q}{\partial T}\right)_v \tag{28}$$

$$h = RT + RT^2\left(\frac{\partial \ln Q}{\partial T}\right)_v \tag{29}$$

with the relation

$$h = e + Pv \tag{30}$$

holding for any type of gas, whether calorically perfect, thermally perfect, or chemically reacting. The expressions for the modal partition functions are given in the previous section. Taking the derivatives of the logarithms and using Eq.(28) we get

$$e_i^{trans} = \frac{3}{2}R_iT \tag{31}$$

$$e_i^{rot} = R_iT \tag{32}$$

and

$$e_i^{vib} = \frac{h\nu_i}{kT}\frac{1}{\left(e^{\frac{h\nu_i}{kT}} - 1\right)}R_iT \tag{33}$$

Again, for the electronic energy, the lack of a closed form partition function leaves us with

$$e_i^{el} = R_i T^2 \left(\frac{\partial \ln Q_i^{el}}{\partial T} \right)_v \tag{34}$$

where $R_i = R_{UGC}/MM_i$ is the specific gas constant. The translational and rotational modes are assumed to be fully excited.

For a mixture of N species, the total mixture sensible internal energy is

$$e = \sum_{i=1}^{N} c_i e_i \tag{35}$$

where c_i is the mass fraction of species i, given by

$$c_i = X_i \frac{MM_i}{MMG} = \frac{P_i}{P} \frac{MM_i}{MMG} \tag{36}$$

Similarly, the specific enthalpy for a mixture of N species is given by

$$h = \sum_{i=1}^{N} c_i h_i \tag{37}$$

$$h_i = e_i + R_i T + \left(\Delta h_f \right)_i^0 \tag{38}$$

where again, c_i is the mass fraction and h_i is the specific enthalpy for species i. The internal energy at each required temperature and pressure is calculated using Eqs. (31)-(34) combined with Eqs. (35) and (36).The solution procedure required a previous call to the equilibrium composition subroutine to input the partial pressures and mixture molecular mass. The electronic derivatives appearing in Eqs. (31) through (34) are calculated using a 4^{th}-order four-point Richardson extrapolation with $\Delta T = .01K$. The derivatives are taken with a frozen principal quantum number cutoff. This was done for ease of calculation and to avoid the problem other authors[4,5] experienced with large computational derivatives being obtained if the temperature and pressure state corresponded to a partition function jump due to the addition or subtraction of another electronic level. The specific enthalpy is not computed using Eq.(37) , rather Eq.(30) is used written in the form

$$h = e + Pv = e + \frac{R_{UCG}T}{MMG} \tag{39}$$

because both e and MMG are now known and it is a rather simple, yet completely applicable relation.

b. Computation of Specific Heats

The specific heat at constant pressure is defined as

$$c_p = \left(\frac{\partial h}{\partial T}\right)_p \tag{40}$$

From Eq.(37) we have $h = \Sigma c_i h_i$, putting this into the above we get

$$c_p = \left(\frac{\partial h}{\partial T}\right) = \frac{\partial}{\partial T}\left(\sum c_i h_i\right)_p = \sum c_i \left(\frac{\partial h_i}{\partial T}\right)_p + \sum h_i \left(\frac{\partial c_i}{\partial T}\right)_p \tag{41}$$

The mass fractions are input to the thermodynamic subroutine, thus are known. The $(\partial h_i/\partial T)_p$ for each species is calculated using Eq.(38) together with the appropriate modal energy derivatives from Eqs. (31)-(34). The first and second electronic derivatives were taken using 4-point fourth-order Richardson Extrapolation[11] using T=.01K for h. They were again taken assuming a frozen principal quantum number cutoff through the derivative steps. The absolute specific enthalpy, h_i, for each species is calculated using Eq.(38) , and the energies previously calculated. The composition derivatives $(\partial c_i/\partial T)_p$ are evaluated numerically using Eq.(36). For each of the four terms, a call to the equilibrium composition subroutine is made at the appropriate temperature ($T+\Delta T$, $T+\Delta T/2$, $T-\Delta T/2$, $T-\Delta T$) keeping pressure constant. The step length for the temperature is $\Delta T = .01K$.

The specific heat at constant volume is defined as

$$c_v = \left(\frac{\partial e}{\partial T}\right)_v \tag{42}$$

From Eq.(35) we have $e = \Sigma c_i e_i$, putting this into the above we get

$$c_v = \left(\frac{\partial e}{\partial T}\right)_v = \frac{\partial}{\partial T}\left(\sum c_i e_i\right)_v = \sum c_i \left(\frac{\partial e_i}{\partial T}\right)_v + \sum e_i \left(\frac{\partial c_i}{\partial T}\right)_v \tag{43}$$

thus

$$c_v = \sum c_i \left(\frac{\partial e_i}{\partial T}\right)_v + \sum e_i \left(\frac{\partial c_i}{\partial T}\right)_v \tag{44}$$

Unfortunately, this cannot be easily evaluated for the following reason. The state variables the appear in the specific energy and especially in the calculation of the equilibrium composition are pressure and temperature. A partial derivative can be taken easily with respect to temperature or pressure because we have the ability to directly hold the other constant. But here, we are required to take derivatives with respect to temperature, holding volume v (specific volume) constant. Since pressure and temperature are our chosen state variables, there is no direct way to do this. Authors such as Drellishack[4,5], Peng[12], and Penski[13] use a complex method involving partial derivatives of compressibility, energy, and enthalpy in Jacobian-like form. But since in this research the gas was treated as perfect, or at most weakly imperfect, an easier and more fundamental method of obtaining c_v is found.

The general relation[14]

$$c_p - c_v = \left[\left(\frac{\partial e}{\partial v}\right)_T + P\right]\left(\frac{\partial v}{\partial T}\right)_p \tag{45}$$

is applicable to all gases, weather calorically perfect, thermally perfect, ideal or non-ideal, and even chemically reacting. We want to transform $(\partial e/\partial v)_T$ in to something easier to calculate. If $e=e(v,T)$ and $e=e(P,T)$ then it can be shown that

$$c_v = c_P - P\left[1 - \left(\sum e_i \frac{\partial c_i}{\partial P}\right)_T \left(\frac{1}{MMG}\left(\frac{\partial MMG}{\partial v}\right)_T + \frac{1}{v}\right)\right]\left(\frac{\partial v}{\partial T}\right)_P \tag{46}$$

Which, although looks complicated is actually a much easier method given the present situation of T and P as state variables. c_p is known, as are the e_i's, MMG, and specific volume (from $v = 1/\rho = R_{UGC}*T/P*MMG$) because the composition is already known and the internal energies have already been calculated from the previous section. The composition derivative $(\partial c_i/\partial P)_T$ is evaluated by a 4-point fourth-order Richardson Extrapolation with $\Delta P=.01$ N/m^2 = h. The specific volume derivative $(\partial v_i/\partial T)_P$ is evaluated using the same technique by evaluating the molecular mass at the four Richardson step points variant on T by

$$\left(\frac{\partial v}{\partial T}\right)_P = \frac{R_{UGC}}{P}\frac{\partial}{\partial T}\left(\frac{T}{MMG}\right)_P \tag{47}$$

with $\Delta T = .01K$. The derivative $(\partial MMG_i/\partial v)_T$ requires the use of an iterative technique. First Δv is calculated at each T and P as $\Delta v = .01 * v_1$. Then at each Richardson point, a v^{req} is calculated and a variable P^{iter} is guessed as

$$P^{iter} = P \frac{v_1}{v^{req}} \tag{48}$$

The equilibrium composition subroutine is called using $P=P^{iter}$ and T=T. A new value of v, called v^{calc} is obtained by

$$v^{calc} = \frac{R_{UGC} T}{P^{iter} MMG} \tag{49}$$

If the absolute value of the difference $v^{calc}-v^{req}$ is not less than 10^{-9} and the maximum number of iterations has not been reached (in this case 150), then the pressure is updated to

$$P^{iter} = P^{iter} + \frac{v^{calc} - v^{req}}{v^{calc}} \times \frac{R_{UGC} T}{v^{calc} MMG} \tag{50}$$

and the iteration process continues. Convergence to required accuracy is usually obtained to from within 10-40 iterations. There are some convergence problems at low pressures (P=.001 atm) and high temperatures (T>25,000 K), but that was rare. Once convergence is achieved the calculated molecular mass was set to the appropriate numerical derivative term. The specific heat c_v was then calculated using Eq. (46).

The ratio of specific heats (γ) is then calculated by

$$\gamma \equiv \frac{c_P}{c_v} \tag{51}$$

which is also its definition.

CALCULATION OF THE TRANSPORT COEFFICIENTS

In high-temperature flows, the onset of excited internal energy modes, and especially chemical reactions such as dissociation and ionization, may have a profound effect on the way a gas transports its mass, momentum, and energy. The microscopic molecular transport of mass, momentum, and energy, arising from macroscopic nonequilibrium in composition, flow velocity, and temperature, give rise to the macroscopic phenomena of diffusion, viscosity, and heat conduction, respectively[3]. In this research, the transport coefficients of viscosity (μ) and thermal

conductivity (k) are calculated using the most recent methods and data available. The viscosity and thermal conductivity are calculated including the possibility of molecular dissociation, first atomic ionization, and second atomic ionization. The internal energy modes of translation, rotation, vibration, and electronic excitation are included when possible and applicable. Knowledge of the unique equilibrium chemical composition and of the equilibrium thermodynamic properties are required for the calculation of the transport coefficients and are obtained from methods described in the previous sections.

A diatomic base gas, in this case N_2, with the inclusion of possible dissociation, molecular first ionization, first atomic ionization, and second atomic ionization gives six possible chemical species, namely N_2, N_2^+, N, N^+, N^{++}, and e^-. These species give rise to twenty-one possible independent binary interactions, which in this case are illustrated as x's and o's in table 1. Due to the lack of available collision cross section data, and due to the complexity of a large multicomponent gas transport calculation, some binary interactions and chemical species exclusions are made. All interactions involving the molecular ion (N_{2+}) are ignored. This reduces the system to a five component transport model. The exclusion of N_2^+ is based on the fact that it is at all times a minor species and has negligible effects on the transport properties. The low concentration is evident from the previous equilibrium composition calculations. Peng[12] and Penski[13] made the same assumption. Capitelli and Devoto[15] made a similar assertion but not the same assumption, and instead used crude estimated instead of absolute exclusions. Also, the interactions involving N_2-N^+, N_2-N^{++}, and N-N^{++} were ignored because of the low probability that any of these species will co-exist to any significant degree, as evident from the composition calculations. Similar assumptions are made in the works of Peng,[13] Penski,[14] and Capitelli.[15] These assumptions now leave us with the twelve possible binary interactions

	N_2	N_2^+	N	N^+	N^{++}	e^-
N_2	o	x	o	x	x	o
N_2^+		x	x	x	x	x
N			o	o	x	o
N^+				o	o	o
N^{++}					o	o
e^-						o

Table 1. Nitrogen interaction model.

for the transport calculations, as indicated by an o in table 1. Although the e^--N_2 interaction is a minor interaction, it is included because data was available.

a. Calculation of the Viscosity

The exact kinetic representation for the viscosity of a multicomponent gas is given by Hirshfelder[16] as

$$\mu = \frac{\begin{vmatrix} H_{ij} & X_i \\ \hline X_j & 0 \end{vmatrix}}{|H_{ij}|} \tag{52}$$

where

$$H_{ii} = \frac{X_i^2}{\mu_{ii}} + \sum_{\substack{k=1 \\ k \neq i}}^{n} \frac{2X_i X_k}{\mu_{ik}} \frac{MM_i MM_k}{(MM_i + MM_k)^2} \left[\frac{5}{3A_{i,k}^*} + \frac{MM_k}{MM_i} \right] \tag{53}$$

and

$$(H_{ij})_{i \neq j} = -\frac{2X_i X_j}{\mu_{ij}} \frac{MM_i MM_j}{(MM_i + MM_j)^2} \left[\frac{5}{3A_{i,j}^*} - 1 \right] \tag{54}$$

In the above formulas μ_{ii} is the viscosity of a pure substance, given by

$$\mu_{ii} = C \frac{\sqrt{MM_i T}}{\sigma_{ii}^2 \Omega_{ii}^{(2,2)^*}} \tag{55}$$

and μ_{ij} is the binary gas viscosity, given by

$$\mu_{ij} = C \sqrt{\frac{2MM_i MM_j T}{(MM_i + MM_j)}} \frac{1}{\sigma_{ij}^2 \Omega_{ij}^{(2,2)^*}} \tag{56}$$

Also, in the above formulas, X_i's are the mole fractions given by Eq.(26), MM_i are the molecular masses, and A_{ij}^* is the dimensionless ratio of collision integrals, expressed as

$$A_{ij}^* = \frac{\Omega_{ij}^{(2,2)^*}}{\Omega_{ij}^{(1,1)^*}} \tag{57}$$

The $\Omega_{ij}^{(l,s)^*}$'s are the dimensionless collision integrals

$$\Omega_{ij}^{(l,s)^*} = \frac{\left[\Omega^{(l,s)}\right]}{\left[\Omega^{(l,s)}\right]_{rig.sph}} \tag{58}$$

where (l,s) = (1,1) corresponds to the diffusion integral and (l,s) = (2,2) corresponds to the viscosity and thermal conductivity integral. They have the physical significance of being the deviation of any particular model from an idealized hard sphere model. The σ_{ij}'s are the collision diameter. And C is a constant equal to 8.4422×10^{-25} when working in MKS units. The only difference between the averaged collision (transport) cross section and the $\sigma^2\Omega^{(l,s)^*}$ is a numerical constant equal to π ($\sigma^2\Omega^{(l,s)^*} = Q/\pi$).[16,17]

Calculating the viscosity using Eq.(52) is still rather complicated and has proven to be unnecessary.[18] Instead, Eq.(52) can be replaced by its equivalent infinite series representation, which is[19]

$$\mu = \sum_{i=1}^{n} \frac{X_i^2}{H_{ii}} - \sum_{i=1}^{n} \sum_{\substack{j=1 \\ j \neq i}} \frac{X_i X_j H_{ij}}{H_{ii} H_{jj}} + \ldots - \ldots \tag{59}$$

Armaly and Sutton[19] have shown that the diagonal elements of matrix H_{ij} are much larger than the off diagonal elements, so much so, that the off diagonal elements of H_{ij} can be neglected. This leaves the much simpler expression for the multicomponent viscosity as

$$\mu = \sum_{i=1}^{n} \frac{X_i^2}{H_{ii}} \tag{60}$$

This is modified by canceling an X_i, such that

$$\mu = \sum_{i=1}^{n} \frac{X_i}{H_{ii}^*} \tag{61}$$

where

$$H_{ii}^* = \frac{X_i}{\mu_{ii}} + \sum_{\substack{k=1 \\ k \neq i}}^{n} \frac{2X_k}{\mu_{ik}} \frac{MM_i MM_k}{(MM_i + MM_k)^2} \left[\frac{5}{3A_{i,k}^*} + \frac{MM_k}{MM_i} \right] \tag{62}$$

Although the previous simplification seems trivial, it as actually quit computationally valuable. Canceling out the X_i from each term leaves H_{ii}^*'s second term, the summation, not dependant on X_i. This helps reduce the number of 0/0 composition possibilities in a general purpose

computational calculation.

The multicomponent viscosity of the gas is then calculated using Eqs. (61) and (62). The composition is assumed to be known. The data for the collision integrals is sparse, but every attempt was made to find the most recent $\sigma^2\Omega^{(1,1)^*}$ and $\sigma^2\Omega^{(2,2)^*}$ for every reaction. When one or the other was unavailable approximations had to be made. Armally and Sutton[19,20], Flori and Biolsi[21], and Freeman and Oliver,[22] have all shown that the ratio A_{ij}^* is only a rather weak function of temperature. Its magnitude is essentially governed by the general type of interacting particles. Armally[19] gives the general guidelines that $A_{ij}^*=1.25$ for all interactions with the exception of atom interactions with its own ion. In that case the following values are recommended: $A_{ij}^*=0.18$ for $H\text{-}H^+$, $A_{ij}^*=0.025$ for $He\text{-}He^+$, $A_{ij}^*=1.10$ for $C\text{-}C^+$, and for all other homonuclear atom-atomic ion interactions the value of A_{ij}^* for $C\text{-}C^+$ should be used. Freeman and Oliver[22] have also shown that although A_{ij}^* is a relatively weak function of temperature, its temperature dependance increases the greater the pressure. Thus, because of the pressure range used on this research, the assumption of constant A_{ij}^* was only used when absolutely necessary, in this case to get $\sigma^2\Omega^{(2,2)^*}$ for the $e^-\text{-}N$ interaction and $\sigma^2\Omega^{(2,2)^*}$ for the $e^-\text{-}N_2$ interaction. An interesting point is that if A_{ij}^* is set equal to 5/3 in all expressions, then what's left is the mixture rule proposed by Wilke. Wilke's viscosity mixture rule has been proven to fail drastically for any significant degree of ionization.[13,19,23] This happens for the apparent reason that A_{ij}^* is never close to the value 5/3 for ion-ion ar atom-ion interactions. The calculation of the interactions with charged particles were made using the screened coulomb potential.[24] The debye length is taken as the characteristic dimension for coulomb transport ($\sigma^2\Omega^{(l,s)^*} = \lambda_D^2\Omega^{(l,s)^*}$) which in this research is calculated as[25]

$$\lambda_D = \left(\frac{\epsilon_0 kT}{n_{e^-} e^2}\right)^{\frac{1}{2}} \tag{63}$$

in MKS units. The coulomb cross sections were calculated only if the degree of ionization was greater than 10^{-8}. If not, the cross sections were set equal to a constant $10^{-20}m^2$. This reduced the effect of having large, physically incorrect values of λ_D at low degrees of ionization. Although calculations were done at rather extreme temperature and pressure conditions, quantum effects on the cross sections were ignored.[24,26] The interpolated values of the collision integrals at all required points are obtained using a cubic-spline interpolation technique. The calculations for both the viscosity and the collision integral interpolation procedure are done in Fortran.

b. Calculation of the Thermal Conductivity

The thermal conductivity (k) for the reacting mixture is the sum of three components, which are translational, internal, and reactive. The basic translational relation for the thermal conductivity is the familiar Euken's relation

$$k^{trans} = \frac{5}{2}\mu c_v^{trans} \tag{64}$$

Anderson[2] and Vincentti & Kruger[3] give a modified Euken relation to take into account internal

energy modes by stating that, in general,

$$k = k^{trans} + k^{internal} \tag{65}$$

where

$$k^{internal} = \mu c_v^{internal} = \mu\left(c_v^{rot} + c_v^{vib} + c_v^{el}\right) \tag{66}$$

thus

$$k = \mu\left(\frac{5}{2}c_v^{trans} + c_v^{rot} + c_v^{vib} + c_v^{el}\right) \tag{67}$$

Also, for a chemically reacting gas , there is additional energy transport due to diffusion, thus giving as additional component to the thermal conductivity, called the reactive thermal conductivity (k_r). Since the gas under consideration is homonuclear with limited reaction simultaneity, the reactive component of the thermal conductivity is expressed as[12,27]

$$k_r = \sum_{p=1}^{\substack{no.of\\ reactions}} \frac{R\left(T\dfrac{\partial \ln K_p}{\partial T}\right)^2}{\sum_{i=1}^{\nu}\sum_{j=1}^{\nu}\dfrac{RT}{PD_{ij}}\dfrac{\nu_i}{X_i}\left(\nu_i X_j - \nu_j X_i\right)} \tag{68}$$

where D_{ij} is the binary diffusion coefficient given by[12]

$$D_{ij} = 8.4144\times10^{-24}\frac{T^{\frac{3}{2}}}{\sigma_{ij}^2\,\Omega_{ij}^{(1,1)^*}\,P}\sqrt{\frac{MM_i + MM_j}{2MM_iMM_j}} \tag{69}$$

Thus the governing equation for the thermal conductivity is now

$$k = \mu\left(\frac{5}{2}c_v^{trans} + c_v^{rot} + c_v^{vib} + c_v^{el}\right) + k_r \tag{70}$$

where k_r is given by Eq.(68).

For a practical evaluation of k, Eq.(70) needs to be modified further. Recall from Section 2 that c_v is a rather tricky quantity to get. The calculation of c_v is not accomplished through modal contributions (c_v^{trans}, c_v^{rot}, etc.), but instead calculated as a whole from chemical thermodynamic

relations and knowledge of c_p using Eq.(46). Thus, there is no general was of obtaining the specific modal contributions and Eq. (70) must be modified as to use the total c_v. From Eq.(64), we have

$$c_v^{trans} = \frac{2}{5}\frac{k^{trans}}{\mu} \tag{71}$$

the total c_v is

$$c_v = c_v^{trans} + c_v^{rot} + c_v^{vib} + c_v^{el} = c_v^{trans} + c_v^{internal} \tag{72}$$

now, re-arranging the above equation and putting this into Eq.(70) we have

$$k = \mu\left(\frac{5}{2}c_v^{trans} + c_v - c_v^{trans}\right) + k_r = \mu\left(c_v + \frac{3}{2}c_v^{trans}\right) + k_r \tag{73}$$

Upon simplification of Eq.(73) and using Eq.(64) again we are left with

$$k = \frac{3}{5}k^{trans} + \mu c_v + k_r \tag{74}$$

where c_v is now the total gas c_v. The middle quantity is an equivalent internal thermal conductivity. And k_r is given by Eq.(68).

The translational component of the thermal conductivity, k^{trans}, appearing in Eq.(74) is obtained from kinetic theory. The translational component of the multicomponent thermal conductivity can be expressed as[20,16,21]

$$k^{trans} = \frac{\begin{vmatrix} L_{ij} & X_i \\ X_j & 0 \end{vmatrix}}{|L_{ij}|} \tag{75}$$

where

$$L_{ii} = -4\frac{X_i^2}{k_{ii}^{trans}} - \sum_{\substack{k=1 \\ k\neq i}}^{n} \frac{2X_iX_k}{k_{ik}^{trans}\left(MM_i + MM_k\right)^2 A_{ik}^*}\left[\frac{15}{2}MM_i^2 + \frac{5}{2}MM_k^2 + 4MM_iMM_kA_{ik}^*\right] \tag{76}$$

and

$$L_{ij} = \frac{2 X_i X_j MM_i MM_j \left(10 - 4A_{ij}^*\right)}{\left(MM_i + MM_j\right)^2 k_{ij}^{trans} A_{ij}^*} \tag{77}$$

where X_i is the mole fraction of the i^{th} component, A_{ij}^* is the dimensionless ration of collision integrals given by Eq.(57), k_{ii}^{trans} is the thermal conductivity of a pure gas, and k_{ij}^{trans} is the thermal conductivity of a binary gas. The pure gas thermal conductivity is given as

$$k_{ii}^{trans} = C \sqrt{\frac{T}{MM_i}} \frac{1}{\sigma_{ii}^2 \Omega_{ii}^{(2,2)^*}} \tag{78}$$

and the binary gas thermal conductivity ,k_{ij}, is given by

$$k_{ij}^{trans} = C \sqrt{\frac{T\left(MM_i + MM_j\right)}{2 MM_i MM_j}} \frac{1}{\sigma_{ij}^2 \Omega_{ij}^{(2,2)^*}} \tag{79}$$

where C is a constant equal to 2.6335×10^{-23} on MKS units. The $\Omega_{ij}^{(2,2)^*}$ are the dimensionless viscosity and thermal conductivity integrals. And σ_{ij} is the collision diameter. The usage, theory, and equivalence to the familiar cross sections were explained in the previous section.

As with the viscosity calculation (refer so Sect. 2) the expression for k^{tr} given by Eq.(75) is simplified by first expanding it in its series representation as[20]

$$k^{trans} = -4 \sum_{i=1}^{n} \frac{X_i^2}{L_{ii}} + 4 \sum_{i=1}^{n} \sum_{\substack{j=1 \\ j \neq i}} \frac{X_i X_j L_{ij}}{L_{ii} L_{jj}} + \ldots - \ldots \tag{80}$$

where is has been shown that the off diagonal elements L_{ij} are much smaller than the diagonal elements. Thus a very good approximation for the multicomponent translational thermal conductivity is

$$k^{trans} = -4 \sum_{i=1}^{n} \frac{X_i^2}{L_{ii}} \tag{81}$$

and, upon reducing Eq.(81) for the same reason as done with viscosity, we are left with

$$k^{trans} = -4\sum_{i=1}^{n} \frac{X_i}{L_{ii}^*} \tag{82}$$

where

$$L_{ii}^* = -4\frac{X_i}{k_{ii}^{trans}} - \sum_{\substack{k=1 \\ k\neq i}}^{n} \frac{2X_k}{k_{ik}^{trans}(MM_i + MM_k)^2 A_{ik}^*}\left[\frac{15}{2}MM_i^2 + \frac{5}{2}MM_k^2 + 4MM_iMM_kA_{ik}^*\right] \tag{83}$$

The multicomponent total thermal conductivity is then calculated using Eq.s(), (), and (). The viscosity (μ), the specific heat at constant volume (c_v), the equilibrium composition, and the collision integral data are assumed known (calculated previously).

RESULTS AND DISCUSSION

The electronic partition function and the cutoff principal quantum numbers for atomic nitrogen are shown in Figs. 1 and 2, respectively. Here we see that due to the cutoff criterion of the electronic partition function, a function which is dependant on both density and degree of ionization, the electronic partition function is now a function of two state variables, namely pressure and temperature. The cutoff principal quantum number and the partition function both increase with increasing temperature and decrease with increasing pressure. This general behavior is present for all other species, which due to brevity are not shown. The degree of ionization, shown in Fig. 3 illustrates that increasing pressure retards ionization. This trend is also observed for the degree of dissociation pictured in Fig. 4. The total mixture thermal conductivity is displayed in Fig. 5. We see that highly non-monotonic variation occur in reactive regions where the reactive component of the thermal conductivity dominates. Beyond the dissociation region, although there is some contribution due to ionization reactions, the translational component dominates. The mixture viscosity, pictured in Fig. 6, shows that the viscosity increases with temperature, independent of pressure, until reaction occur in the gas. The changes that arise in the presence of chemical reactions are due to changes in the mixture molecular mass or in the average collision cross sections. The large increases that result in the maxima are due to the dissociation of N_2. The decrease that follow these maxima are due to the increasing amount of ionization in the mixture. This is caused by the charged particle interactions which have large coulomb cross sections. The specific heats, given in Figs. 7 and 8, are strong functions of temperature, especially at low pressures where the composition changes generally happen more rapidly and the dc_i/dT terms dominate. The ratio of specific heats is shown in Fig. 9. It starts at low temperatures at the expected value of 1.4 (for a diatomic gas with translation and rotation excited). As the temperature increases we observe a non-pressure-sensitive rise due to increasing vibration excitation. As chemical reaction occur, large non-monotonic variations occur for the same reasons explained earlier for the specific heats. Figures 10 and 11 show that the enthalpy and internal energy both increase with temperature and increase and pressure decreases in reactive regions primarily due to the changes in molecular mass. Figure 12 clearly indicates that

the Prandtl number is nowhere near constant, especially at high temperatures, as some frequently assume (with as assumed constant value of 0.75). There is a massive decrease with dissociation that can cause it to vary by a factor of almost ten.

ACKNOWLEDGMENTS

The support of this work by AFOSR/NA is gratefully appreciated. The authors would also like to thank R.E. Peterkin Jr., USAF Phillips Laboratory, Kirtland AFB, NM for continued hospitality.

REFERENCES

[2]Anderson, John D. Jr. 1989. Hypersonic and High-Temperature Gas Dynamics. Mcgraw-Hill.

[14]Anderson, John D. Jr. 1990. Modern Compressible Flow. Mcgraw-Hill.

[19]Armaly, B. F., K. Sutton. 1980. "Viscosity of Multicomponent Partially Ionized Gas Mixtures Associated with Jovian Entry." AIAA 80-1495.

[20]Armaly, B. F., K. Sutton. 1981. "Thermal Conductivity of Partially Ionized Gas Mixtures." AIAA 81-1174.

[11]Atkinson, L. V., P. J. Harley, J. D. Hudson. 1989. Numerical Methods with FORTRAN 77: A Practical Introduction. Addison-Wesley.

[23]Blake, Lynn H. 1970. "Approximate Transport Calculations for High-Temperature Air." AIAA J. 8.9: 1698-1700.

[27]Butler, James N., Richard S. Brokaw. 1957. "Thermal Conductivity of Gas Mixtures in Chemical Equilibrium." J. Chem. Physics. 26.4 June: 1636-1643.

[15]Capitelli, M., R. S. Devoto. 1973. "Transport Coefficients of High-Temperature Nitrogen." Phys. Fluids. 16.11 Nov: 1835-1841.

[25]Chen, Francis F. 1984. Introduction to Plasma Physics and Controlled Fusion v1: Plasma Physics. Plenum Press.

[17]Devoto, R. S. 1973. "Transport Coefficients of Ionized Argon." Phys. Fluids. 16.5 May: 616-623.

[5]Drellishak, K. S., D. P. Aeschliman, A. B. Cambel. 1963. "Partition Functions and Thermodynamic Properties of Nitrogen and Oxygen Plasmas." Phys. Fluids. 8.9 Sept: 1590-1600.

[4]Drellishak, K. S., C. F. Knopp, A. B. Cambel. 1963. "Partition Functions and Thermodynamic Properties of Argon Plasma." Phys. Fluids. 6.6 Sept: 1280-1288.

[1]Duclos, D. P., D. P. Aeschliman, A. B. Cambel. 1963. "Approximate Equation for a Perfect Gas Plasma." ARS. J. April: 641-642.

[21]Flori, Beverly, Luis Biolsi. 1981. "Transport Properties Associated with Entry into the Atmosphere of Titan." AIAA 81-0278.

[22]Freeman, G. N., C. C. Oliver. 1970. "High-Temperature Thermodynamic and Transport Properties of Planetary CO_2-N_2 Atmospheres. AIAA J. 8.9 Sept: 1687-1693.

[26]Hahn, H. S., E. A. Mason, F. Smith. 1971. "Quantum Transport Cross Sections for Ionized Gases." Phys. Fluids. 14.2 Feb: 278-287.

[7]Herzberg, Gerhard. 1961. Molecular Spectra and Molecular Structure, 2nd ed. New York: Von Nostrand.

[16]Hirschfelder, Joseph O. 1964. Molecular Theory of Gases and Liquids, 2nd ed. New York: Wiley.

[24]Mason, E. A., R. J. Munn, J. Smith. 1967. "Transport Coefficients of Ionized Gases." Phys. Fluids. 10.9 Aug: 1827-1832.

[8]Moore, Charlotte E. 1993. Tables of Spectra of Hydrogen, Carbon, Nitrogen, Oxygen Atoms and Ions. Edited by Jean W. Gallager. Boca Raton: CRC Press.

[12]Peng, T. C., A. L. Pindroh. 1962. Improved Calculation of Gas Properties at High Temperatures. The Boeing Company, Aerospace Division, Flight Technology Department. Report No. D2-11722.

[13]Penski, K. (appx. 1967). "Theoretical Calculation of Transport Properties in Nitrogen Equilibrium Plasma." (unidentified journal) 189-202.

[9]Press, William H. et al. 1989. Numerical Recipes: The Art of Scientific Computing - FORTRAN Version. Cambridge U. Press.

[18]Saxena, S. C., A. Tanzman. 1974. "A Note on the Calculation of Viscosity for Multicomponenet Gas Mixtures." High Temperature Science. 6: 215-220.

[3]Vincenti, Walter G., Charles H. Kruger Jr. 1965. Introduction to Physical Gas Dynamics. New York: Wiley.

[6]Schmahl, Christopher S. 1996. A Computational Study of Shocked Flow Heat Transfer with Improved Equation of State and Transport Properties - A Case Study for Nitrogen. Master's Thesis. The Ohio State University.

[10]Powell, M.J.D. 1970. " A Hybrid Method for Nonlinear Algebraic Systems." in Numerical Methods for Nonlinear Equations. ed. by P. Rabinowitz. Ch. 4. pp 61-73. Gordon and Breach: New York

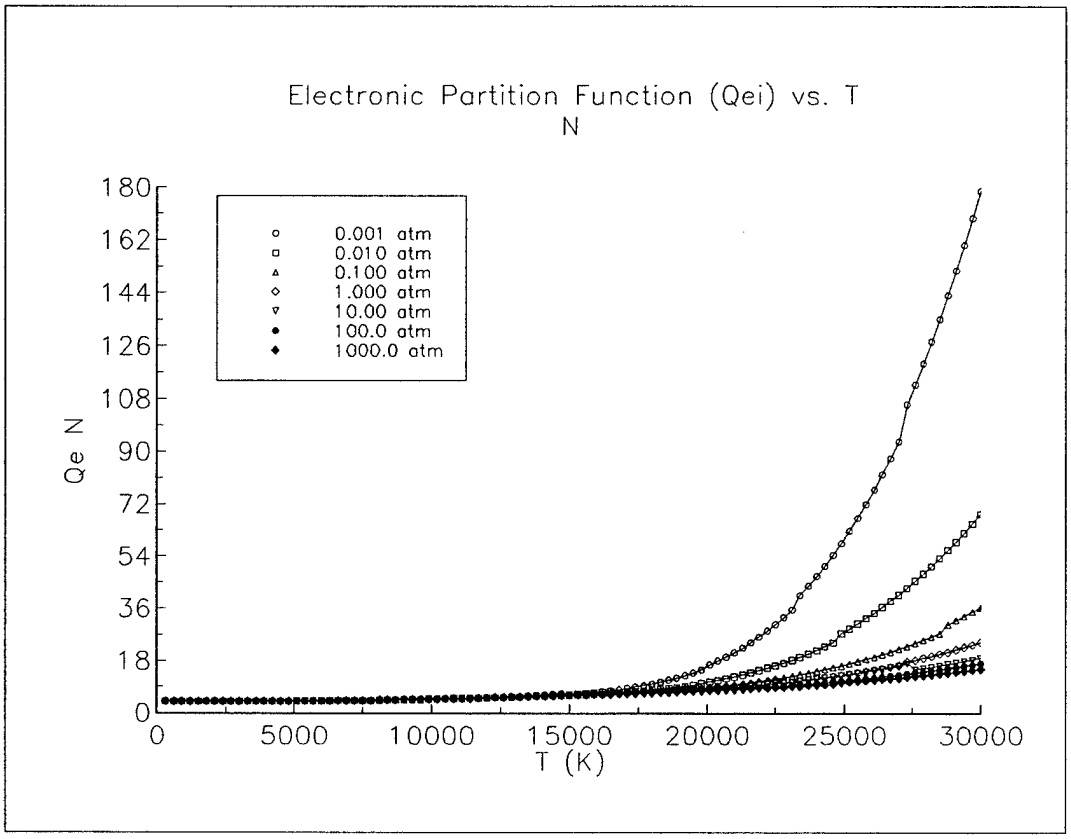

Figure 1. Electronic partition function of N.

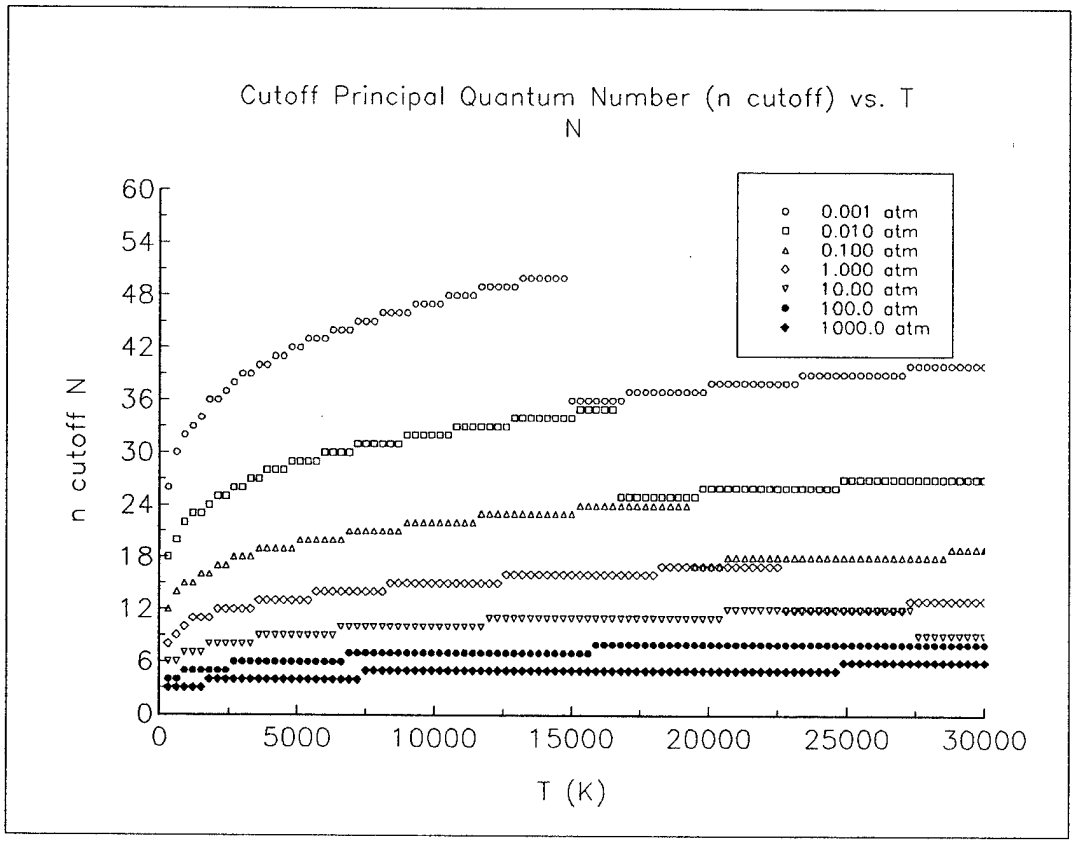

Figure 2. Cutoff principal quantum numbers for N.

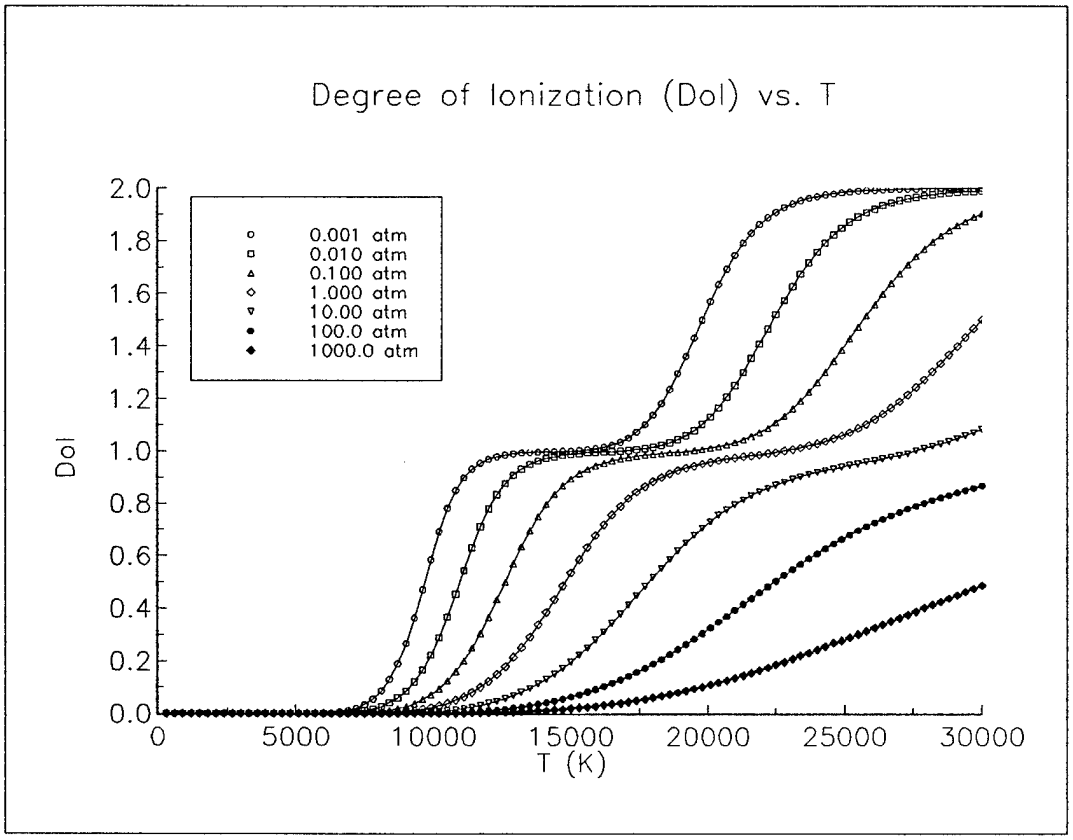

Figure 3. Degree of ionization vs. temperature.

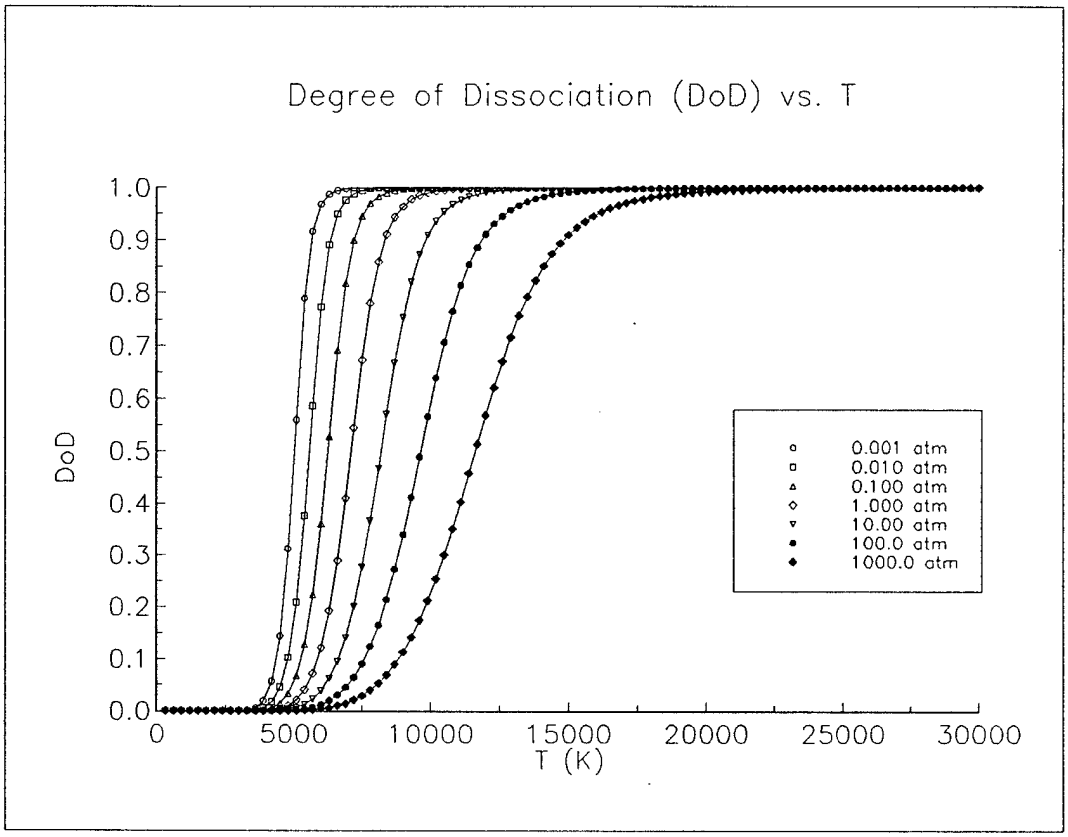

Figure 4. Degree of dissociation vs. temperature.

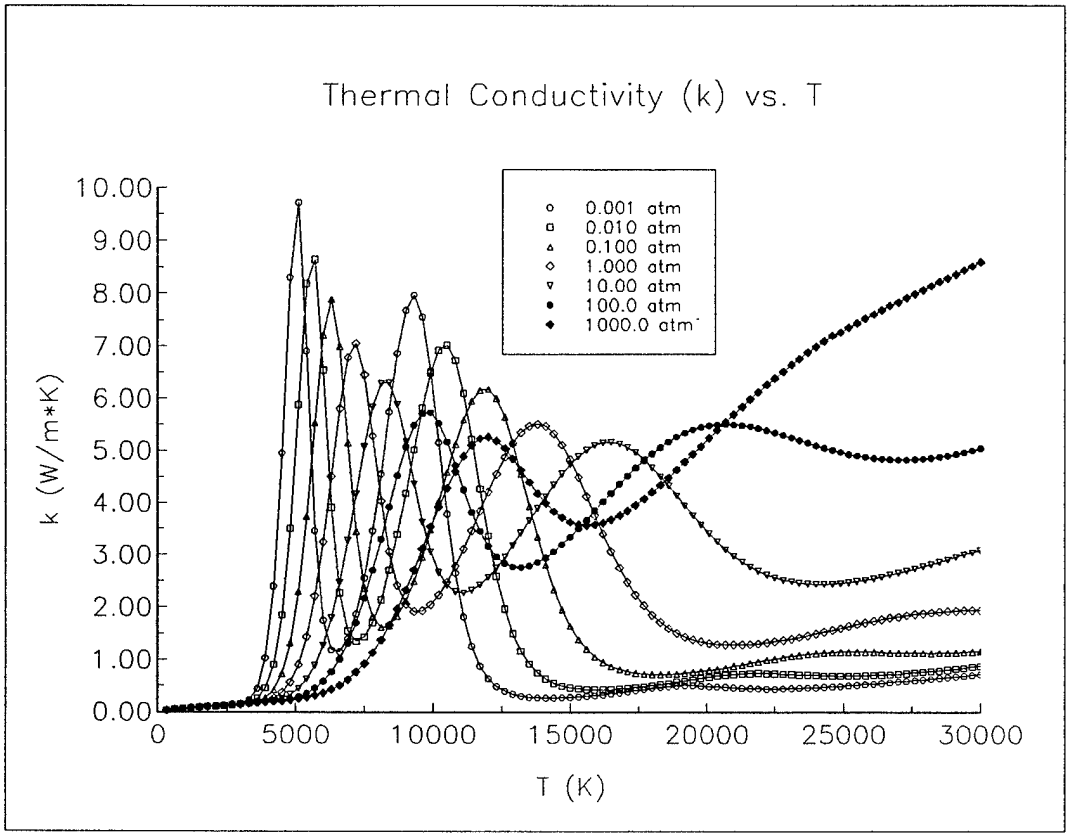

Figure 5. Total mixture thermal conductivity.

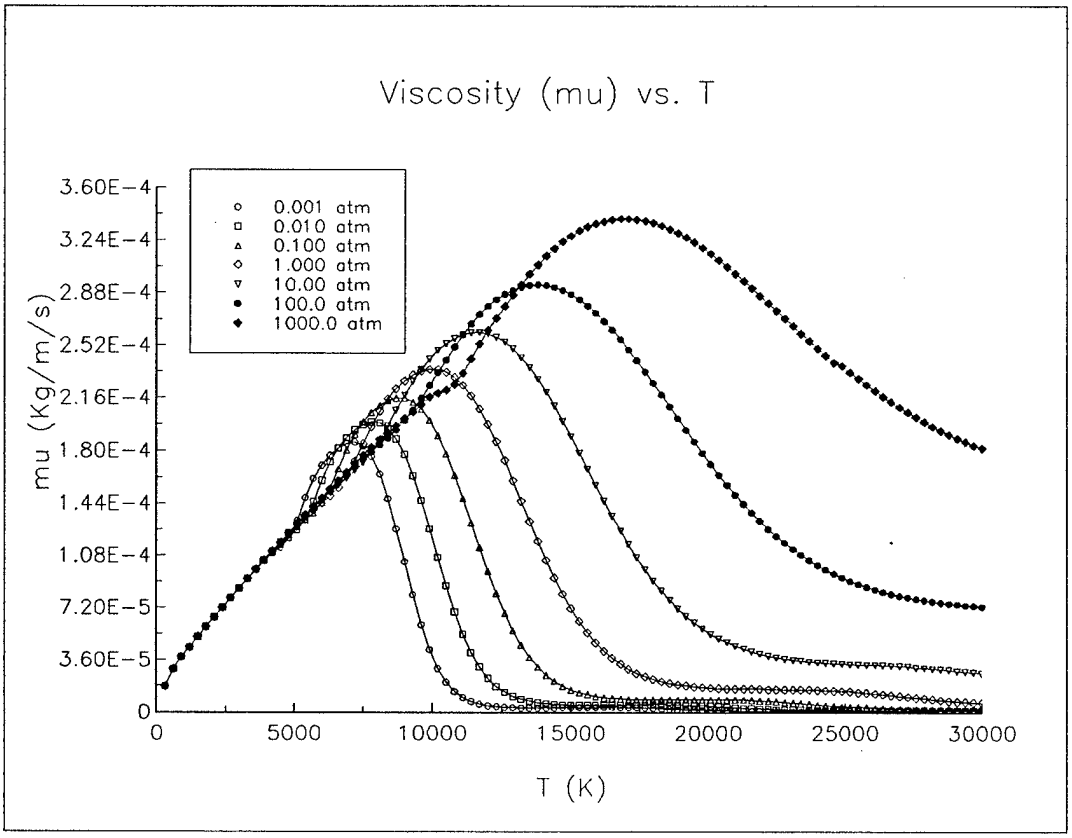

Figure 6. Mixture viscosity.

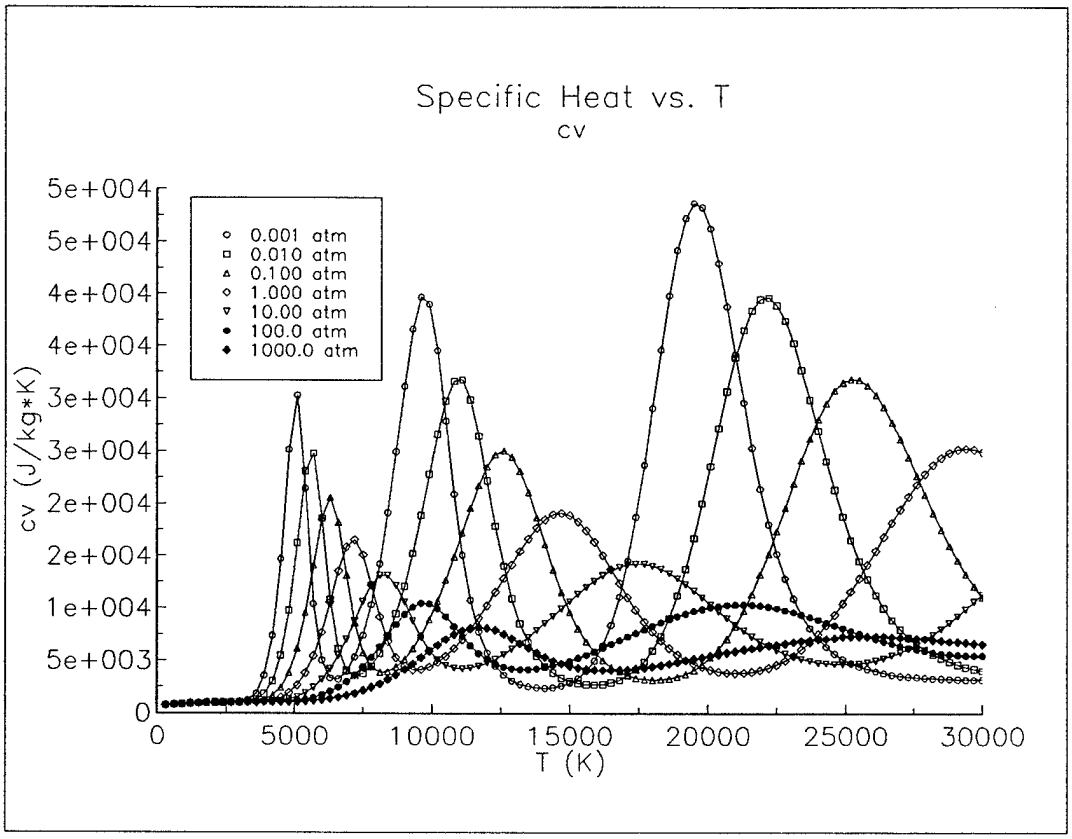

Figure 7. Specific heat at constant volume.

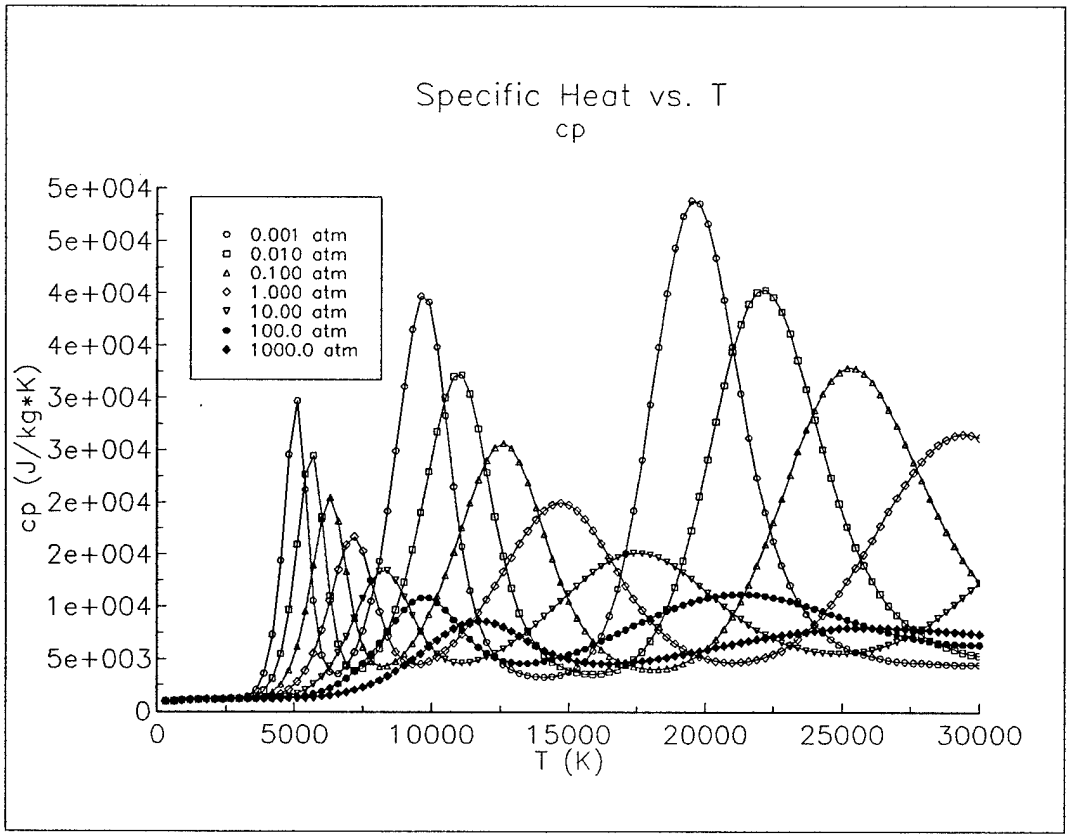

Figure 8. Specific heat at constant pressure.

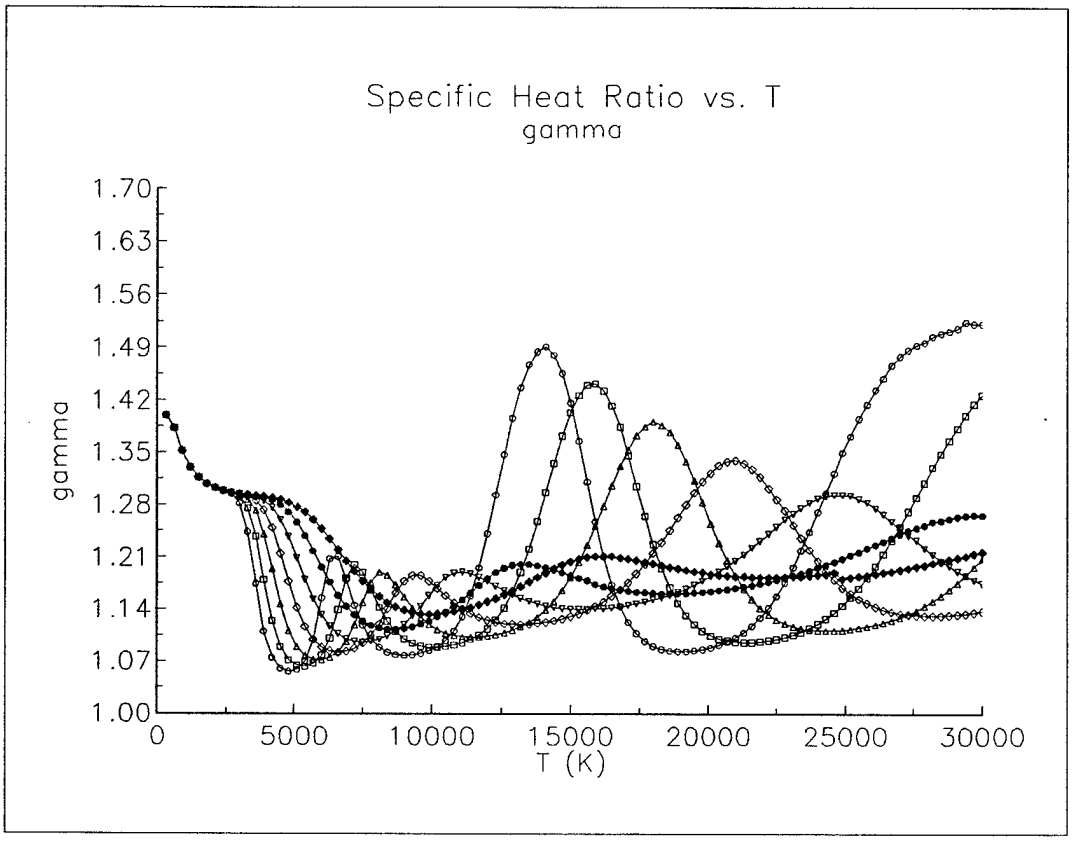

Figure 9. Ratio of specific heats.

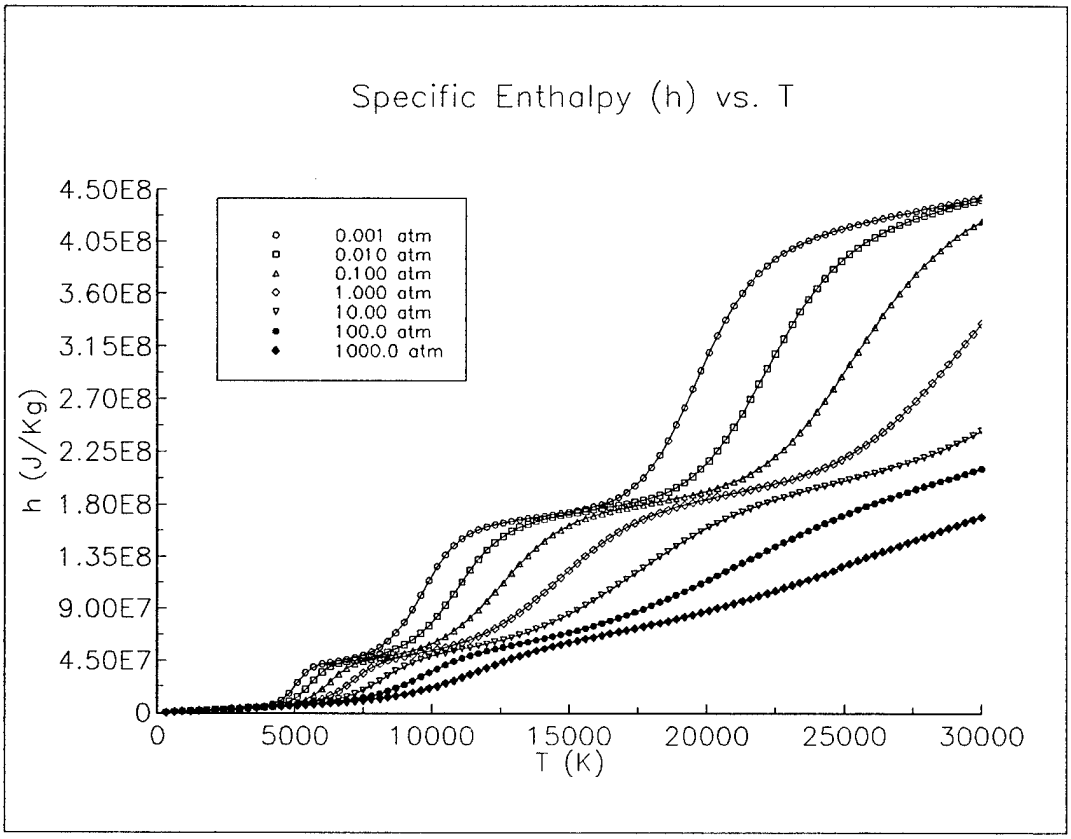

Figure 10. Mixture enthalpy vs. temperature.

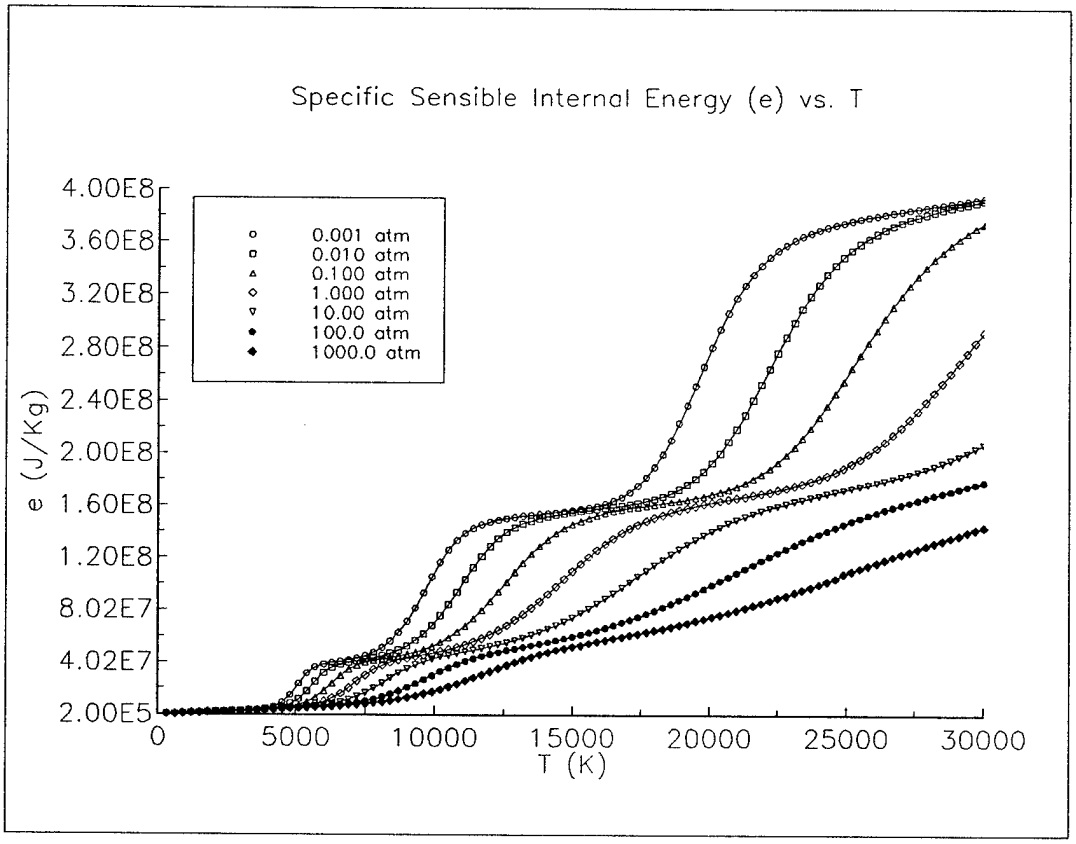

Figure 11. Mixture sensible internal energy vs. temperature.

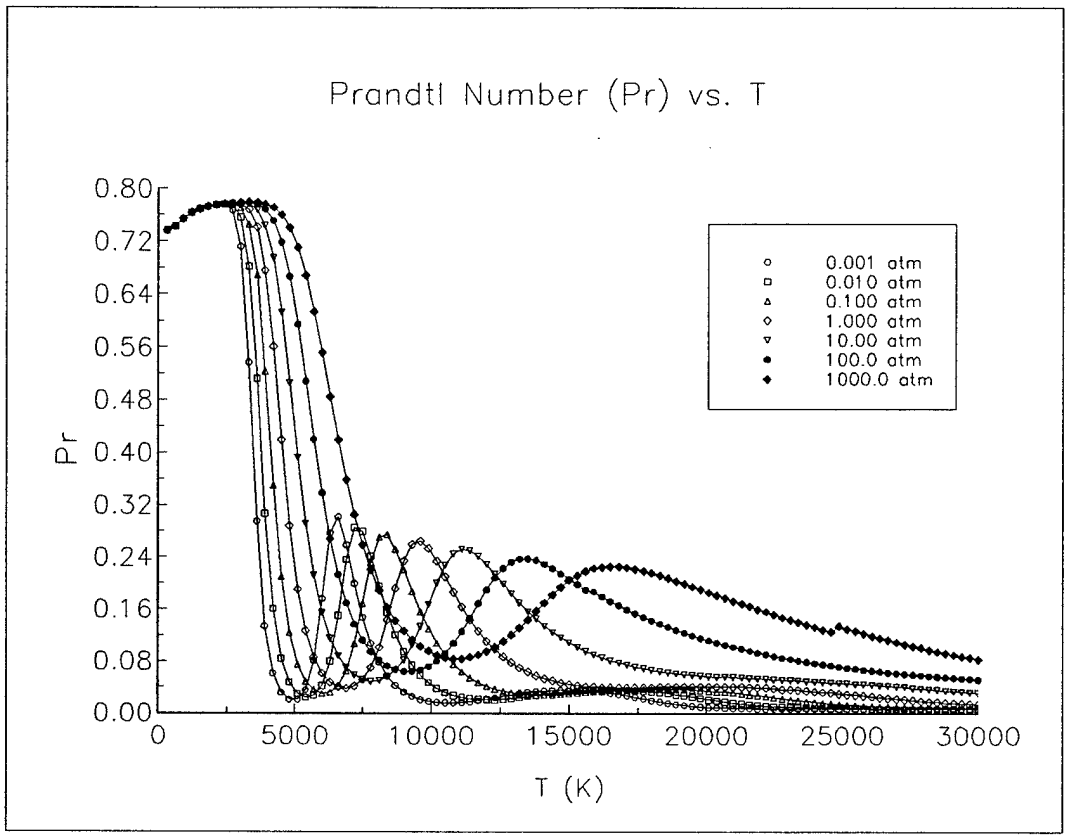

Figure 12. Prandtl number vs. temperature.

APPENDIX V

Use of an Adaptive Grid to Model Thermal Diffusion in Problems with Severely Non-Monotonic Transport Properties

USE OF AN ADAPTIVE GRID TO MODEL THERMAL DIFFUSION IN PROBLEMS WITH SEVERELY NON-MONOTONIC TRANSPORT PROPERTIES

C. S. Schmahl[1], P. J. Turchi.[2], R. E. Peterkin[3]

Abstract

Modeling of thermal diffusion in problems where the thermal conductivity is a severely non-monotonic function of temperature is studied numerically. The thermal conductivity of a partially-ionized, molecular gas, including transport due to variations in chemical state, exhibits non-monotonic variations by factors of three to five in the temperature range from 1000 - 20,000 K. This range corresponds to conditions near surfaces in both internal and external high-speed flows, and in various devices for material processing. A detailed study of the effects of numerical gridding on the accuracy of the solution of the thermal diffusion equation is performed with MACH2, a 2-1/2 dimensional, time dependent, arbitrary Lagrangian-Eulerian (ALE) adaptive-grid magnetohydrodynamic (MHD) code. Data from an advanced reactive thermal-conductivity model for nitrogen is provided in tabular form. An adaptive mesh based on variations in the thermal conductivity, rather than the temperature or temperature gradient, allows increased accuracy of calculations with a smaller number of computational cells. Comparisons with uniform gridding indicate that, when such an adaptive mesh is used with the severely non-monotonic transport coefficient provided by the advanced thermal-conductivity model, differences in thermal flux can exceed 100%, especially at early times.

1. Graduate Research Associate, Department of Aerospace Engineering, Applied Mechanics and Aviation, The Ohio State University, Columbus, OH.
3. Professor, Department of Aerospace Engineering, Applied Mechanics and Aviation, The Ohio State University, Columbus, OH. AIAA Associate Fellow.
2. Technical Leader, Center for Plasma Theory and Computation, Air Force Research Laboratory, Kirtland AFB, NM.

Introduction

In several categories of aerospace and industrial systems, partially-dissociated, partially-ionized gases are in contact with solid surfaces. These systems include hypersonic flight vehicles, plasma thrusters, and arc furnaces. The equation-of-state of such a gas is quite complex and results in transport coefficients for thermal conduction and viscous flow that can be severely non-monotonic functions of temperature and pressure. Solution of problems of considerable engineering significance, such as heat transfer to ablating surfaces, depend on accurately modeling transport across regions that span a temperature range from 1,000 - 20,000 K. Over this range, calculations for even relatively simple molecular gases, such as nitrogen, indicate non-monotonic variations of thermal conductivity by factors of three to five. Numerical modeling is essential in order to analyze heat transfer under these circumstances. The question of accuracy and efficiency in performing such modeling is the subject of this paper. Two points of interest are examined: 1) the relation of the calculational grid to the physical properties of the problem, and 2) the use of adaptive gridding based on the thermal conductivity, rather than the temperature or temperature gradient, in order to capture the effects of variation in transport properties with temperature and density.

Example of Thermal Conductivity Variation

The equilibrium chemical composition, thermodynamic, and transport properties for nitrogen have been calculated[1]. Six possible species are included: N_2, N_2^+, N, N^+, N^{++}, and e^-. The calculations are performed with the inclusion of molecular dissociation and vibrational excitation, single molecular ionization, both single and double atomic ionization. Single electronic excitation is included with a variable electronic partition-function cutoff for atomic species (based on distance between neighboring perturbations to the potential function of an isolated atom or ion). The thermodynamic state ranges for the calculations are: $300\ K < T < 30{,}000\ K$ and $10^{-3}\ atm < p < 10^{3}\ atm$.

Figure 1 displays that the thermal conductivity of the mixture can exhibit highly non-monotonic variations, especially in state regions where chemical reactions are dominant. For use with MACH2, a 2-1/2 dimensional ALE MHD code[2], the chemical thermodynamic and transport data is provided in the format of SESAME tables[3].

Numerical Modeling of Unsteady Heat Transfer

It is necessary to choose the time step for numerical integration according to proper characteristic times based on both the temporal behavior of the boundary conditions and the cell size needed to capture the spatial dependence of the solution. In general, with the thermal diffusivity defined as

$$K \equiv \frac{k}{\rho c_v} \tag{1}$$

the characteristic length for unsteady thermal diffusion scales as

$$x_c = \sqrt{K t_c} \tag{2}$$

where t_c is the characteristic time scale for the boundary condition, such as the rise time of a sinusoidal pulse or the elapsed time from the impulsive application of a constant temperature or heat flux.

To capture the distribution of temperature within the medium, the cell size must, of course,be much smaller than this characteristic length scale:

$$\delta x = f_x x_c \tag{3}$$

where $f_x << 1$.

The computational time step, at least for explicit calculations, must be much less that the characteristic time for diffusion across the cell-size:

$$\delta t = f_t \frac{(\delta x)^2}{K} \tag{4}$$

where $f_t << 1$. Thus, the time step is related to the characteristic time of the problem by two factors, f_x and f_t, such that:

$$\delta t = f_t (f_x)^2 t_c \tag{5}$$

Note that for impulsive application of boundary conditions, for which t_c equals the elapsed time, numerical calculation will always be inaccurate at very early times. Also the number of cycles required to complete computation of a problem of duration t_c is

$$N = \frac{1}{f_t (f_x)^2} \tag{6}$$

For $f_t = f_x = 0.1$, N = 1000 cycles. This is overcome by the use of an implicit scheme.

In computations presented here, in which the cell size is changing throughout the computation, the maximum time step allowed is chosen to be equal to the characteristic time step to minimize the influence of errors that might otherwise result from improperly chosen time steps for the smallest cell, with $f_t=1$.

One-Dimensional Thermal Flux on a Uniform Grid

Computations were performed for three values of evenly-spaced cells (n = 64, 32, and 16), respectively, Figure A displays the temperature profile for unsteady, one-dimensional, heat transfer between two surfaces impulsively imposed across a medium initially at a uniform temperature (equal to the average value of the two surfaces) with a constant thermal conductivity. Figure B compares the error in calculations of temperature as a function of time between the surfaces, at several times, in terms of the differences between local values of temperature (for n = 64, 32, and 16, respectively) and the local value obtained analytically[4]. This error is normalized by the mean value and given as a cell averaged quantity across the grid. This is calculated as:

$$E = \sqrt{\sum_{i=1}^{no.cells} \left| \frac{T_{anal} - T_{calc}}{T_c} \right|^2} \times 100 \quad (7)$$

Accuracy at early times improves as the cell size becomes smaller compared to the characteristic length for diffusion. Smaller cell size, however, within the strict requirement of Eqn. 4, requires a larger number of computational cycles. This requirement is certainly ameliorated by the use of implicit solution of the difference equations, but at the potential loss of accuracy even within stable, converged solutions. The use of nonuniform cell size permits a reduction in the total number of calculations and memory requirements, if the reduced number of cells can be concentrated in regions where important variations are occurring.

Adaptive Gridding

The benefit of using a calculational grid with variable resolution is well established. Often, the grid will be determined by the shape of flow boundaries and by the distribution of flow functions such as mass density. Figures 4 and 5 display the percent differences in flux of the solutions for a unsteady heat transfer problem using the tabular conductivity with a grid that is concentrated in regions of highest temperature gradient to that of an ordinary fixed grid. This is done for 16 and 32 cells, respectively.

Here we see that the largest differences happen at earlier times, especially near the domain mid-range, and decrease as time continues. Larger differences appear in the 32 cell case. The

magnitudes being approximately double that of the 16 cell simulation.

Grid Based on Thermal Conductivity

The code has the capability to adapt the grid according to the magnitude of the thermal conductivity and, separately or in combination, to gradients in the thermal conductivity. The decision to have the ability to adapt the grid on either magnitudes or gradients is based on the assumption that both may be important depending on the physical situation or the transport model.

The specific amount of adaptation provided be each control is determined by the following procedure. This is accomplished by continuously adjusting the grid to the squares of the logarithmic derivatives, accumulated of course, throughout the spatial and temporal coordinates. The exact sensitivity of the calculational grid is defined by user defined input parameters which modify the code internal adaptive weight function accordingly.

The ability to adapt according to the thermal conductivity in this manner has four major features. Enough cells are placed in regions where large amounts of thermal diffusion are important. The true maxima/minima of conductivity are captured in descretized space when dealing with highly non-monotonic transport model, thus minimizing the risk of missing important values by approximations in using the tabular data. The thermal conductivity is a function of both pressure and temperature, so the grid directly adapts on one function instead of two, thus minimizing computational work. Finally, the exact correlation of the transport model with flow structure can be delineated.

To test the adaptive-gridding scheme, the unsteady, two-wall heat transfer problem is again considered. As pictured in Fig 2, the left wall is at 1.0 ev, the right at 0.5 Ev, and the gas is initially at a uniform temperature of 0.75 Ev. Before using the more complex tabular model (for Fig. 1), it is useful to employ a generic ersatz, analytical model for a severely non-monotonic variation in thermal conductivity. A sinusoidal form is chosen for this task. To test the adaptive grid algorithm, we impose a sinusoidally-varying thermal diffusivity on the interval [0,1]:

$$K(x) = K_0[\ 1 + b\sin(2n\pi x)\ ] \qquad (8)$$

For $K_0 = 0.25\ m^2 / s$, b = 0.5, and n = 4, the resulting conductivity profile is illustrated in Figure 3.

Twelve different runs were performed utilizing the sinusoidal thermal-conductivity model given by Eqn. 6, under four different adaptivity conditions. Three runs using a plain non-adaptive grid were performed as baseline computations using 64, 32, ad 16 cells, respectively. The results of the 64 cell run are shown in Fig. 8. The results of the 32 and 16 cell runs exhibited similar behavior. The 64 cell grid simulation using the adaptive grid based on thermal conductivity magnitude is shown in Fig 9. The grid density for this case is shown in Fig. 10.

Figures 11 and 12 show the percent difference for the sinusoidal conductivity model between the uniform grid and the grid adapting to the magnitude for the 16 and 32 cell cases, respectively. The difference being defined as:

$$E(x_a,t_a) = \frac{Q_a(x_a,t_a) - \overline{Q}_f(x_a,t_a)}{\overline{Q}_f(x_a,t_a)} \times 100 \qquad (9)$$

where Q_f(xa,ta) is the interpolated value of flux from the fixed grid simulation at each adaptive grid point. (This interpolation procedure is performed using a multi-dimensional cubic spline interpolation). The differences indicated are very small except in the mid-range where a rather large variation occurs. For the 32 and 16 cell cases, much larger errors exist near the middle reaching consistent maxima of approximately 78% for the 32 cell case and 66% for the 16 cell case. Note the small deviation even at late times for both of these cases.

Calculations with the true non-monotonic conductivity model of Fig. 1, under the same general parameters as the simulations with the idealized, sinusoidal form, yield similar results. Figure 13 shows the flux distribution with no adaptivity. Figure 14 shows the resultant flux distribution with full adaptivity. The percent difference between the fixed grid and fully adaptive grid for 64 cells is shown in Fig. 15. We see that the differences present in the tabulated runs are generally much greater that present in the sinusoidal model. Figure 15 shows a rather large maxima in the mid-range with a maximum of approximately 28%. Note that the left wall maxima is still present in this case along with the 32 and 16 cell cases shown in Figs. 16 and 17. Figures 18 through 20 show the grid densities for these three cases.

Concluding Remarks

Calculation of a multi-component, chemically-reacting transport model for nitrogen revealed that in certain state regimes the thermal conductivity exhibits highly non-monotonic behavior[1]. This prompted the modification of the MACH2 computer code to adapt the computational grid to the magnitude and gradient of the thermal conductivity and the gradient of the thermal conductivity. As time progresses, such an adaptive grid increases the accuracy of the solution by concentrating the grid in the appropriate regions to capture severe variations in thermal conductivity. This adaptation also helps to stabilize the numerical solution at boundaries with impulsive initial conditions. The largest percentage differences between results with the

new gridding scheme and uniform gridding occur at early times, but errors persist even at late times in the calculations.

In addition to avoiding significant errors in calculation of heat flux (in excess of 70% in some instances), the use of a gridding scheme that follows the behavior of the thermal conductivity will be important in attempts to understand the structure of nonuniform regions between relatively cold boundaries and high temperature, molecular flows. Aerospace problems, including heat transfer and ionization in hypersonic boundary-layers, and the current distribution in ablation-fed plasma thrusters, will certainly depend on accurate modeling of transport properties, but also require that numerical computations capture the complexity of such modeling.

Acknowledgements

This work was sponsored by the Air Force Office of Scientific Research, Directorate of Aerospace Sciences, Washington, DC, and the USAF Phillips Laboratory, Kirtland AFB, NM. A portion of the effort by the first author was performed as a graduate student in the AFOSR Summer Research Program at the Phillips Laboratory.

References

1. Schmahl, Christopher S., A Computational Study of Shocked Flow Heat Transfer With Improved Equation of State and Transport Properties - A Case Study For Nitrogen. Master's Thesis. The Ohio State University. 1996

2. Peterkin, Robert E., A. J. Giancola, J. E. Sturtevant. 1992. MACH2: A Reference Manual - Fifth Edition. Mission Research Corporation. Albuquerque, NM. Report Number ABQ-R-1490.

3. Favorite SESAME reference

4. Carslaw and Jaeger ? [Reference for analytic solution]

5. Reference for adaptive gridding techniques.

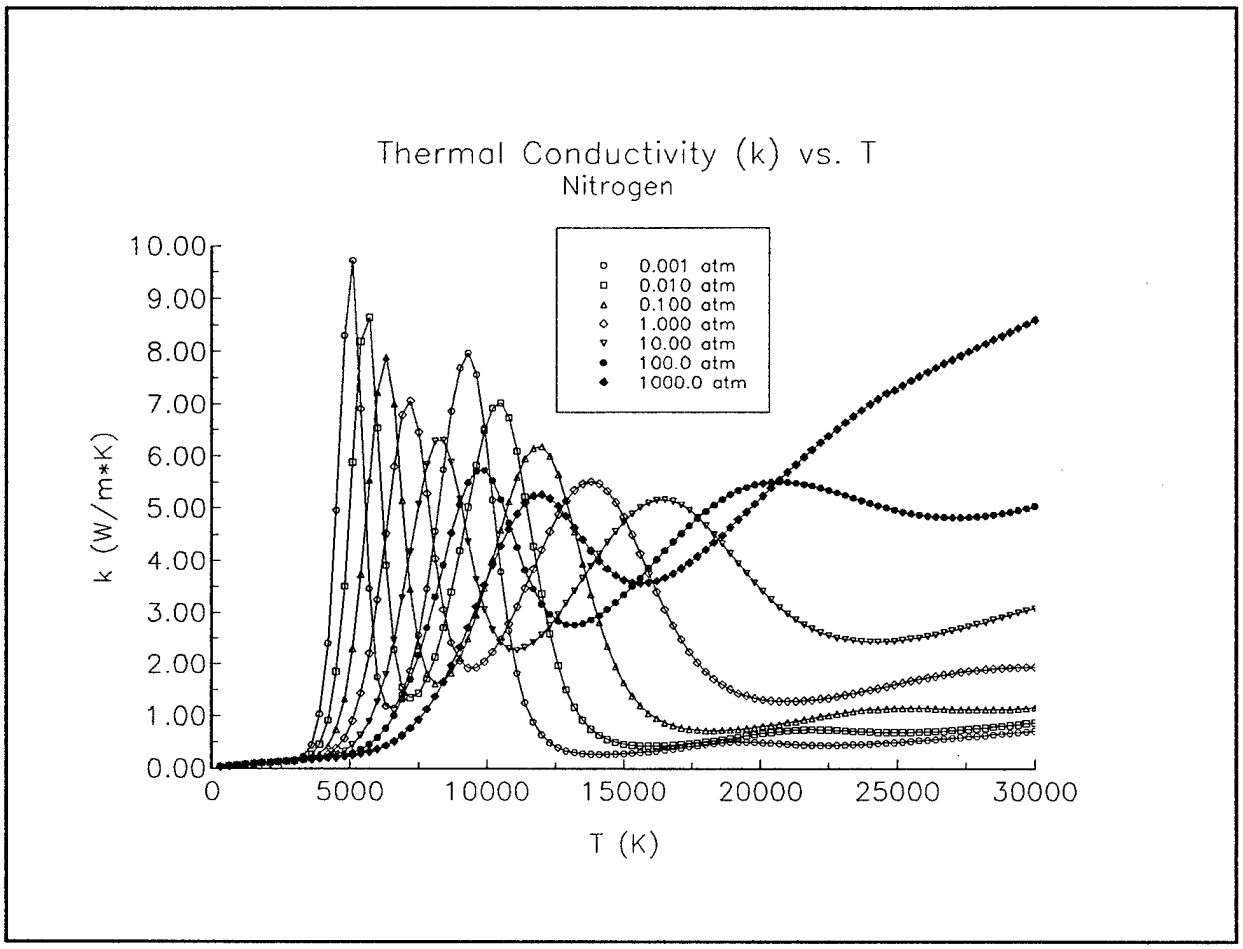

Figure 1. Total mixture thermal conductivity for nitrogen.

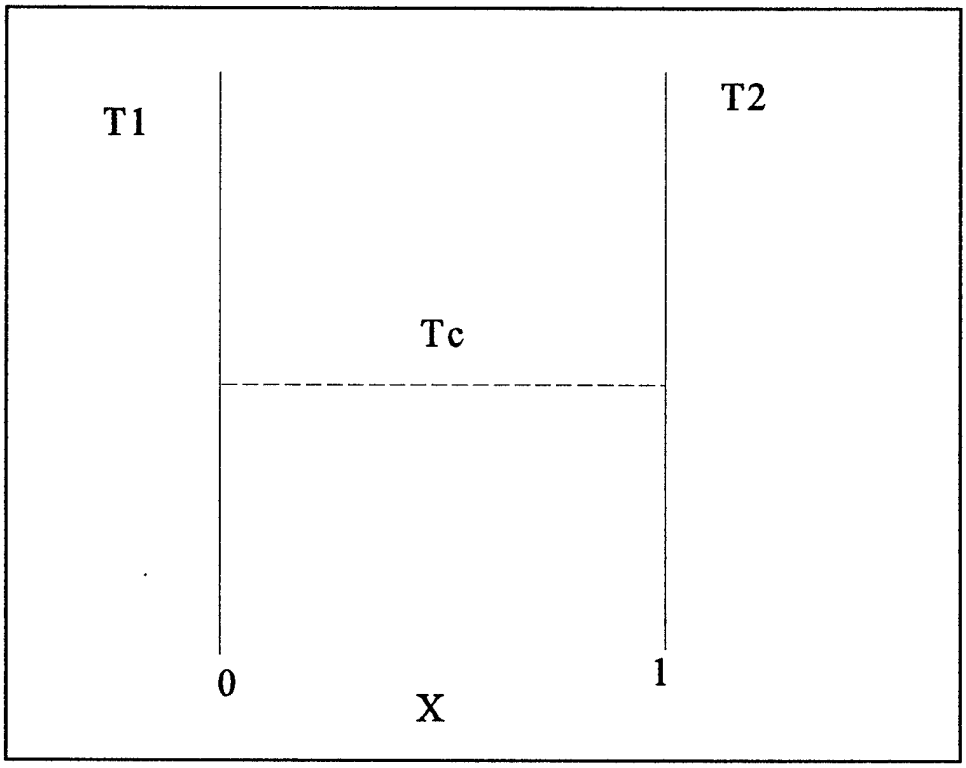

Figure 2. Illustration of problem.

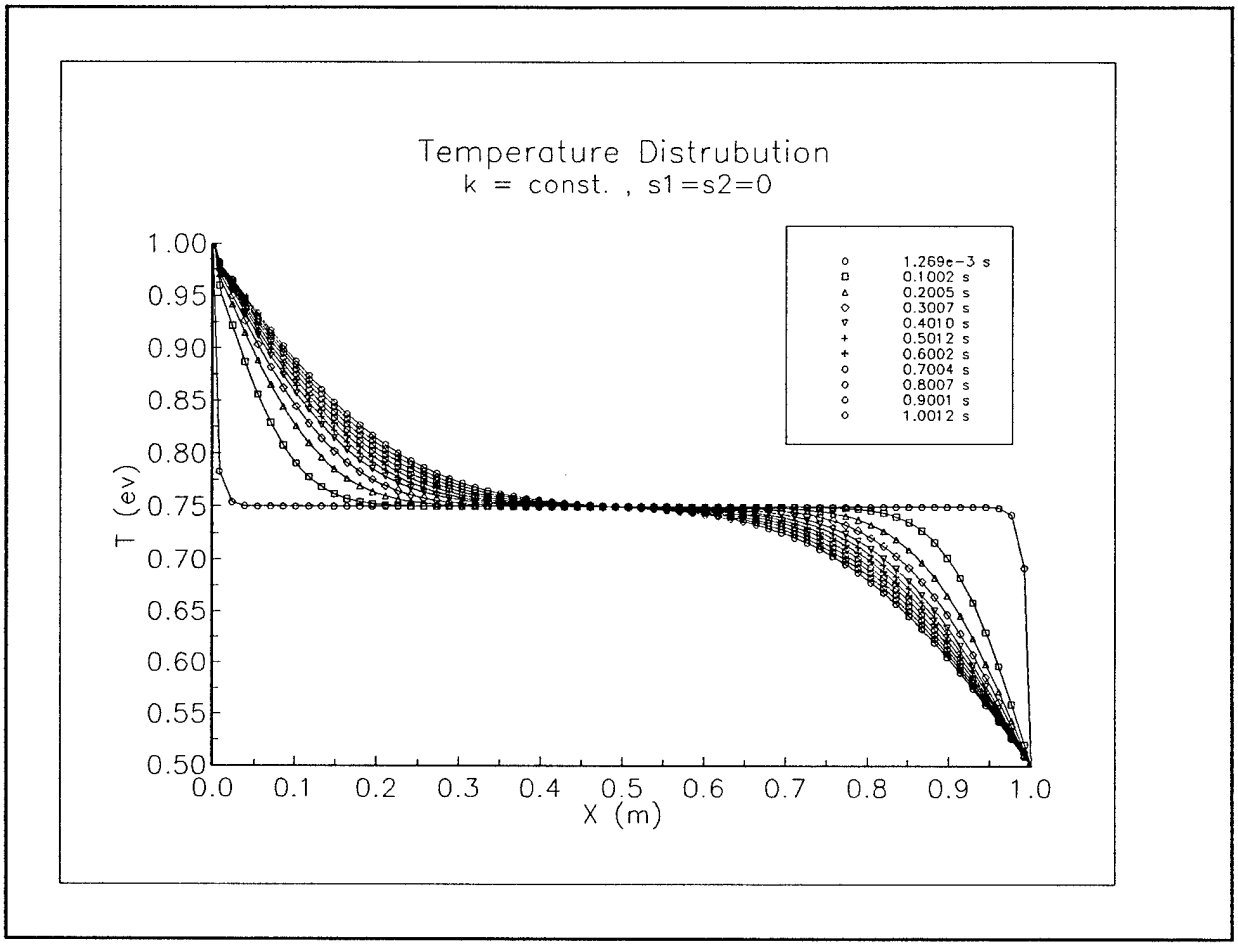

Figure 3. Temperature distribution. No adaptivity. Constant conductivity.

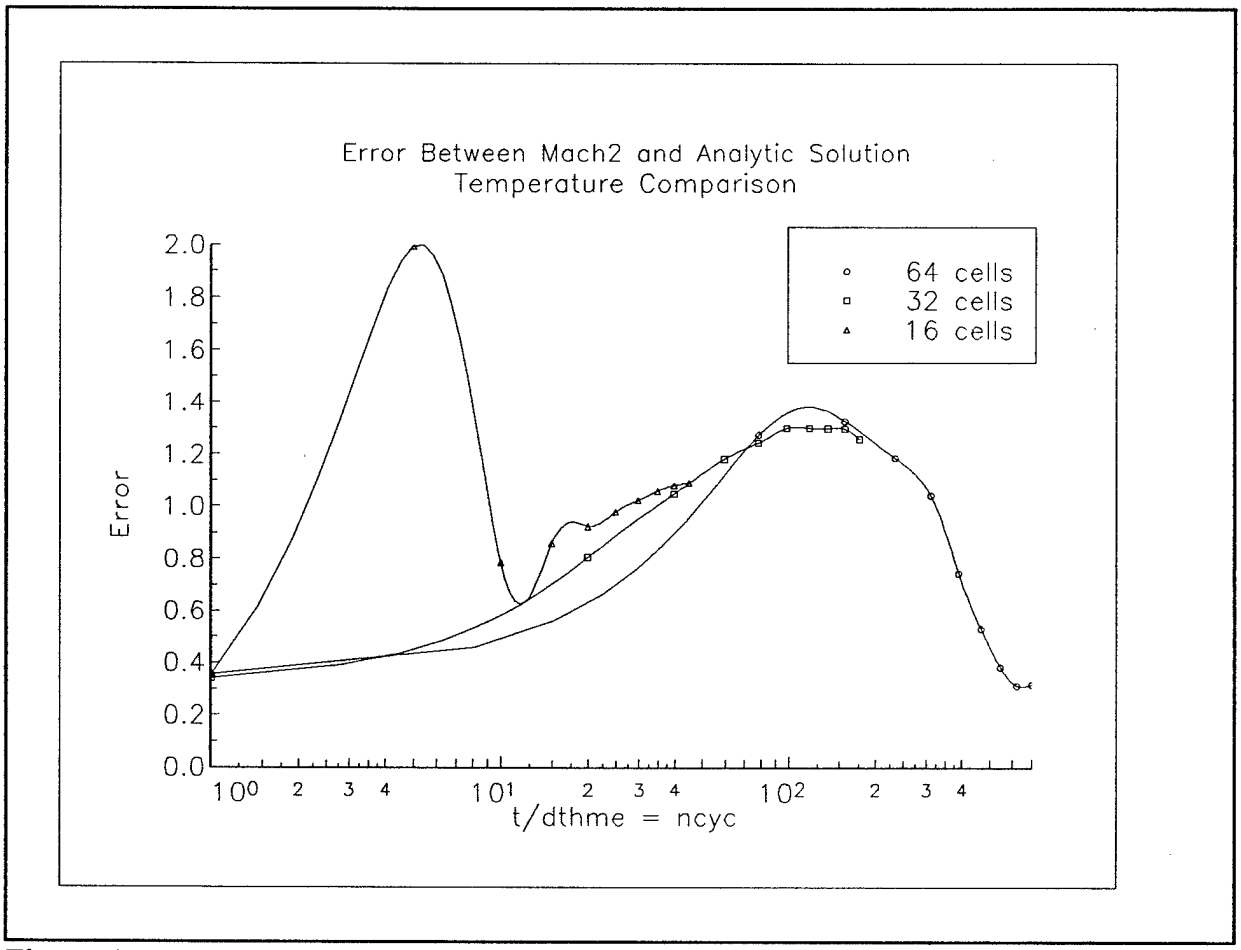

Figure 4. Error between Mach2 calculations and analytic solution.

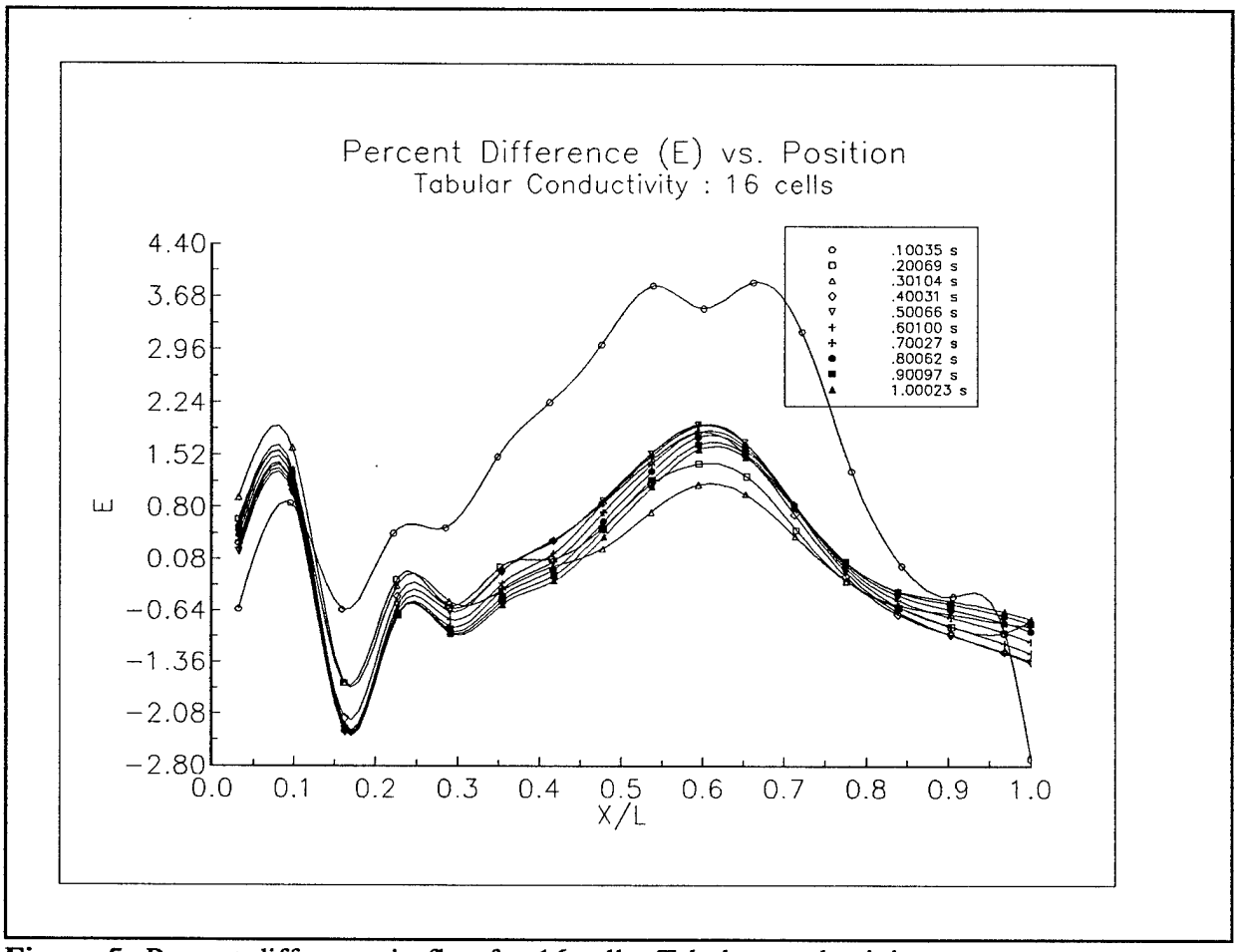

Figure 5. Percent difference in flux for 16 cells. Tabular conductivity.

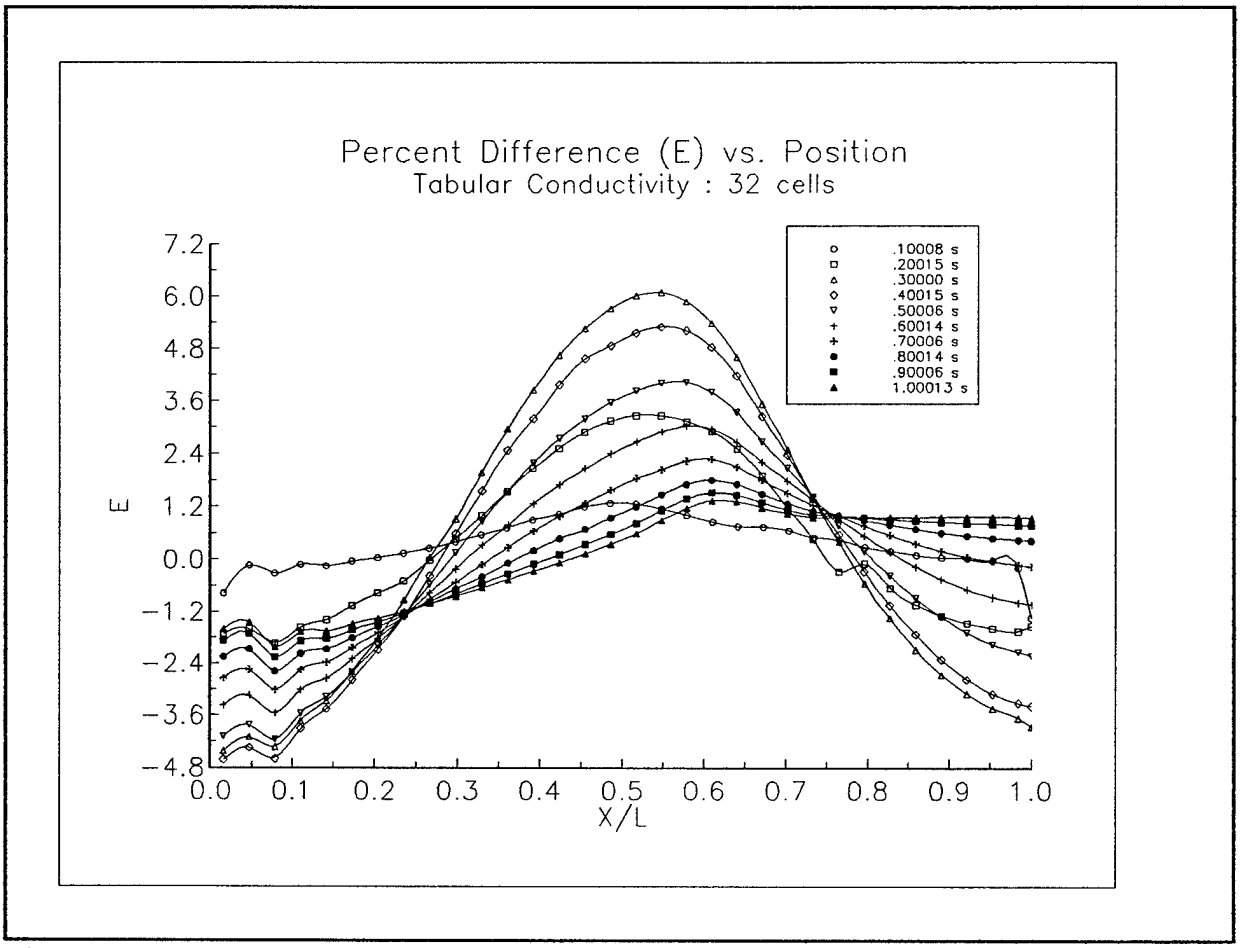

Figure 6. Percent difference in flux for 32 cells. Tabular conductivity.

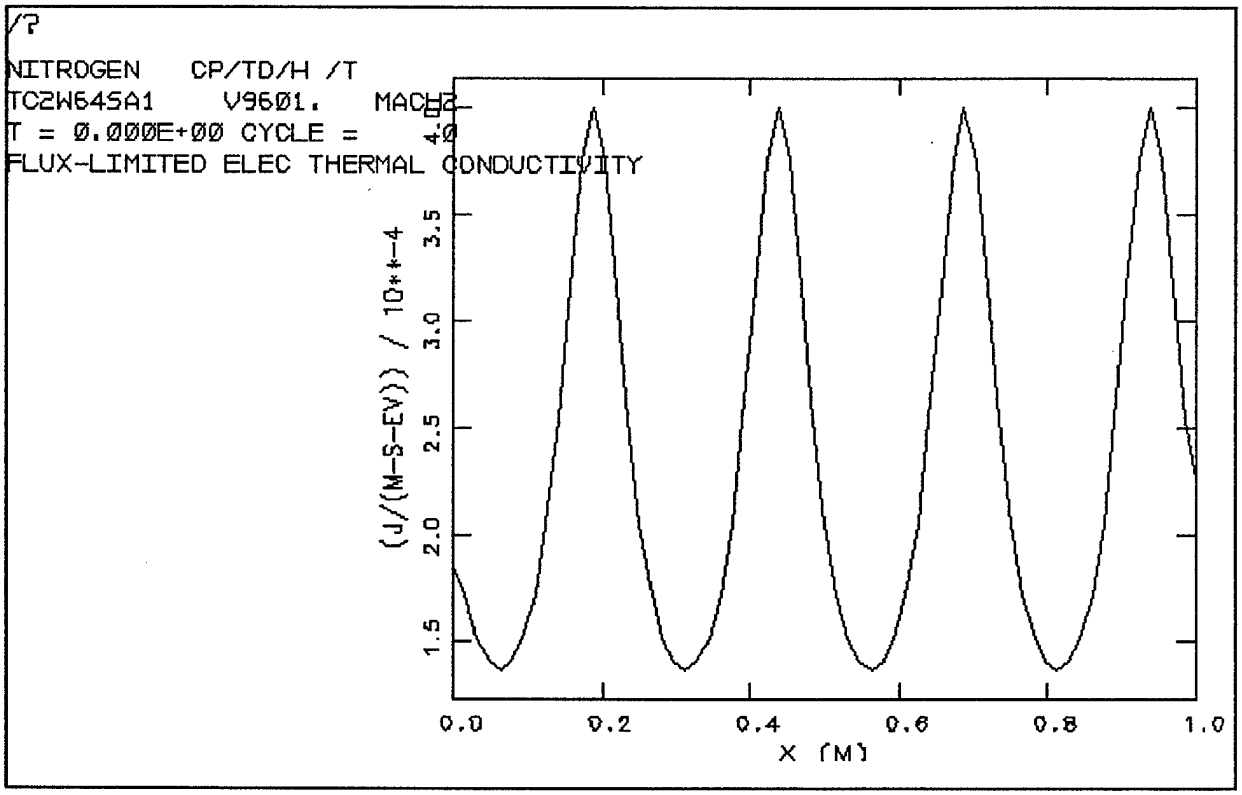

Figure 7. Conductivity profile given by Equation 8.

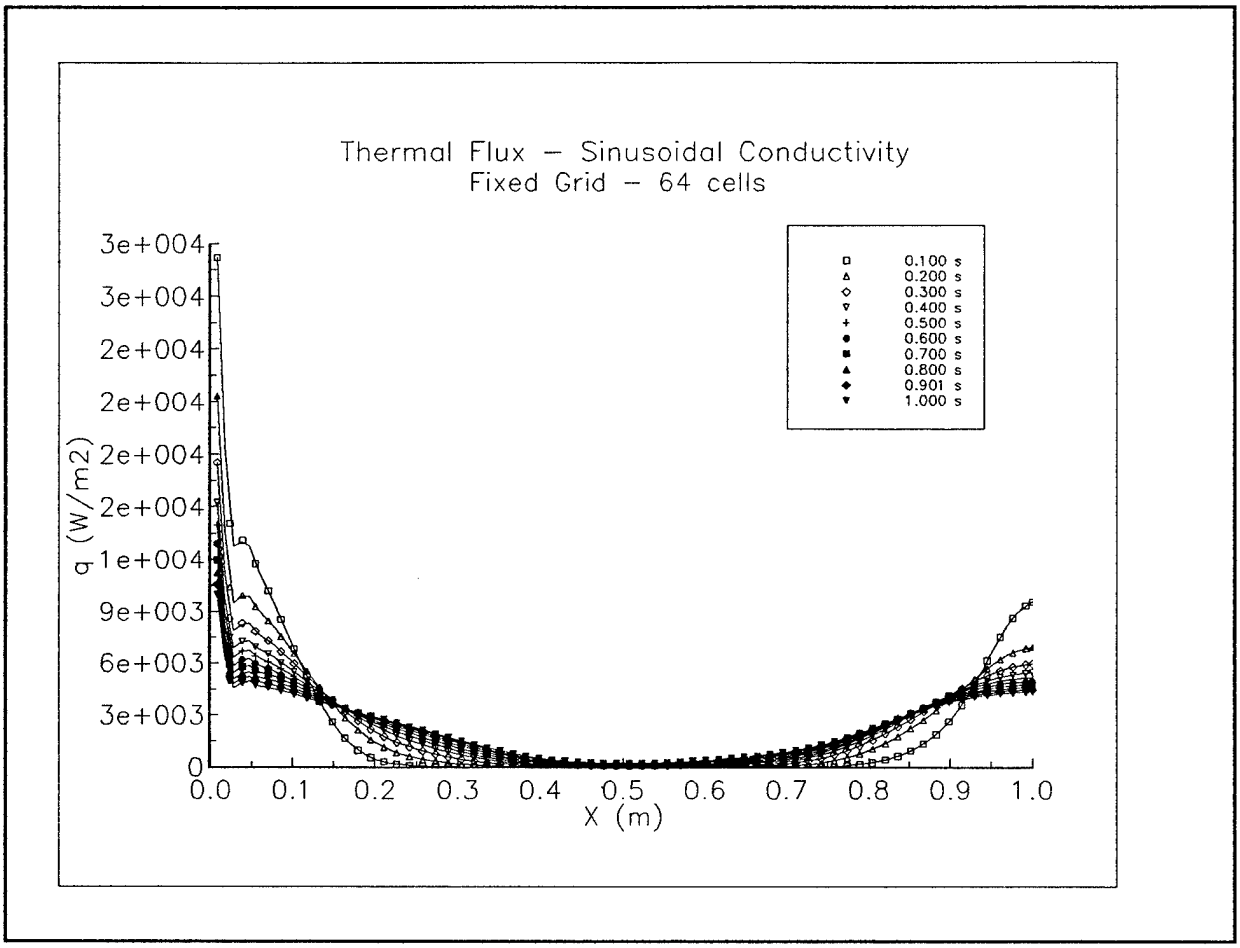

Figure 8. Thermal flux, fixed grid

APPENDIX VI

Thermochemical Properties of Vapor Phase PTFE (Teflon) Under Conditions of Thermal Nonequilibrium

THERMOCHEMICAL PROPERTIES OF VAPOR PHASE PTFE (TEFLON) UNDER CONDITIONS OF THERMAL NONEQUILIBRIUM

C. S. Schmahl and P. J. Turchi
The Ohio State University
Columbus, Ohio
USA

ABSTRACT

The chemical composition and thermodynamic properties of tetrafluoroethylene (C_2F_4) is calculated with a two-temperature LTE formulation. Twenty-five chemical species are included in the analysis. The equilibrium constants are calculated using the most recent spectroscopic data available. Calculations are performed for pressures from 0.001 atm to 1.0 atm and for temperature ranges of 0.05 ev to 5 ev for both heavy particle and electron temperatures.

INTRODUCTION

Knowledge of the chemical, thermodynamic, and transport properties of a gas is required in almost any gasdynamic analysis. Accurate thermochemical and transport properties become particularly important in high-temperature applications such as the pulsed plasma thruster. In this paper, we shall concentrate on calculating the equilibrium composition of a gas mixture. This is the necessary first step for determining the thermodynamic and transport properties of a gas.

There are three primary thermochemical states possible for a gas. A calorically perfect gas has specific heats that are constant, and the enthalpy and internal energy are only functions of temperature. A thermally-perfect gas, in which variable vibrational and electronic excitation are taken into account, has specific heats, enthalpy, and internal energy that are all functions of temperature. If the conditions are right for chemical reactions to occur, then we can treat the gas as an equilibrium chemically-reacting gas for which properties area all functions of temperature and pressure. Even this can be generalized by stating that the reacting gas is in local thermodynamic equilibrium (LTE). This means that a local Boltzmann distribution exists at each point in the flow at the local temperature. We will extend this statement further for the case of a two temperature LTE gas modeled here. In this paper we calculate the chemical composition of gaseous Teflon.

Very little information exists on the thermochemical properties of PTFE and its chemical constituents, especially in the plasma state. This is unfortunate for high-temperature thermochemical and transport data is needed for such devices as pulsed plasma thrusters[1,2], ablative re-entry heat shields, electronic components (such as capacitors), plasma etching systems, and upper atmosphere modeling. Nonequilibrium properties are particularly important when studying electric discharges near Teflon surfaces and other nonequilibrium flows.

POSSIBLE SPECIES, REACTIONS, AND EQUILIBRIUM EQUATIONS

In this paper, we calculate the chemical composition of tetrafluoroethylene (C_2F_4). The analysis will include vibrational and electronic excitation, dissociation, first molecular ionization, and first through fourth monatomic ionization. Throughout of the analysis, we shall assume a perfect gas, where intermolecular forces are non-existent or negligible. This might seem a strange assumption when the gas is in the plasma state due to the presence of Coulomb collisions, but it is a widely used and accepted approximation.[3]

For a polyatomic base gas, C_2F_4 in our case, with the possibility of undergoing full dissociation, singular molecular ionization, and up to fourth monatomic ionization, we first assume there are twenty-five possible chemical species, which are C_2F_4, C_2F_2, CF_2, CF_2^+, CF_3, CF_3^+, CF_4, C_2, CF, CF^+, F_2, F_2^+, C^Z (Z=-1,4), F^Z (Z=-1,4), and e^-'s. For a gas containing twenty-five chemical species, which is composed of three elements (C, F, e^-), we are required to have twenty-two (25-3=22) independent chemical reaction equations (laws of mass action). The reactions considered here are

$$CF_2 \rightleftharpoons CF + F \tag{1}$$

$$CF \rightleftharpoons C + F \tag{2}$$

$$F_2 \rightleftharpoons 2F \tag{3}$$

$$CF_2 \rightleftharpoons CF_2^+ + e^- \tag{4}$$

$$CF \rightleftharpoons CF^+ + e^- \tag{5}$$

$$C^{Z-1} \rightleftharpoons C^Z + e^- \quad \prod_{Z=0}^{4} \tag{6}$$

$$C_2F_4 \rightleftharpoons 2CF_2 \tag{7}$$

$$F_2 \rightleftharpoons F_2^+ + e^- \tag{8}$$

$$F^{Z-1} \rightleftharpoons F^Z + e^- \quad \prod_{Z=0}^{4} \tag{9}$$

$$C_2F_4 \rightleftharpoons C_2F_2 + F_2 \tag{10}$$

$$C_2F_4 \rightleftharpoons CF_3 + CF \tag{11}$$

$$C_2F_4 \rightleftharpoons CF_4 + C \tag{12}$$

$$C_2 \rightleftharpoons 2C \tag{13}$$

In actuality, there are other possible reactions that could yield the same chemical species. But, for an equilibrium calculation, the reactions chosen are arbitrary as long as they are linearly independent and account for all possible species.

Writing these reactions in terms of equilibrium relations for the partial pressures, we have

$$K_{p,j}(T) = \prod_i p_i^{\nu_i} \tag{14}$$

where the $K_{p,j}$ are the equilibrium constants for the reaction (j) at the equilibrium temperature T, in terms of the partial pressures. Using the appropriate formulations, they may also be put in terms of concentrations, K_c, or number densities, K_n. It is important to note in the above equations that the equilibrium constants are written as functions of temperature only, as most authors point out. However, they may be functions of two or more state variables depending on whether such things as thermal non-equilibrium assumptions or electronic partition function cutoff is taken into account.[4]

In addition to twenty-two independent equations relating the twenty-five unknown partial pressures, we need three more equations to solve for the gas composition. The three chosen are; conservation of nuclei, Dalton's Law, and charge neutrality. The ideal thermal gas law for each species is written in the form

$$p_i = n_i k T_i \tag{15}$$

where

$$p = \sum p_i \tag{16}$$

For charge neutrality, we have

$$\sum_{i=1}^{25} Z n_{iz} = 0 \tag{17}$$

In terms of partial pressures, this becomes (for ideal gases)

$$\sum_{i=1}^{25} Z\left(\frac{1}{T_i}\right) p_{iz} = 0 \tag{18}$$

For conservation of nuclei, we write

$$\left(n_{C_2F_4}\right)_0 = \frac{1}{2}\left(n_C\right)_0 = \frac{1}{4}\left(n_F\right)_0 \tag{19}$$

where

$$\left(n_C\right)_0 = \sum_{i=1}^{25} N n_{i_{C_N}} \tag{20}$$

and

$$\left(n_F\right)_0 = \sum_{i=1}^{25} N n_{i_{F_N}} \tag{21}$$

where $(n_{C2F4})_0$ is the total number of tetrafluoroethylene molecules available for dissociation and ionization (ie. the number of C_2F_4 molecules present if the gas was non-reacting at some initially low temperature). Dividing Eq. (20) by Eq. (21) and utilizing Eq. (19) gives us the nuclei conservation statement, where the number densities are related to the partial pressures by Eq. (15).

CALCULATION OF THE EQUILIBRIUM CONSTANT - PARTITION FUNCTIONS

To solve the system of equations, we only need values for the equilibrium constants which may be calculated from equilibrium statistical mechanics. In terms of partition functions Q_i, the law of mass action for a general system is

$$K_N(T) = \prod N_i^{\nu_i} = e^{\frac{-\Delta\varepsilon_0}{kT}} \prod Q_i^{\nu_i} \tag{22}$$

or alternatively, substituting $n_i = N_i/V$ we have

$$K_n(T) = \prod n_i^{\nu_i} = \left(\frac{1}{V}\right)^{\Sigma\nu_i} e^{\frac{-\Delta\varepsilon_0}{kT}} \prod Q_i^{\nu_i} \tag{23}$$

where ν_i is the stoichiometric mole number for species (i), that is, the coefficients in the balanced chemical equation, $\Delta\varepsilon_0$ is the reaction energy (change in zero-point energy) and Q_i is

the total partition function for species (i). Thus, for a given reaction and thermodynamic state, the only unknowns in Eq. (23) are the Q_i's.

For a system in thermodynamic equilibrium, we have

$$N_j^* = N\frac{g_j e^{-\frac{\varepsilon_j}{kT}}}{\sum g_j e^{-\frac{\varepsilon_j}{kT}}} \tag{24}$$

which gives the number of particles N_j^* in energy level ε_j with g_j degenerate states. We define the partition function, Q, as the sum in the denominator of Eq. (24)

$$Q \equiv \sum g_j e^{-\frac{\varepsilon_j}{kT}} \tag{25}$$

which is, in general, a function of T and V. It is typical to express the total energy as the sum of translational and internal energies. Note that Eqs. (23) and (24) contain only one temperature. For the two temperature case considered in this research we make the assumption that the heavy-particle gas composed of neutrals and ions, has a Maxwellian distribution in velocities and a Boltzmann distribution in energies at a heavy-particle temperature , T. The electron gas, composed of both free and bound electrons is in equilibrium with an electron temperature T_e defined by their Maxwellian velocity distribution. Note that, in this analysis, we are ignoring the interaction between electronic and vibrational states. Thus, we have defined a two-temperature LTE situation. Equation (22) is the standard statistical representation of the equilibrium constant for a one temperature system. For the multi-temperature system analyzed here we expect a different representation. There has been some controversy about the correct form of the multi-temperature Saha equation[5,6,7,8]. Derivations using kinetic arguments yield the same form as Eq. (22) but with T replaced by T_e in the Boltzmann factor. This formulation has long been consistent with the general assumption that ionization is in equilibrium with the electron temperature and just replacing T by T_e as an approximation. Other derivations using pure thermodynamic arguments obtain a Saha equation in which both temperatures appear. This inconsistency was examined in detail by Van de Sanden[5], et al. and was found that these representations were derived using the standard form of the generalized law of mass action, that is

$$\sum_n \mu_n \nu_n = 0 \tag{26}$$

which is proven incorrect for a multi-temperature system because it may violate the second law of thermodynamics for the system as a whole. Van de Sanden found the correct form to be

$$\sum_n \frac{\mu_n \nu_n}{T_n} \tag{27}$$

Which when used in the thermodynamic derivation results in a Saha equation equivalent to that obtained by the kinetic one. Thus in this research the equilibrium constant for ionization reactions is Eq. (22) with T_e in the exponential term.

For a molecule we have

$$\varepsilon = \varepsilon_{trans} + \varepsilon_{rot} + \varepsilon_{vib} + \varepsilon_{el} \tag{28}$$

and for an atom

$$\varepsilon = \varepsilon_{trans} + \varepsilon_{el} \tag{29}$$

where ε is the sensible energy, measured above the zero-point energy ε_0. Quantum mechanics gives us theoretical values for the quantized energies of a particle, at least for the translational, rotational, and vibrational modes.[9] Along with the assertion that particle energy is simply the sum of the modal energies, that is, the internal energies are uncoupled, which is a consequence of the more fundamental assumption of a separable Hamiltonian, the partition function is expressed as the product of the modal partitions Q_j, where

$$Q = \prod Q_j \tag{30}$$

with j extending over all modes, that is, translational, rotational, vibrational, and electronic modes. Armed with the quantized values for the modal energies, and the associated degeneracies we can calculate the modal partition functions which are given here in reduced form, without proof as[10]

$$Q_{trans} = \left(\frac{2\pi mkT}{h^2} \right)^{\frac{3}{2}} \times V \tag{31}$$

$$Q_{rot} = \frac{8\pi^2 IkT}{\sigma h^2} \tag{32}$$

$$Q_{vib} = \frac{1}{1 - e^{-\frac{h\nu}{kT}}} \tag{33}$$

where σ is a factor which arises from the symmetry requirements of the wave function in the exchange of an identical particle. It is equal to 1 for heteronuclear molecules (ex. CF), and equal to 2 for homonuclear molecules (ex. F_2). This number may take other values depending on the complexity of the molecular structure. The rotational and vibrational partition functions are derived assuming that the molecule is a rigid rotator and harmonic oscillator, respectively. For any general polyatomic molecule of N atoms, if we still assume a separable Hamiltonian then we can factor the partition function as in Eq. (30) with the product extending not only over all fundamental modes but also over all modal degrees of freedom.[11] For a polyatomic molecule composed of N atoms, there is a total of 3N geometric degrees of freedom. Translation requires 3 degrees of freedom thus there are a total of 3N-3 degrees of freedom available for the internal modes. For linear polyatomic molecules the rotation can be completely specified by two angles, thus taking up two more degrees of freedom. This leaves 3N-5 degrees of freedom for vibration. The rotational partition function if still given be Eq. (32). For nonlinear molecules three angeles are necessary thus there are a total of 3N-6 geometric degrees of freedom for vibration. The rotational partition function in this case is given by[11]

$$Q_{rot} = \sigma^{-1} \pi^{\frac{1}{2}} \left(\frac{8\pi^2 kT}{h^2} \right)^{\frac{3}{2}} (I_A I_B I_C)^{\frac{1}{2}} \tag{34}$$

For each case the total vibrational partition function is taken as the product of each of the vibrational degrees of freedom with the partition function for each degree of freedom given by Eq. (33). As stated earlier, we have assumed uncoupled energy modes. That is, we assume that the energy exchange between energy modes is small. As a result each energy mode which is equilibrium at its temperature, in our case either T or T_e, is statistically independent from all others. Thus for our multi-temperature system we can write

$$Q = \prod Q_i(T_i) \tag{35}$$

where T_i is the equilibrium temperature of the mode.

Note that the Boltzmann factor, $e^{-\beta\epsilon j}$, in the above equations for the partition functions is written as derived in the standard one-temperature system case. That is, where $\beta = 1/Kt$. It has been known for a long time that certain molecules have the tendency to have their vibrational modes to be a strong function of electron temperature, that is $T_v = T_e$ instead of T. Atmospheric gasses, especially nitrogen are well known for this property[12,13]. This phenomena is thought to be largely due to the propensity of the molecule for vibrational resonance. Since we are dealing with a gas mixture containing twelve molecular species a more formal examination of the situation is required to support our assumptions. We define a parameter η which quantifies the fractional energy exchange between thermal systems, in our case it is the fractional energy exchange between systems at the equilibrium electron temperature, ie. the electron gas, and other internal modes. From the results derived in Appendix 1 we find that our Lagrange multiplier β becomes

$$\beta = \frac{\eta T_H + (1-\eta)T_e}{k T_H T_e} \tag{36}$$

At this point in time, research is being done on how to set the η parameter effectively. Consistent with the assumptions made thus far we have for the interaction of free electrons and bound electrons $\eta = 1$ thus $\beta = 1/Kt_e$ for Q_e. And for the interaction of free electrons and the translational, rotational, and vibrational modes $\eta = 0$ thus $\beta = 1/Kt_h$ for the partition functions for these modes.

For electronic energy there is no closed form general expression for the quantized energy levels, thus the electronic partition function must be left as an infinite series in the form

$$Q_{el} = \sum_{j=0}^{\infty} g_j e^{-\frac{\varepsilon_j}{kT}} \tag{37}$$

Equation (37) is the true theoretical representation of the electronic partition function for an *isolated* particle. In theory there are an infinite number of electronic levels extending from the ground state energy ($\varepsilon_0 = 0$) to the ionization potential, which is the amount of energy needed to remove an electron from its ground state to infinity (ie. undergo a bound-free transition). The electronic partition function is a diverging series because although the energy approaches a finite limit, the degeneracy increases as the square of the principal quantum number, so the series diverges.[14]

In actuality, the electronic series in not infinite because a particle in the real world is never truly isolated. Due to various interparticle interactions that arise in any finite density medium, the series will actually terminate at some principal quantum number, n^{cutoff}. The evaluation of n^{cutoff} and its associated effect of ionization potential lowering is the subject of some controversy and was explored in detail in another work.[4] Results from that work give the correct cutoff criterion as

$$n^{cutoff} = \sqrt{\frac{1 - \frac{1}{2}(\alpha_i)^{\frac{1}{2}}}{\tilde{a}}} \times n_p^{-\frac{1}{6}} \tag{38}$$

where $\tilde{a}=Z_{eff}*e^2/2*IP$. The lowered ionization potential is given by

$$\overline{IP} = IP\left(1 - \frac{1}{n_{cutoff}^2}\right) \tag{39}$$

The K_n's are converted to K_p's using the relation

$$(40) \quad K_{p,j}(T) = (k)^{\Sigma \nu_i} \left(\prod_i T_i^{\nu_i} \right) K_{n,j}(T)$$

The required molecular and atomic data, which are too numerous to give here, are taken from the works of Chase,[15] Moore,[16,17] Rosenstock,[18] Herzberg,[19] Buckely,[20] and Paulino and Squires.[21]

SOLUTION OF THE EQUILIBRIUM EQUATIONS

The equations given in the previous section to calculate the equilibrium composition in terms of partial pressures, given T , T_e and P, provide a closed set of twenty-five coupled nonlinear algebraic equations for which there is no analytic solution and numerical methods must be used. The numerical solution of systems of nonlinear equations is universally very difficult and is a topic of current research. As of yet, there are no appropriate numerical methods for solving coupled nonlinear systems of algebraic equations from arbitrary starting vectors.[22] One of the most commonly used methods and the one used previously for nitrogen research,[4] is the Newton-Raphson method. The Newton-Raphson method usually exhibits excellent convergence qualities when the starting vector (initial guesses for the roots) is near the actual root. For a homonuclear diatomic gas a good initial guess can usually be obtained through Saha-type statistical arguments using weighted averages due to limited reactive simultaneity. In this case though, since we are dealing with a polyatomic heteronuclear gas, it was initially assumed that we could not get close enough to the root for Newton-Raphson to work properly. Many hybrid techniques have been proposed but most fail when the Jacobian becomes singular, or at stationary point.[23,24] The solution procedure initially chosen for this research is the one proposed by Powell.[25] Powell's technique exhibits almost guaranteed convergence even for poor initial guesses. It also has the ability to correctly handle stationary points. The price of this behavior is that the convergence is linear until very close to the root then it converges quadratically like the standard Newton-Raphson. Thus, the total number of iterations required is greatly increased resulting in much longer runtimes, up to 200 minutes per isobar on a workstation . Thus, it was decided that the Newton-Raphson method would be used combined with a raster processing iteration procedure throughout the computational thermodynamic space.

Given T, T_e, and P, an initial equilibrium composition is approximated using simple Saha-type arguments assuming totally uncoupled physical process at low T and T_e, then partial pressures are backed out using weighted approximations or the initial guess was set equal to the previous converged root at the last temperature and pressure and stepped up in temperature on each isobar in small increments of from 0.1 to 10 K for heavy particle temperatures and 1 K to 100 K for electron temperatures. The completely closed system is solved at each point using the Newton-Raphson procedure, which iterates until the sum of the absolute values of the corrections is less than the chosen tolerance, ζ, where

The K_n's are converted to K_p's using the relation

$$(40) \quad K_{p,j}(T) = (k)^{\Sigma \nu_i} \left(\prod_i T_i^{\nu_i} \right) K_{n,j}(T)$$

The required molecular and atomic data, which are too numerous to give here, are taken from the works of Chase,[15] Moore,[16,17] Rosenstock,[18] Herzberg,[19] Buckely,[20] and Paulino and Squires.[21]

SOLUTION OF THE EQUILIBRIUM EQUATIONS

The equations given in the previous section to calculate the equilibrium composition in terms of partial pressures, given T , T_e and P, provide a closed set of twenty-five coupled nonlinear algebraic equations for which there is no analytic solution and numerical methods must be used. The numerical solution of systems of nonlinear equations is universally very difficult and is a topic of current research. As of yet, there are no appropriate numerical methods for solving coupled nonlinear systems of algebraic equations from arbitrary starting vectors.[22] One of the most commonly used methods and the one used previously for nitrogen research,[4] is the Newton-Raphson method. The Newton-Raphson method usually exhibits excellent convergence qualities when the starting vector (initial guesses for the roots) is near the actual root. For a homonuclear diatomic gas a good initial guess can usually be obtained through Saha-type statistical arguments using weighted averages due to limited reactive simultaneity. In this case though, since we are dealing with a polyatomic heteronuclear gas, it was initially assumed that we could not get close enough to the root for Newton-Raphson to work properly. Many hybrid techniques have been proposed but most fail when the Jacobian becomes singular, or at stationary point.[23,24] The solution procedure initially chosen for this research is the one proposed by Powell.[25] Powell's technique exhibits almost guaranteed convergence even for poor initial guesses. It also has the ability to correctly handle stationary points. The price of this behavior is that the convergence is linear until very close to the root then it converges quadratically like the standard Newton-Raphson. Thus, the total number of iterations required is greatly increased resulting in much longer runtimes, up to 200 minutes per isobar on a workstation . Thus, it was decided that the Newton-Raphson method would be used combined with a raster processing iteration procedure throughout the computational thermodynamic space.

Given T, T_e, and P, an initial equilibrium composition is approximated using simple Saha-type arguments assuming totally uncoupled physical process at low T and T_e, then partial pressures are backed out using weighted approximations or the initial guess was set equal to the previous converged root at the last temperature and pressure and stepped up in temperature on each isobar in small increments of from 0.1 to 10 K for heavy particle temperatures and 1 K to 100 K for electron temperatures. The completely closed system is solved at each point using the Newton-Raphson procedure, which iterates until the sum of the absolute values of the corrections is less than the chosen tolerance, ζ, where

$$\zeta = \frac{\epsilon P}{\left(\frac{T_e}{T} + \frac{T}{T_e}\right)} \tag{41}$$

where $\epsilon = 10^{-4}$ or until a maximum of 20,000 iterations are performed. Convergence to the tolerance is usually obtained quickly. An additional convergence check is performed after each completed iteration so that the total isobaric deviation is not allowed to exceed 5%. The correct composition is now known to within desired accuracy. The mixture molecular is computed using the expression

$$MMG = \sum_{i=1}^{25} X_i MM_i \tag{42}$$

where X_i is the mole fraction of species i, obtained using

$$X_i \equiv \frac{\eta_i}{\eta} = \frac{n_i}{n_{tot}} \tag{43}$$

where n_{tot} is, of course, just the total number of particles.

CALCULATION OF THE THERMODYNAMIC PROPERTIES

For a given temperature and pressure, the complete gas composition is calculated using the techniques in the previous section. Often, however, it is necessary to have the thermodynamic properties of the gas. In this research, the calculated thermodynamic properties are specific enthalpy (h), specific internal energy (e). The specific heats (c_p and c_v), and consequently the ratio of specific heats (γ), were not calculated for there is some ambiguity as to the definition of specific heat for a multi-temperature system and they are rarely used in high-temperature calculations anyway.

On a microscopic scale, a particle (atom or molecule) may possess energy due to its translational, rotational, vibrational, and electronic modes. This is expressed as

$$e_i = e_i^{trans} + e_i^{rot} + e_i^{vib} + e_i^{el} \tag{44}$$

where e is the total specific internal energy. Note that e is actually the total specific sensible internal energy and is measured above the zero point ($e=e-e_{0,i}$ where $e_{0,i}$ is the summation of the zero point energies for the individual modes of translation, vibration, and electronic. The rotational mode has no zero point energy. In terms of partition functions, the energy and enthalpy for a one temperature system is expressed as[10]

$$e = RT^2\left(\frac{\partial \ln Q}{\partial T}\right)_v \tag{45}$$

$$h = RT + RT^2\left(\frac{\partial \ln Q}{\partial T}\right)_v \tag{46}$$

with the relation

$$h = e + Pv \tag{47}$$

holding for any type of gas, whether calorically perfect, thermally perfect, or chemically reacting. The expressions for the modal partition functions explained earlier. Taking the derivatives of the logarithms and using Eq. (45) we get

$$e_i^{trans} = \frac{3}{2}R_iT \tag{48}$$

$$e_i^{rot} = R_iT \tag{49}$$

and

$$e_i^{vib} = \frac{h\nu_i}{kT}\frac{1}{\left(e^{\frac{h\nu_i}{kT}} - 1\right)}R_iT \tag{50}$$

Again, for the electronic energy, the lack of a closed form partition function leaves us with

$$e_i^{el} = R_iT^2\left(\frac{\partial \ln Q_i^{el}}{\partial T}\right)_v \tag{51}$$

where $R_i = R_{UGC}/MM_i$ is the specific gas constant. The translational and rotational modes are assumed to be fully excited. For a multi-temperature system, composed of *n* subsystems each in equilibrium at their own temperature T_n, as long as the subsystems are statistically independent then the fundamental thermodynamic relations may be applied to each temperature subsystem separately[5], thus we write Eqs. (45) and (46) as

$$e = RT_n^2 \left(\frac{\partial \ln Q_n(T_n)}{\partial T_n} \right)_v \tag{52}$$

$$h = RT_n + RT_n^2 \left(\frac{\partial \ln Q_n(T_n)}{\partial T_n} \right)_v \tag{53}$$

For a mixture of N species, the total mixture sensible internal energy is

$$e = \sum_{i=1}^{N} c_i e_i \tag{54}$$

where c_i is the mass fraction of species i, given by

$$c_i = \frac{m_i}{m} = \frac{\rho_i}{\rho} \tag{55}$$

Similarly, the specific enthalpy for a mixture of N species is given by

$$h = \sum_{i=1}^{N} c_i h_i \tag{56}$$

$$h_i = e_i + R_i T + (\Delta h_f)_i^0 \tag{57}$$

where again, c_i is the mass fraction and h_i is the specific enthalpy for species i. The internal energy at each required temperature and pressure is calculated using Eqs. (48)-(51) combined with Eqs. (54) and (55).The solution procedure required a previous call to the equilibrium composition subroutine to input the partial pressures and mixture molecular mass. The electronic derivatives appearing in Eq. (51) are calculated using a 4th-order four-point Richardson extrapolation with ΔT = .01K. The derivatives were taken with a frozen principal quantum number cutoff. This was done for ease of calculation and to avoid the problem other authors[14] experienced with large computational derivatives being obtained if the temperature and pressure state corresponded to a partition function jump due to the addition or subtraction of another electronic level.

RESULTS AND DISCUSSION

The chemical composition in terms of the mole fractions at 1 atm. and T_e/T = 1.0 from 580.2 K to 58,020 K is shown in Fig. 1. We see the same rapid dissociation of C_2F_4 as observed by Paulino and Squires[21] due to the inherent weakness of the carbon double bond in this molecule

as a result of the repulsive electronic weakening of the bond. The results are consistent with those obtained by Kovitya.[26] Figure 2 shows a view of the composition on a logarithmic scale. Figure 3 shows the composition in the low temperature region where molecules dominate. In our case we see that at about 800 K C_2F_4 partially dissociates into C_2F_2 and CF_4, recombines somewhat as temperature increases, creating a region where C_2F_4, CF_2, and CF_3 dominate at about 1700 K. Dissociation of C_2F_4 and CF_2 begins at about 2,000 K into large amounts of CF_3 which is almost completely dissociated by 4,000 K. The primary dissociation products are F and C which reach their maxima at about 5,000 K. Past this temperature ionization begins to occur and singly ionized C and F and electrons dominate the composition. Second ionization begins to occur between 22,500 and 25,000 K. Figures 4 through 9 show representative species compositions of C, C^+, F, F^+, e^- and CF_2 at two different pressures, 1 atm and .1 atm, for the case of thermal nonequilibrium. They are given for four heavy isotherms of .05, .1, 1, and 5 ev. Here we see drastically different behavior due to the highly energetic electrons at their elevated temperature. Dissociation of CF_2 happens rapidly, other molecules exhibited similar behavior. Single and multiple ionization of C and F follows the expected pattern of following the electron temperature, consistent with our original formulation. Figure 8, the electron partial pressure, shows we reach regions where dP_e/dT_e goes to zero. The composition is constant after this for we had assumed that the maximum ionic charge state was four. This suggests that for a correct chemical model at elevated electron temperatures we may need to extend the possible ionic species to a greater charge value. The degree if ionization is shown in Figs. 10 and 11. The results show that it tends to be a stronger function of heavy particle temperature as pressure increases at a given electron temperature. And reduced pressures result in greater degrees of ionization, as is expected. The molecular ionic and electronegative species were found to exist in only very small amounts at all T_e/T values. Figure 12 shows the mixture enthalpy and internal energy for the single temperature case. Here we see that it is a very strong function of temperature throughout the molecular region. Figures 13 and 14 the mixture enthalpy and internal energy for the two-temperature case. We see the most drastic changes with electron temperature in the region below 10,000 K in electron temperature. After this we also see larger differences with pressure for each heavy particle temperature. In future work it is planned to include multi-phase species in like amorphous carbon. Molecular effects that are being evaluated for inclusion in future models include anharmonic vibrations and internal energy mode coupling. Also research is being performed to develop the complete reactive transport model for this complex mixture.

APPENDIX 1

For statistically independent subsystems, the energy, entropy and other thermodynamic quantities are still additive. Thus

$$S = \sum S_n \qquad and \qquad E = \sum E_n \tag{58}$$

Taking the derivatives of the above we get

$$dS = \sum dS_n \qquad and \qquad dE = \sum dE_n \tag{59}$$

Using the proper form for the second law for a multi-temperature system[5]

$$dS \geq \sum \frac{\delta Q_n}{T_n} \tag{60}$$

where $\delta Q_n = dE_n + \delta W_n$, and $\delta W_n = p_n dV$. Then we see that

$$(dS)_{N,T,V} \geq \sum \frac{dE_n}{T_n} \tag{61}$$

Now, for brevity, we invoke the relation, without proof that[27,10]

$$S = kN\ln(Q) + k\beta E \tag{62}$$

And due to the fact that the n subsystems are statistically independent such that the above equation, which is derived for a system in thermodynamic equilibrium also holds for all separate subsystems then we write[5]

$$S_n = kN \ln(Q_n) + k\beta E_n \tag{63}$$

so that

$$(dS)_{N,T,V} = k\beta dE \tag{64}$$

therefore

$$k\beta \sum dE_n = \sum \frac{dE_n}{T_n} \tag{65}$$

For our two-temperature system

$$\sum dE_n = dE_H + dE_e \tag{66}$$

and

$$\sum \frac{dE_n}{T_n} = \frac{dE_H}{T_H} + \frac{dE_e}{T_e} \tag{67}$$

thus

$$k\beta\left(dE_H + dE_e\right) = \frac{T_e dE_H + T_H dE_e}{T_H T_e} \tag{68}$$

Now we define an "economy" between the heavy particle and electron energies, η, which defines the fractional contribution of each to the total energy in any state. Lets express it as

$$E_e = \eta E \tag{69}$$

and

$$E_H = (1 - \eta) E \tag{70}$$

Then

$$dE_e = \eta dE \tag{71}$$

and

$$dE_H = (1 - \eta) dE \tag{72}$$

which upon substitution into Eq. (68), and the subsequent cancellation of dE yields that

$$\beta = \frac{\eta T_H + (1 - \eta) T_e}{k T_H T_e} \tag{73}$$

with the limits that if

$$\eta = \begin{cases} 1 \rightarrow \beta = \dfrac{1}{kT_e} \\ 0 \rightarrow \beta = \dfrac{1}{kT_H} \end{cases} \tag{74}$$

ACKNOWLEDGMENTS

The support of this work by AFOSR/NA is gratefully appreciated. The authors would also like to thank R.E. Peterkin Jr., USAF Phillips Laboratory, Kirtland AFB, NM for continued hospitality.

REFERENCES

[1]Mikellides, P.G., P.J. Turchi, et al. 1997. "Theoretical Studies of a Pulsed Plasma Microthruster." 25th International Electric Propulsion Conference. Aug 24-28, Cleveland, Ohio. IEPC 97-037.

[2]Schmahl, C.S., P.J. Turchi. 1997. " Development of Equation-of-State and Transport Properties for Molecular Plasmas in Pulsed Plasma Thrusters Part I: A Two-Temperature Equation of State for Teflon." 25th International Electric Propulsion Conference, Aug 24-28, Cleveland, Ohio. IEPC-97-124

[3]Duclos, D.P., D.P. Aeschliman, A.B. Cambel. 1963. " Approximate Equation for a Perfect Gas Plasma." ARS J.. April: 641-642.

[4]Schmahl, Christopher S. A Computational Study of Shocked Flow Heat Transfer with Improved Equation of State and Transport Properties - A Case Study for Nitrogen. Master's Thesis. The Ohio State University. 1996.

[5]van de Sanden, M. C. M., et al. 1989. " Thermodynamic Generalization of the Saha Equation for a Two-Temperature Plasma." Phys. Rev. A. 40.9 Nov: 5273-5276

[6]Giordano D., M. Capitelli. 1994. " Two-Temperature Saha Equation: A Misunderstood Problem." J. Thermophysics. 9.4, 803-804.

[7]Morro, Angelo, M. Romeo. 1988. " Thermodynamic Derivation of Saha's Equation for a Multi-Temperature Plasma. " J. Plasma Phys. 39.1, pp 41-51

[8]Potapov, A. V., 1966, "Chemical Equilibrium of Multitemperature Systems" High Temp (USSR). vol. 4, Jan-Feb: pp 48-51.

[9]Liboff, Richard L. 1992. Introductory Quantum Mechanics, 2nd ed. Addison-Wessley.

[10]Vincenti, Walter G., Charles H. Kruger Jr. 1965. Introduction to Physical Gas Dynamics. New York: Wiley.

[11]Mayer, Joseph E., M.G. Mayer. 1977. Statistical Mechanics, 2nd ed. New York: Wiley.

[12]Rich, J. William, S. O. Macheret, I. V. Adamovich. 1996. " Aerothermodynamics of Vibrationally Nonequilibrium Gases." Exp. Thermal and Fluid Sci. 13:1-10

[13]Dunn, Michael G., personal communication.

[14]Drellishak, K.S., C.F. Knopp, A.B. Cambel. 1963. " Partition Functions and Thermodynamic Properties of Argon Plasma." Phys. Fluids. 6.6 Sept: 1280-1288.

[15]Chase, M.W., et al. 1985. JANAF Thermochemical Tables. 3rd ed. J. Phys. and Chem. Ref. Data. 14.1.

[16]Moore, C.E. 1949. Atomic Energy Levels, v1. NBS Circular 467. Jan 15.

[17]Moore, C.E. 1993. Tables of Spectra of Hydrogen, Carbon, Nitrogen, Oxygen Atoms and Ions. ed. by J. Gallagher. Boca Ratan: CRC Press.

[18]Rosenstock, et al. 1977. Energetics of Gaseous Ions. J. Phys. and Chem. Ref. Data. 6.1

[19]Herzberg, G. 1966. Molecular Spectra and Molecular Structure v. 1. 2nd ed. Krieger: Florida.

[20]Buckely, et al. 1995. " Ionization Energies, Appearance Energies, and Thermochemistry of CF_2O and FCO." J. Phys. Chem. 99, pp 4879-4885.

[21]Paulino, Jose A., Robert R. Squires. 1991. " Carbene Thermochemistry from Collision-Induced Dissociation Threshold Energy Measurements. The Heats of Formation of $X^1A_1CF_2$ and $X^1A_1CCl_2$." J. Am. Chem. Soc. 113, 1573-1580

[22]Press, William H. et al. 1989. Numerical Recipes: The Art of Scientific Computing - FORTRAN version. Cambridge University Press.

[23]Broyden, C.G. " Recent Developments in the Solution of Nonlinear Algebraic Systems." Numerical Methods for Nonlinear Algebraic Equations. ed. by P. Rabinowitz. Ch. 4 pp 61-73. Gordon and Breach: New York.

[24]Powell[a], M.J.D. 1970. " A Hybrid Method for Nonlinear Equations." in Numerical Methods for Nonlinear Algebraic Equations. ed. by P. Rabinowitz. Ch.6. pp 87-114. Gordon and Breach: New York.

[25]Powell[b], M.J.D. 1970. " A FORTRAN Subroutine for Solving Systems of Nonlinear Algebraic Equations." in Numerical Methods for Nonlinear Algebraic Equations. ed. by P. Rabinowitz. Ch.7. pp 115-161. Gordon and Breach: New York.

[26]Kovitya, P. 1984." Thermodynamic and Transport Properties of Ablated Vapors of PTFE, Alumina, Perspex, and PVC in the Temperature Range 5000-30,000 K." IEEE Transactions on Plasma Science. PS-12.1 March: 38-42.

[27]Tien, Chang L., J. H. Lienhard. 1971. Statistical Thermodynamics. Hemisphere Publishing

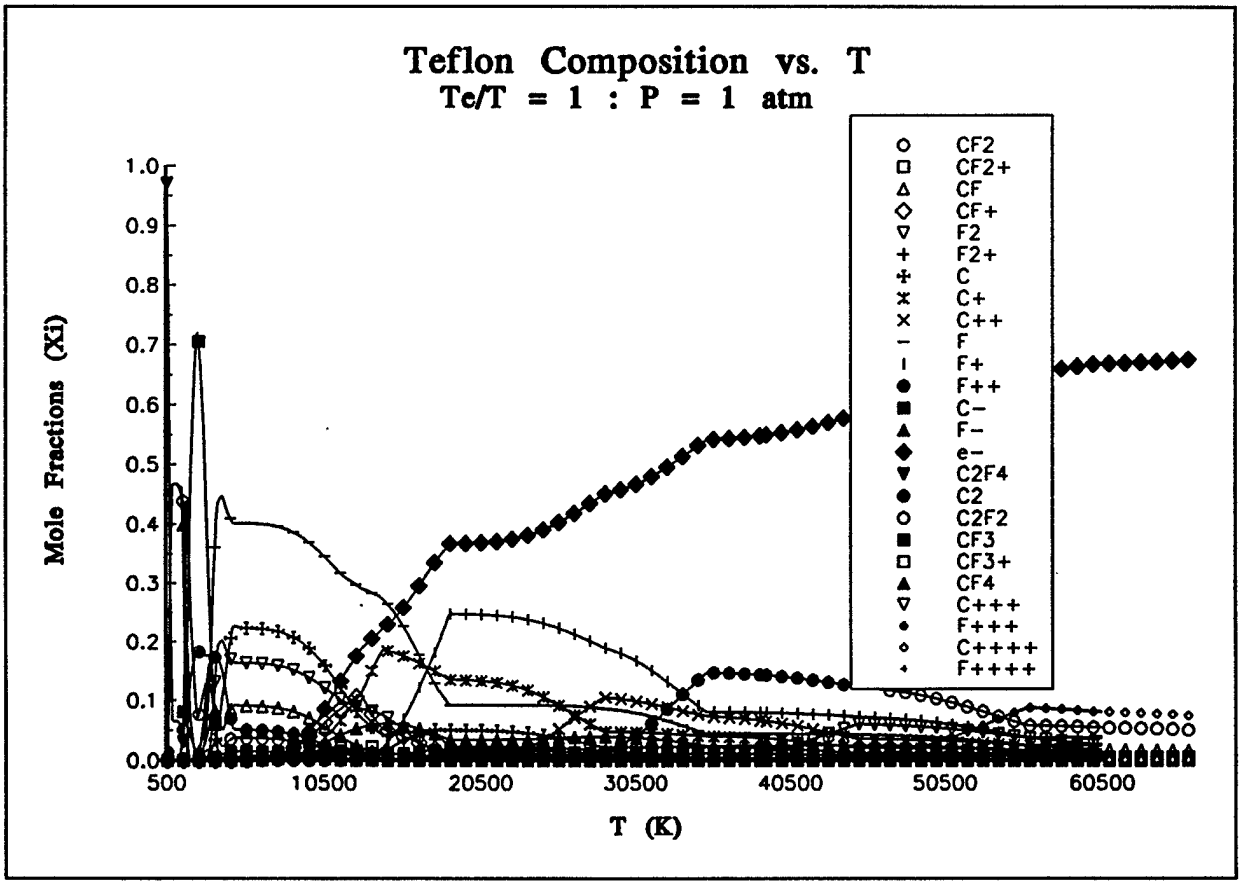

Figure 1. Teflon composition at 1 atm. for isothermal case.

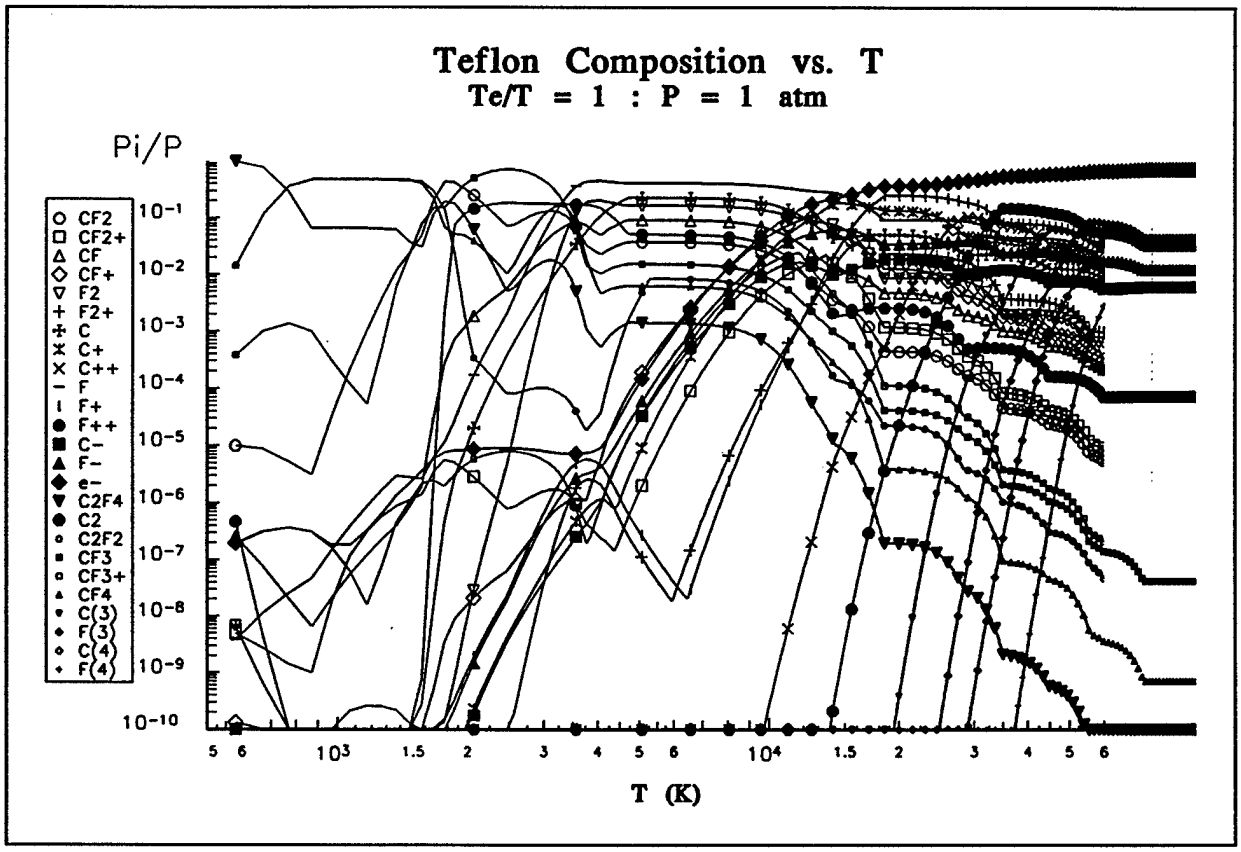

Figure 2. Isothermal Teflon composition at 1 atm. (log-log axis)

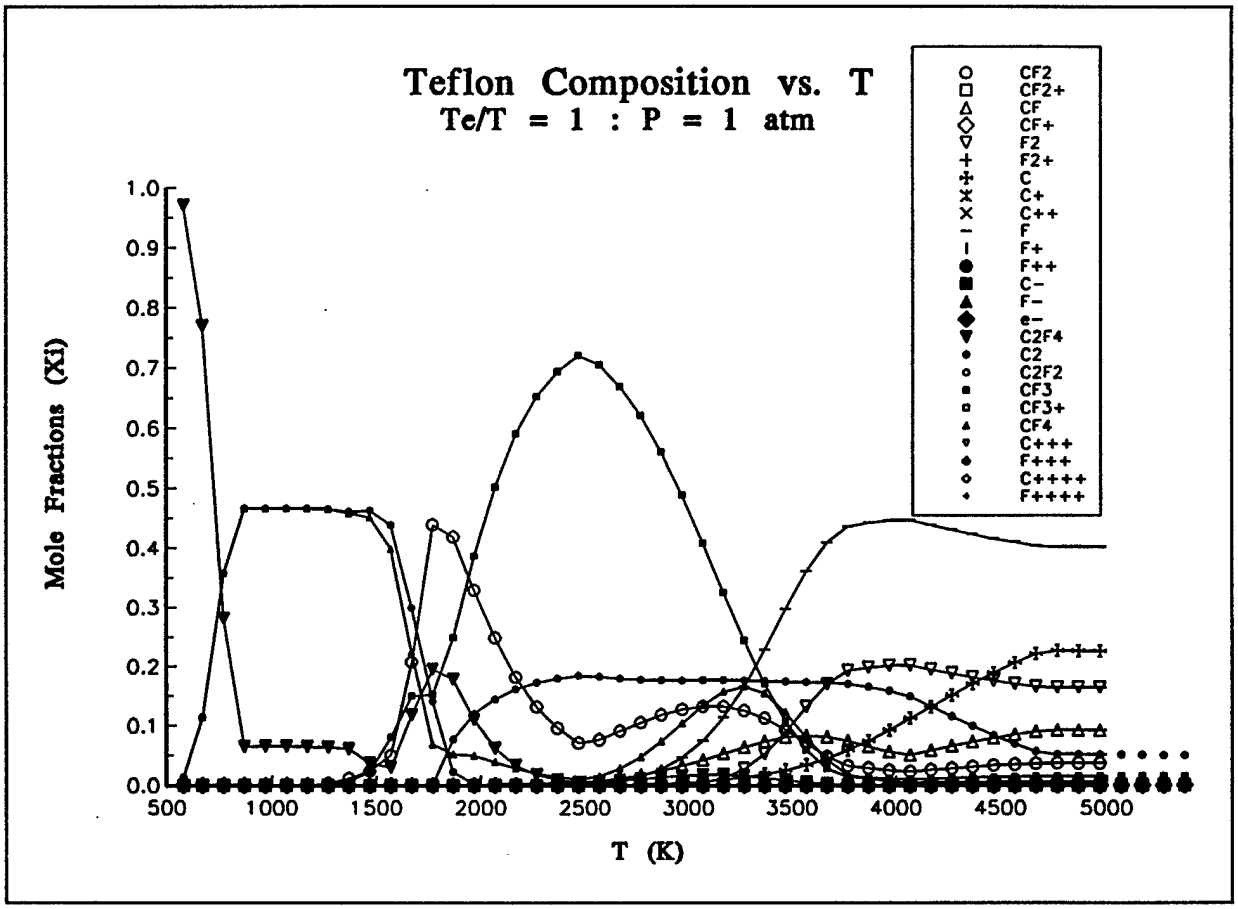

Figure 3. Isothermal Teflon composition for T < 5,000 K.

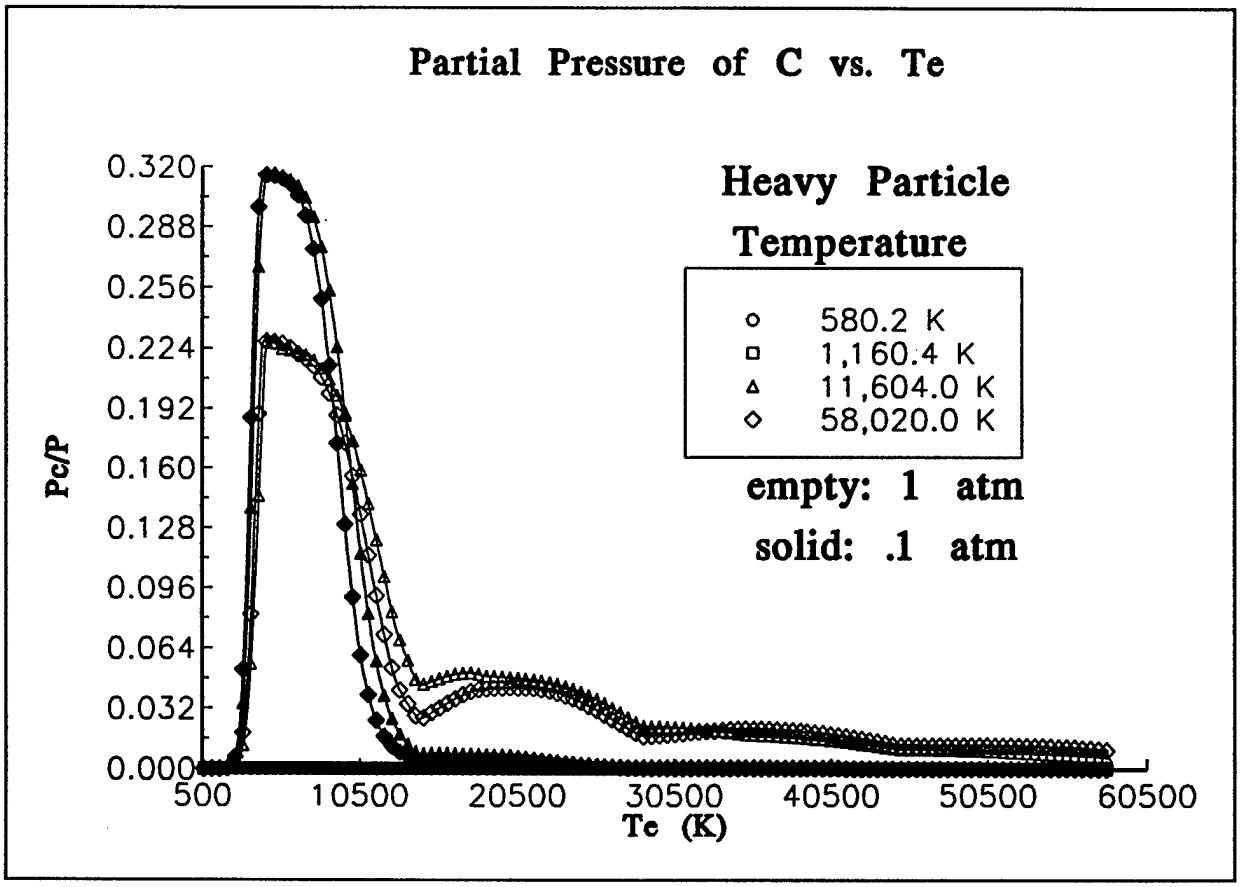

Figure 4. Partial pressure of C vs. Te.

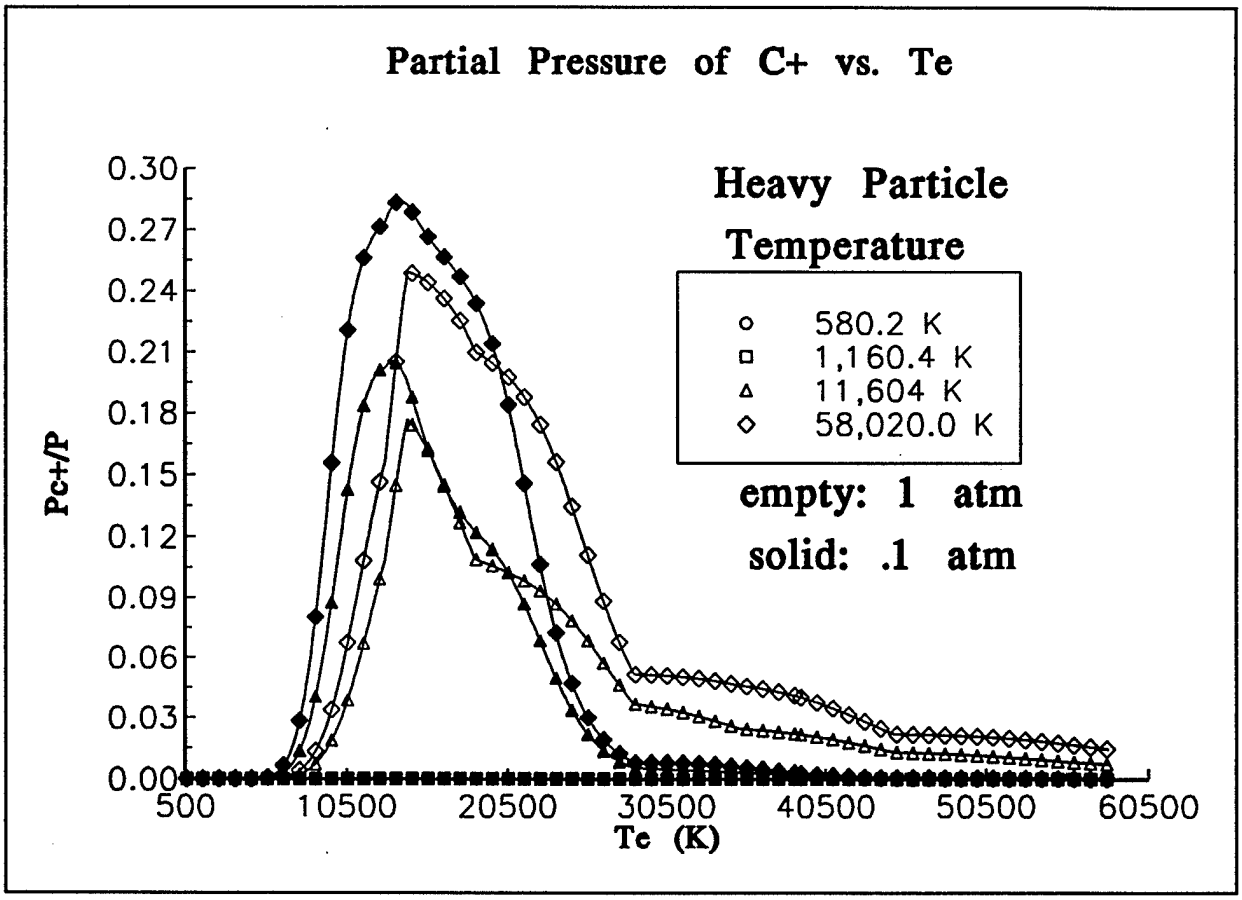

Figure 5. Partial pressure of C^+ vs. T_e.

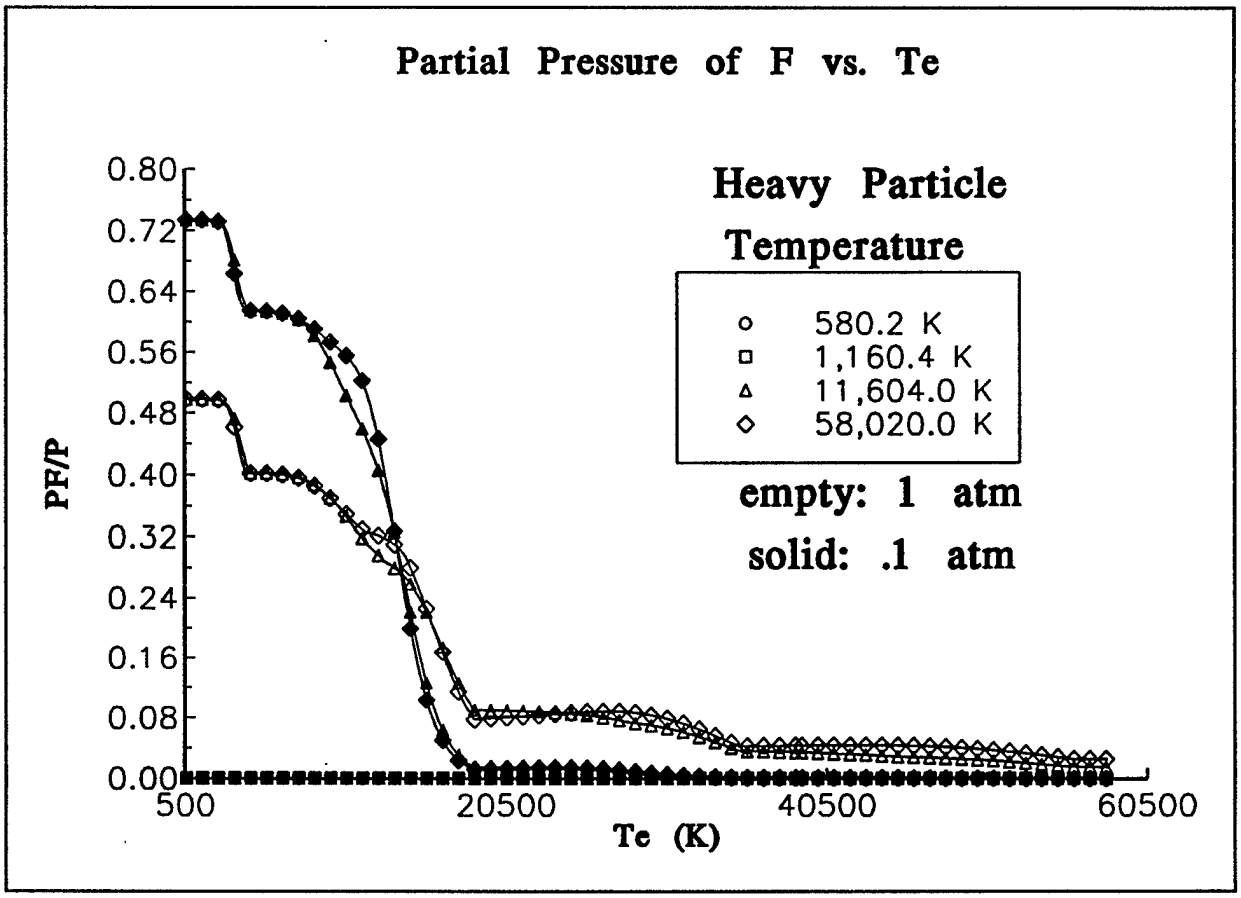

Figure 6. Partial pressure of F vs. T_e.

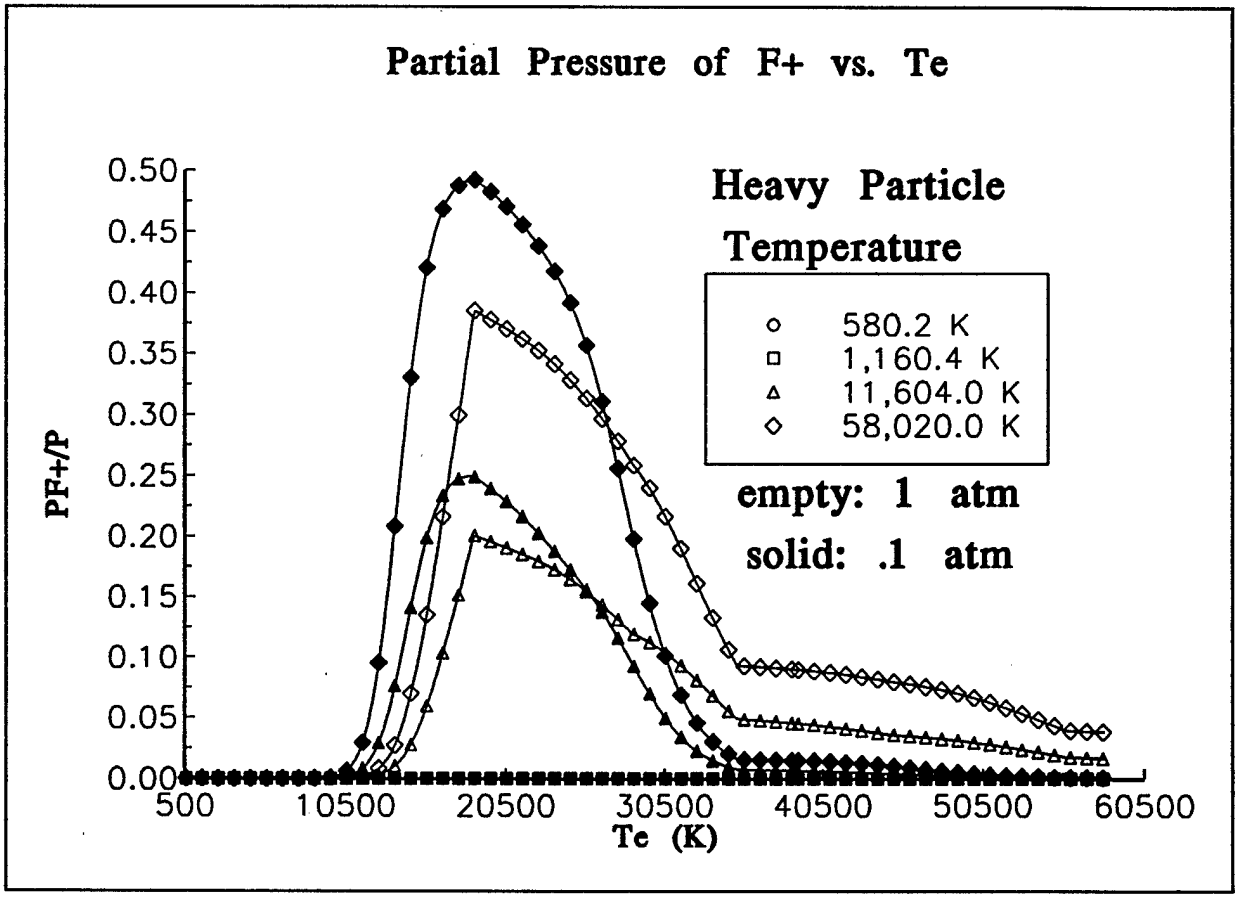

Figure 7. Partial pressure of F^+ vs. T_e.

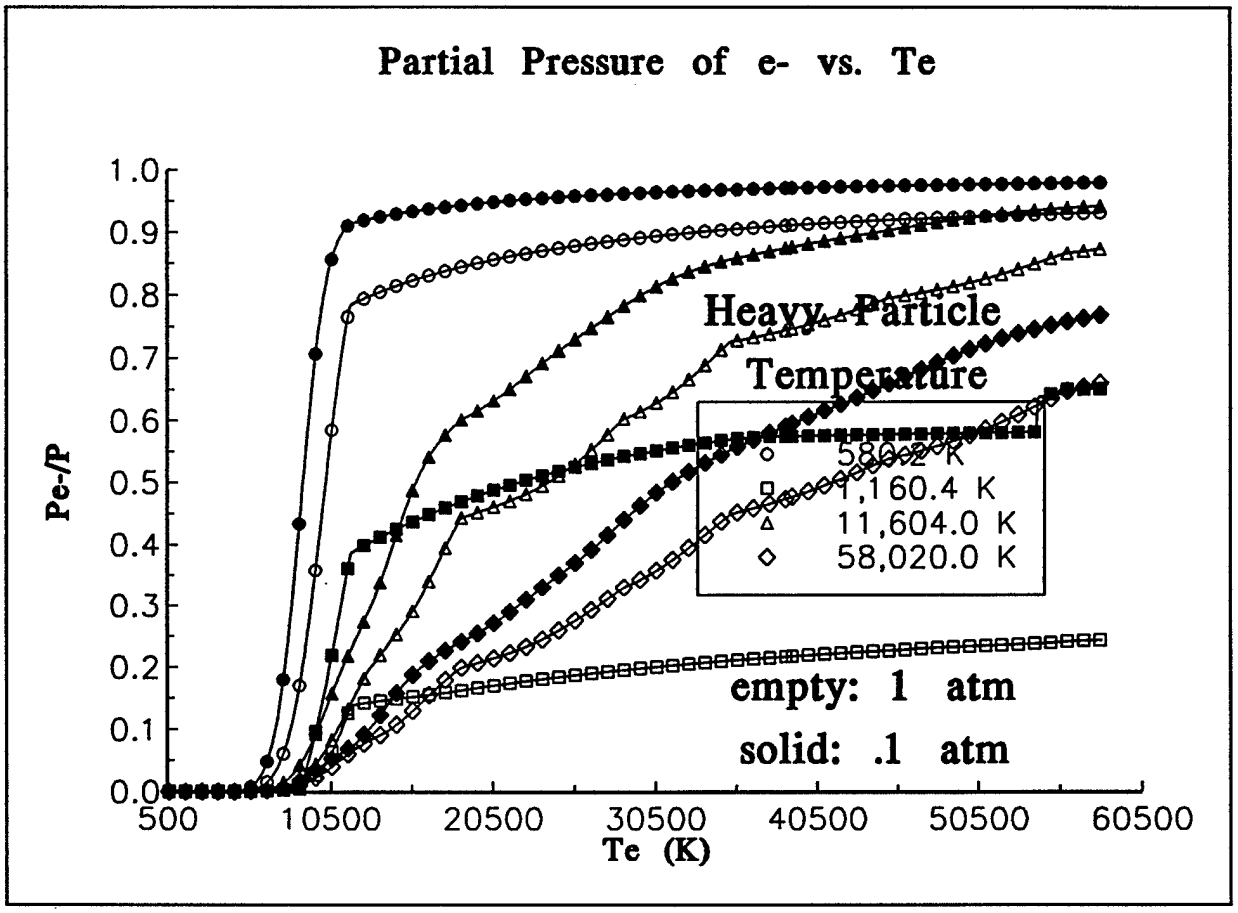

Figure 8. Partial pressure of electrons vs. T_e.

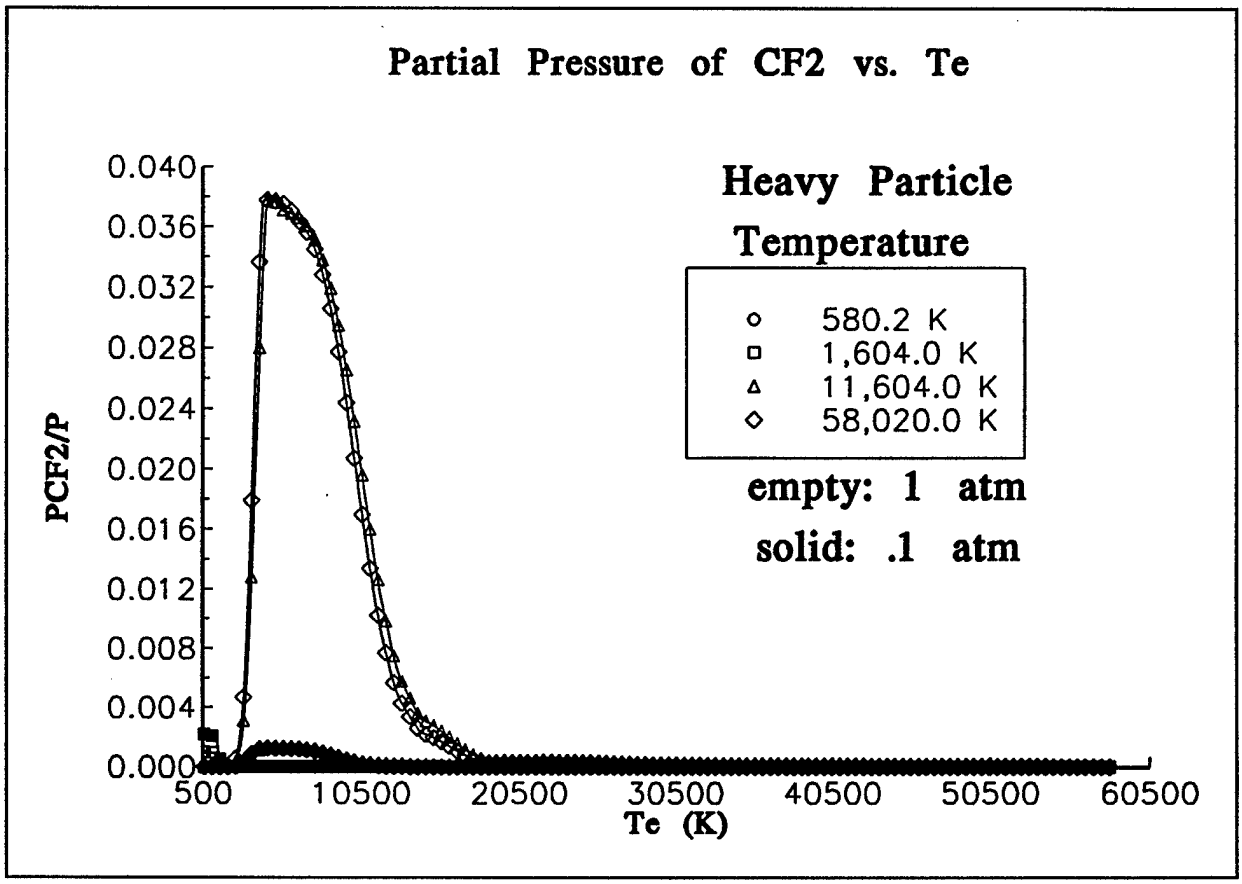

Figure 9. Partial pressure of CF_2 vs. T_e.

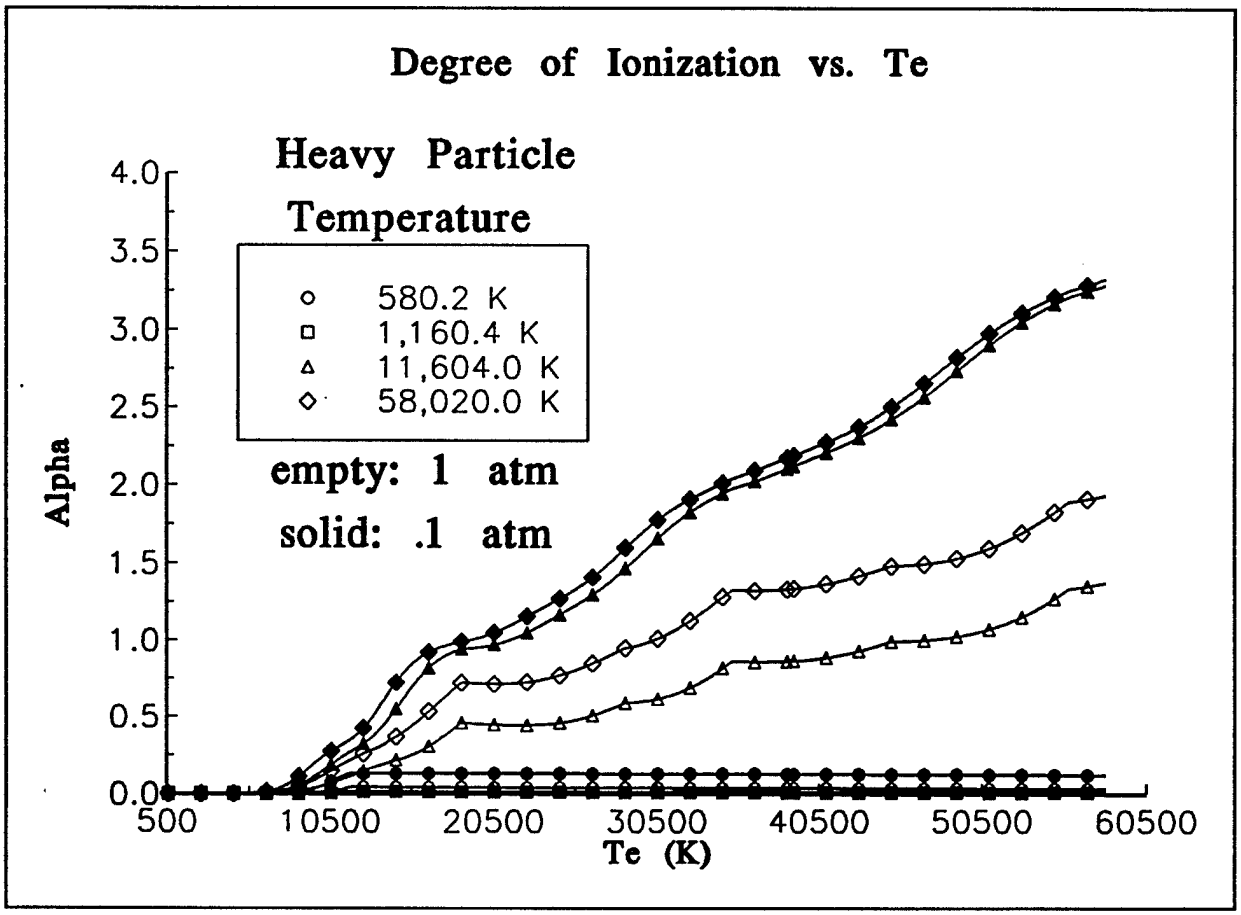

Figure 10. Degree of Ionization vs. T_e

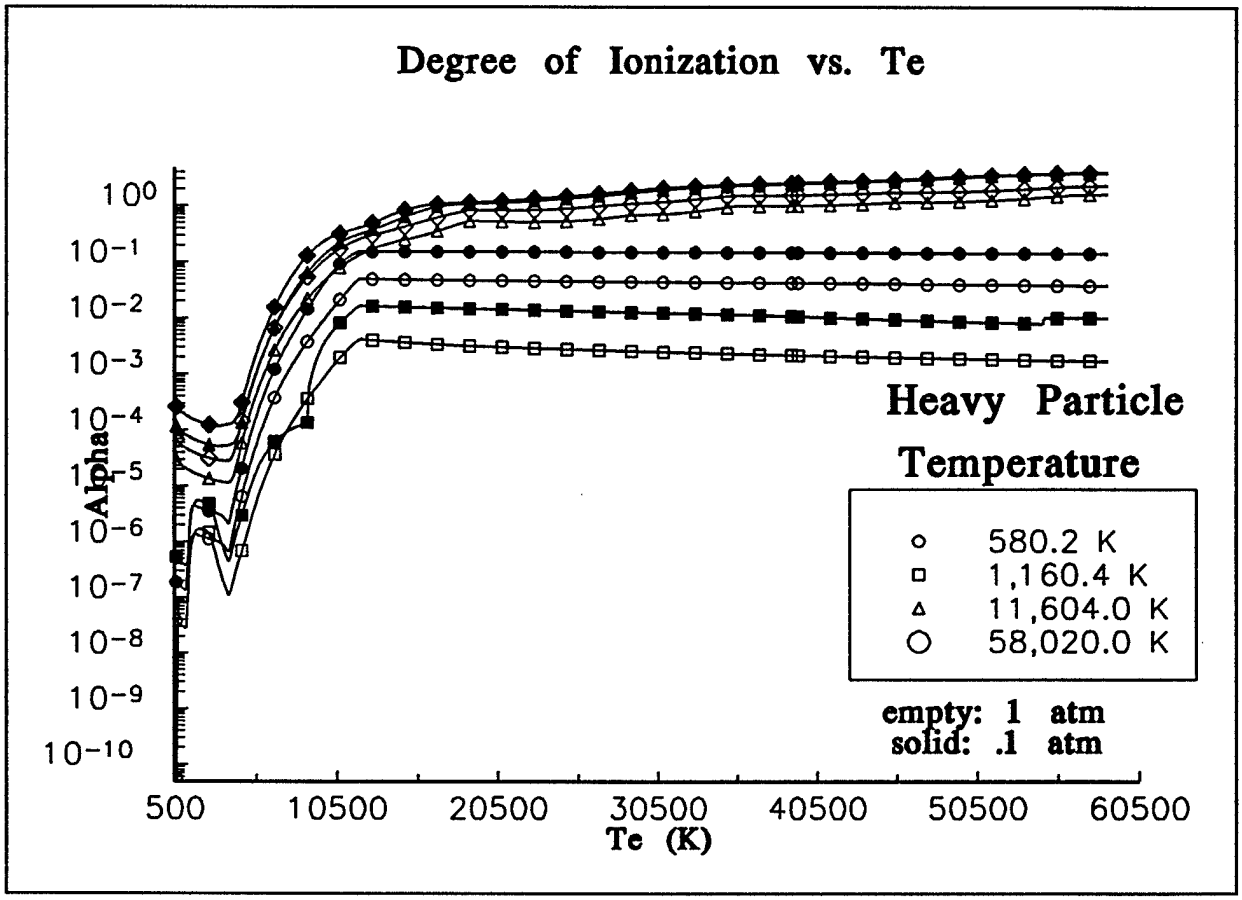

Figure 11. Degree of Ionization vs. T_e, log scale.

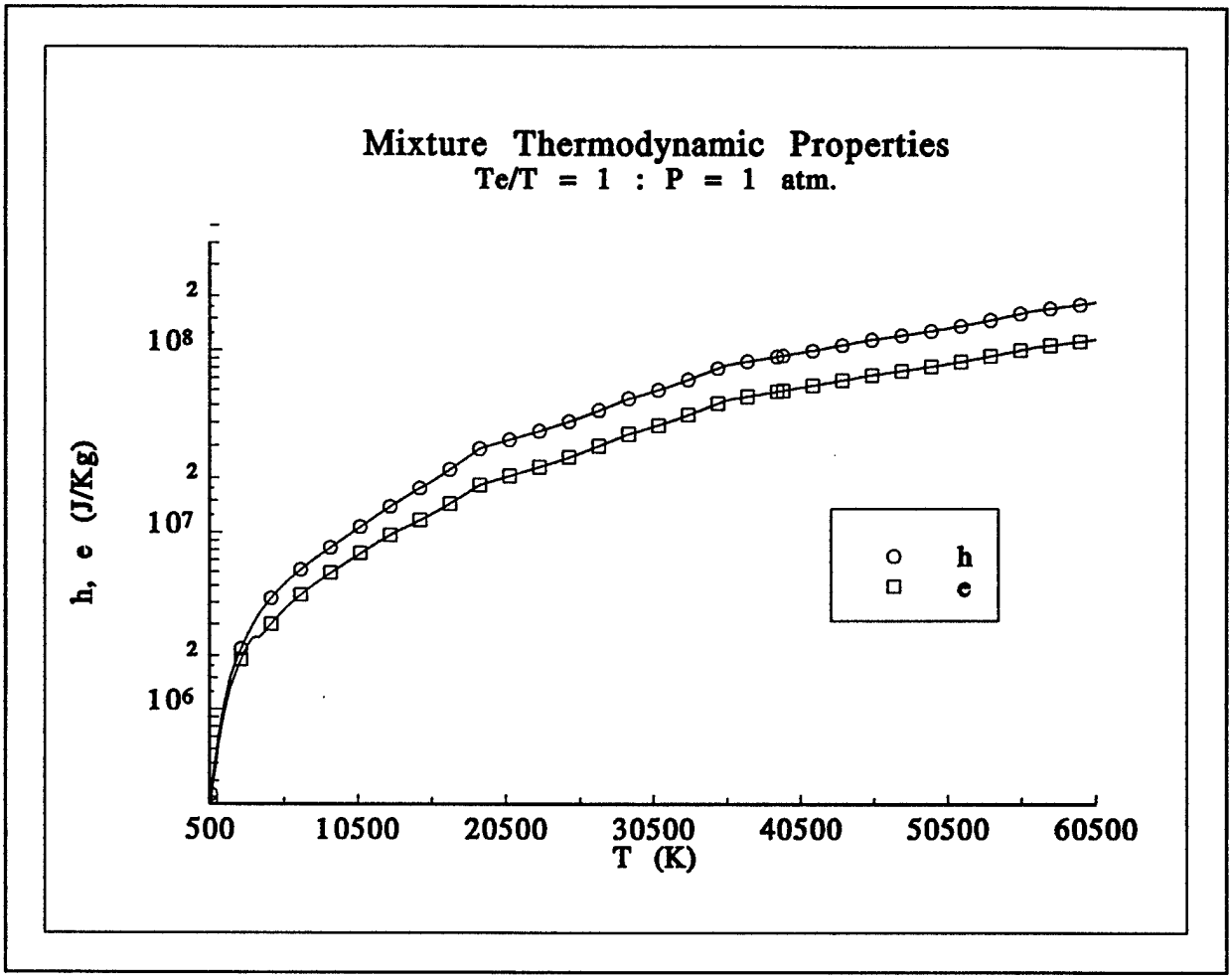

Figure 12. Single temperature mixture enthalpy and internal energy vs. T at 1 atm.

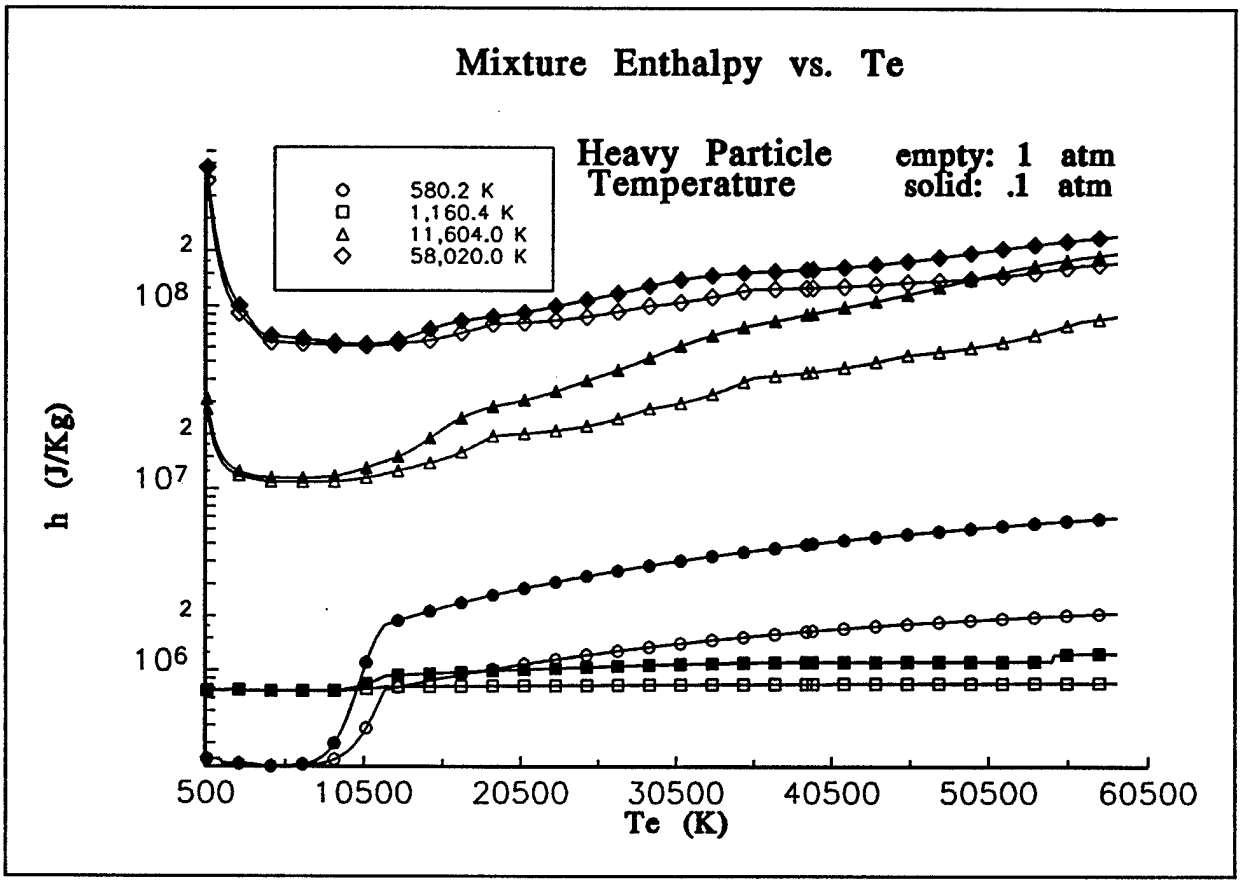

Figure 13. Mixture enthalpy vs. T_e.

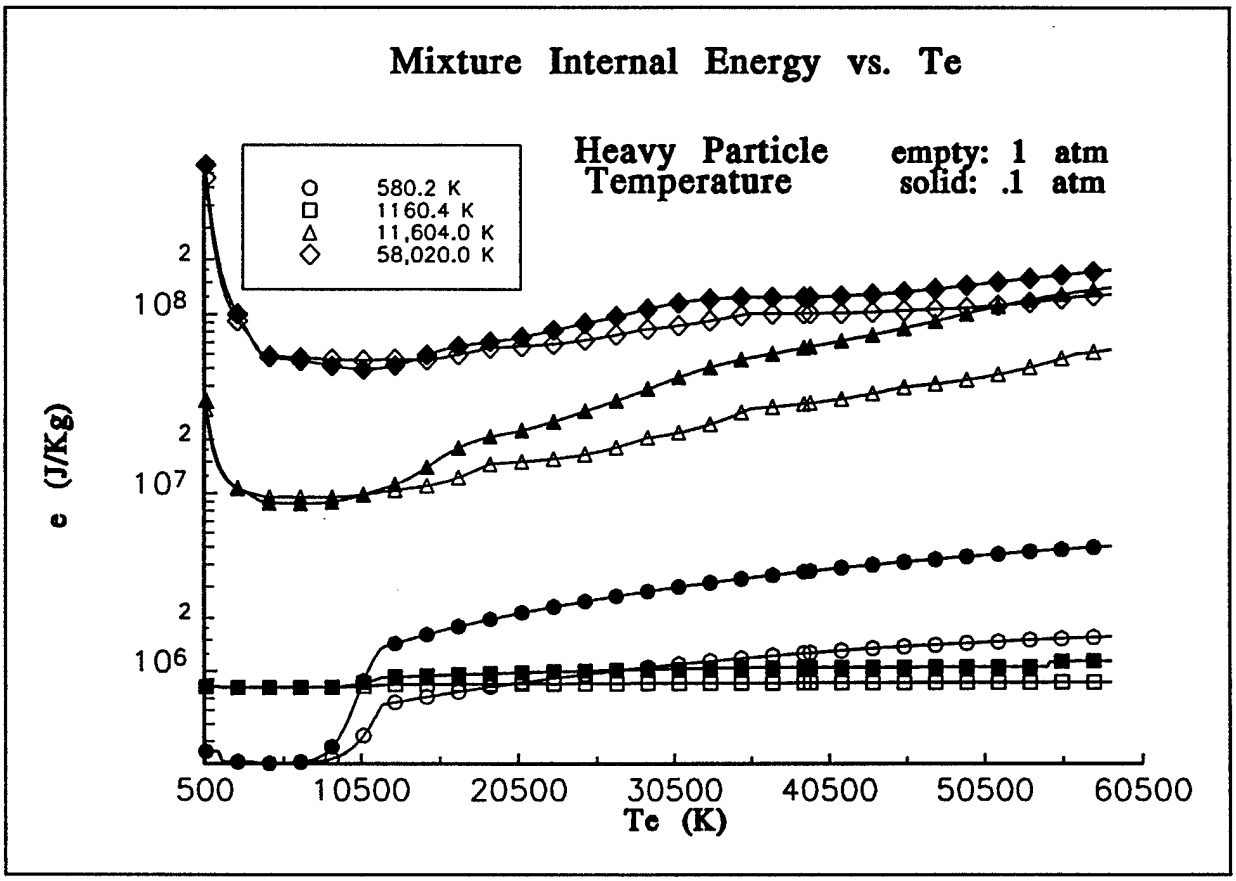

Figure 14. Mixture internal energy vs. T_e.

APPENDIX VII

Modeling of Impedance Collapse in High-Voltage Diodes

MODELING OF IMPEDANCE COLLAPSE IN HIGH-VOLTAGE DIODES

P. J. Turchi [1] and R.E. Peterkin, Jr.[2]

Air Force Research Laboratory
Kirtland AFB, NM, USA

ABSTRACT

Electron-beam diodes driven by fast-rising, high-voltage pulses often operate with cold cathodes for which the presence of a plasma adjacent to the cathode surface is essential to obtain adequate electron emission. A consequence of such surface plasma, however, is closure of the interelectrode gap by plasma motion. The diode impedance decreases with time, adversely affecting the efficiency of coupling to the power source. Plasma closure of the diode gap also limits the length of the electron beam pulse, and the ability to operate the diode repetitively at high frequency. Resistive heating of the plasma competes with work performed in expanding the plasma and heat transfer to the cold-cathode boundary. The resulting closure speed is calculated, using an MHD code, and found to agree well with results of experiments using organic-cloth cathodes at 35 kV. Computed plasma speeds are typically 8 - 12 km/s, and are relatively insensitive to the applied voltage. Gap closure due to the plasma motion calculated numerically corresponds to estimates based on impedance collapse in the experiments.

INTRODUCTION

Closure of the interelectrode space in electron-beam diodes operating with cold-cathodes is a well-known phenomena limiting the performance of such devices. Plasma adjacent to the cathode surface is needed to obtain adequate electron emission for space-charge limited flow in the diode. Such plasma, however, can cross the diode gap, resulting in collapse of the diode impedance during the high-voltage pulse. This behavior adversely affects the efficiency of coupling between the electron beam and the power source, limits the duration of the electron-beam pulse, and may preclude operation at desired repetition rates. It is useful, therefore, to understand factors that determine plasma closure in electron-beam diodes in the context of theoretical modeling that can then be employed to examine directions for improvement. The first step in such modeling consists of simulating existing experiments using techniques that can be extended to more complex possibilities.

The simplest representation of plasma closure in a diode comprises a thin layer of uniform plasma between a solid cathode surface and a region representing the vacuum in the diode gap. The physical model consists of expansion of the plasma across the gap, with resistive heating compensating for the loss of internal energy to work and heat transfer. Even this elementary model is too complex for accurate analytical treatment, so numerical techniques are necessary. Estimates of particle density and temperature for the surface plasma suggest that a continuum approach would be appropriate for the motion of the main portion of the plasma. The MACH2 2-1/2 dimensional MHD code is therefore a reasonable choice of calculational tool. Such a code is, of course, clearly inadequate to model the behavior of an electrically non-neutral, non-continuum flow.

The essential feature, however, that must be calculated in order to compute the dynamics and thermodynamics of the surface plasma is the current density. For MACH2, this merely requires that the resistivity of the "vacuum" region has a value corresponding to space-charge limited flow for the instantaneous values of applied voltage and vacuum gap. For most situations, this resistivity is

---

[1] Professor of Aerospace Engineering, on sabbatical leave from The Ohio State University.

[2] Technical Leader, Center for Plasma Theory and Computation.

sufficiently high to permit magnetic-flux diffusion rapidly through the "vacuum" region, which results in nearly uniform current density normal to the surface of the plasma layer. Thermal expansion of the plasma decreases the effective diode gap, but the resistivity of the vacuum region may be continually adjusted to maintain the proper value of space-charge limited current density during the voltage pulse. While this technique cannot simulate the actual behavior of the particle flow in the vacuum, it is adequate for providing the correct power to the plasma in order to compute the motion of the main portion of the plasma mass. Detailed consideration may then be given to penetration of electric field into the plasma in defining the position of the electron emitting surface. This is accomplished in terms of the local values of the Debye length at the vacuum edge of the plasma, aided by the condition of electric field equal to zero for emission into space-charge limited flow.

USE OF THE MACH2 CODE

The MACH2 code [1] allows numerical solution of the equations for 2-1/2 dimensional, unsteady, MHD flow. It uses an arbitrary Lagrangian-Eulerian (ALE) formulation in combination with a multiple block format that permits application to complex geometries. In addition to classical transport properties and ideal gas formulas, MACH2 operates with the SESAME tables for equation-of-state and transport properties of a variety of materials. Anomalous resistivity coefficients based on plasma/beam microinstabilities are also available, as are options for optically-thin and both equilibrium and non-equilibrium diffusion models for radiative transport. Several opportunities exist as well for coupling plasma dynamics to external electrical sources, including prescribed voltage or current waveforms and self-consistent solution of lumped-element circuitry.

MACH2 is nevertheless a continuum formulation, based on electrical quasi-neutrality and local (two- or three- temperature) thermodynamic equilibrium. Its application to problems in an electron-beam diode is restricted to regions where the plasma density is high enough to satisfy these physical constraints. Plasma created at the cathode surface by explosion of asperities at the cathode surface, or by injection from a continuum plasma source, may satisfy the continuum, quasi-neutral, LTE conditions adequately for the purpose of calculating plasma motion. The very low density, non-neutral region between the emitting surface and the anode certainly does not. MACH2, however, permits the electrical resistivity of a region or material (defined, for example, by its low mass-density) to be assigned quite flexibly. Thus, very low-density material in the vacuum gap can be given, at any instant in the calculation, a value of resistivity that will provide the correct total impedance corresponding to space-charge limited flow. For the applied voltage, therefore, the correct total current will be delivered through the expanding surface-plasma. Implicit in this approach is the approximation that the basically one-dimensional formulation of space-charge limited flow will still be adequate to describe operation of the vacum region. To correct the value of the current from the Child-Langmuir formula, in order to obtain the actual experimental current before significant impedance collapse has occurred due to plasma motion, a value of perveance is calculated. This correction factor is then held constant during diode closure.

MACH2 has not been used to calculate the actual explosion of surface asperities to create the initial plasma. Instead, the conditions of this initial plasma (mass density, electron and heavy-particle temperatures, and initial thickness) are assumed to be uniform, and treated as parameters in analyzing the subsequent plasma expansion. For properties, such as the closure speed, non-dimensionalization suggests that the the actual value of initial mass-density and initial plasma thickness are not crucial. Similarly, low estimates of the initial temperature might be self-correcting due to enhanced resistive heating. (Over-estimates of the temperature, however, will simply cause the plasma to expand too quickly in comparison to experimental data.)

SPECIFICATION OF THE ELECTRON-EMISSION SURFACE

Before proceeding to solve the dynamics of plasma closure, and to examine the sensitivities of the model to the choice of initial plasma conditions, it is necessary to develop a specification for the position of the electron-emitting surface. For the simple case of emission from a solid surface, the diode gap is merely the geometric distance between the electrodes, to the level of atomic dimensions. Emission from a plasma surface is less well-defined and can involve uncertainties in effective diode-gap

on the order of the gradient scale-length for the plasma density, the mean free path for electron-electron collisions, the (local) Debye length in the plasma, or some other condition. For the present calculations, we have chosen to define the electron-emitting surface of the plasma based on the condition that the electron velocity-distribution is significantly distorted from a Maxwellian distribution due to the electric field near the emitting surface. Algebraically, this condition is written as:

$$E(x)\,\lambda_D \geq kT_e \qquad (1)$$

where λ_D is the Debye length based on the local plasma temperature T_e and the local electron density, which varies sharply from the plasma layer to the vacuum region. The local electric field, E(x), would be zero exactly at the emitting surface, as a condition of space-charge limited flow, but has a finite value at a distance of a Debye length into diode gap, i.e., $x = \lambda_D$. The condition of Eqn. 1 is thus satisfied, for any plasma-electron temperature, when the electron density falls below some value. While the condition could equally well have been written with a factor (of order unity) multiplying the electron temperature, the resulting variations in diode gap would usually be less than the resolution of the calculational grid employed in the present work. Furthermore, within the approximation of using the one-dimensional, Child-Langmuir formula for space-charged limited flow, we monitor the diode gap according to Eqn. 1 only at one position along the surface (e.g., half-radius). A more laborious approach involving local calculation of the diode gap is deferred until warranted by substantially two-dimensional motion of the plasma surface and until an appropriate substitute for the Child-Langmuir formula can be developed, (which probably will require a particle-in-cell calculation).

CALCULATIONAL RESULTS

The first application of the present model has been to a set of experiments [2] performed with carbon-cloth cathodes at relatively modest applied voltages (~ 35 kV). These experiments were chosen for simulation because the clean and simple voltage waveform (linear rise and fall surrounding a relatively long constant value) allowed less uncertainty in comparing theoretical and experimental behavior. The experimental arrangement comprises a cylindrical cathode, 2 cm in radius, with a circular endface covered by the emitting carbon-cloth, separated by a gap of 0.5 cm from a screen anode; (the experiments were directed toward virtual-cathode operation for microwave production.) Figure 1 displays the experimental and theoretical waveforms for voltage and current. As previously noted, a perveance factor is included in the calculation to match space-charge limited flow to the experimental current value before significant diode closure has occurred ($t < 50$ ns). This factor is held constant during the subsequent plasma motion. The computed current waveform agrees rather well with the experimental curve scanned from the published oscillogram. Experimental behavior from 210 to 300 ns is difficult to discern due to relatively high amplitude, high-frequency oscillations on the trace; the calculations assume an inductance of 100 nh in series with the diode, which may be somewhat too high.

Figure 2 provides the calculated voltage and current waveforms along with the diode gap. In these calculations, which serve as a baseline for parameter variations, the initial electron and ion temperatures in the plasma layer are 1.0 eV and 0.1 eV, respectively, and the initial plasma (mass) density is 10^{-3} kg/m^3. (These values are chosen arbitrarily, but should be relevant to low temperature plasmas.) The material of the plasma is carbon phenolic, available in the SESAME tables, and was chosen in order to account for the complicated molecular composition of the carbon-cloth cathode, which consists of silk and rayon (vs pure carbon). The effective molecular mass of the phenolic is 9.01 amu. The initial thickness of the surface plasma is 0.5 mm, but rapidly increases to about 1 mm, due to the application of Eqn. 1 to the density distribution computed at early times.

The speed of plasma closure is not constant, but corresponds to an average speed of 8 km/s. This value is consistent with the estimates from the experimentally-observed decrease of diode impedance with time (assuming Child-Langmuir behavior). Such consistency, of course, is directly associated with the good agreement between experiment and theory for the diode current. In addition to the overall behavior of diode impedance -collapse due to plasma motion, the MACH2 simulations

provide detailed descriptions of plasma properties and distributions within the diode. Examples of this information are given in Fig. 3, which displays the shape of the interface between plasma and vacuum, and contours of mass density and electron temperature.

SENSITIVITIES TO PARAMETER CHOICES

The choices of initial values for the plasma layer may be informed by experience, but are certainly arbitrary in the present work. It is necessary, therefore, to explore the effects of other values on the basic behavior of diode closure. Three important parameters are the initial values of electron temperature, ion temperature and mass density. In the following comparisons, the voltage waveform will be maintained, and only one of these parameters will be varied at a time; the other parameters will be held at their values for the baseline case previously discussed.

Figure 4 displays the current and diode gap histories for initial values of electron temperature that are factors of two lower and higher than the baseline case, 0.5 eV and 2.0 eV, respectively. The lower value results in little change in diode gap and corresponding small change in the diode impedance with time; the current follows the voltage waveform. On the other hand, the higher value of initial electron temperature results in substantial faster diode closure and a much higher value of diode current than is observed experimentally. Comparison of the diode gap histories with that of the baseline case indicates the importance of the early development of closure speed on subsequent decrease of the diode gap and rapid increase of diode current (which scales inversely with the square of the gap). Higher current density helps to maintain the plasma internal-energy as the plasma expands across the gap.The early development of closure speed in the higher temperature case is simply a result of higher (electron) pressure.

In Fig. 5, the initial value of electron temperature is 1.0 eV, but the initial values of ion temperature have been increased by factors of five and ten over the baseline case, 0.5 eV and 1.0 eV, respectively. Higher initial temperatures for the ions also means higher plasma pressure (at fixed mass density), so closure speeds develop faster than in the baseline case. There is not as much sensitivity, however, to variation in ion temperature (vs initial electron temperature) because the ions in the baseline case rapidly warm up to above 0.5 eV due to heat transfer from the electrons. The effect of changing the initial value of mass density is much less pronounced because, at fixed initial values of electron and ion temperatures, the plasma pressure scales approximately with the mass density; (variations are possible due to changes in ionization with density). Thus, the basic expansion speed of the plasma remains approximately the same as for the baseline case. The results of this are observed in Fig. 6 for which factors of ten higher and lower values of initial mass density are used.

To the extent that the simulations have captured the actual behavior of diode closure, the agreement of the baseline case with the experimental data suggests that the properties of the initial plasma are reasonably given by electron and ion temperatures of 1 eV and 0.1 eV, respectively. The initial mass density, however, could be higher or lower by almost a factor of ten without disturbing this agreement very much.

EFFECTS OF APPLIED VOLTAGE

The present model can be employed to examine the effects of variation of circuit operation on diode closure. For example, if the same temporal waveform is provided to the diode with different amplitudes, the change in diode closure (and thus diode impedance history) can be predicted. Figure 7 displays the calculated diode gap histories as the amplitude of the applied voltage is increased by factors of 1.5 - 3 over the baseline case. The average closure speed only varies by a factor of 50 % , which agrees with experience in a variety of cold-cathode diodes. The peak speed, however, shows greater sensitivity to applied voltage. Examination of the two-dimensional distributions of plasma in the diode indicate that greater nonuniformity, especially faster closure near the centerline of the diode may be responsible for these higher speeds elsewhere in the diode; (recall that the diode gap is only monitored at mid-radius in these calculations). The basic result of the relative insensitivity of diode impedance-

collapse to applied voltage is, perhaps, the only claim that may be made until the present calculations are extended to more two-dimensional treatment of current flow in the vacuum.

CONCLUDING REMARKS

It appears that MHD codes, such as MACH2, can be successfully employed to study plasma phenomena in high current-density diodes. The basis for this success at present is the application to diode problems for which one-dimensional approximations to the current flow in the vacuum are adequate. Also, by invoking the condition of space-charge limited flow, ($E(0) \simeq 0$), the specification of the electron-emitting surface is facilitated. For two- or three-dimensional problems, recourse to particle-in-cell (PIC) techniques to calculate the local current density through the plasma layer will probably be necessary. For some problems, the development of the current flow and charge distribution in the vacuum may occur on a timescale much shorter than the hydrodynamic expansion times for the surface plasma. This situation may then allow calculation of diode behavior with surface plasmas by a rapid iteration between PIC codes, run for several nanoseconds, and hydrocodes running over a microsecond, without encountering the difficulties of including plasma motion within the PIC code itself.

ACKNOWLEDGEMENTS

This work was performed while one of the authors (PJT) was on sabbatical leave from The Ohio State University, Columbus, OH, and partially supported by the USAF Phillips Laboratory (PL/WS), Kirtland AFB, NM, through the Air Force Office of Scientific Research (AFOSR/NA), Washington, DC.

REFERENCES

1. R.E. Peterkin, Jr., et al, "MACH2: A Reference Manual", Weapons Laboratory, Kirtland AFB, NM.

2. R.J. Adler, et al, Rev. Sci. Instrum. 56 (5) 1985

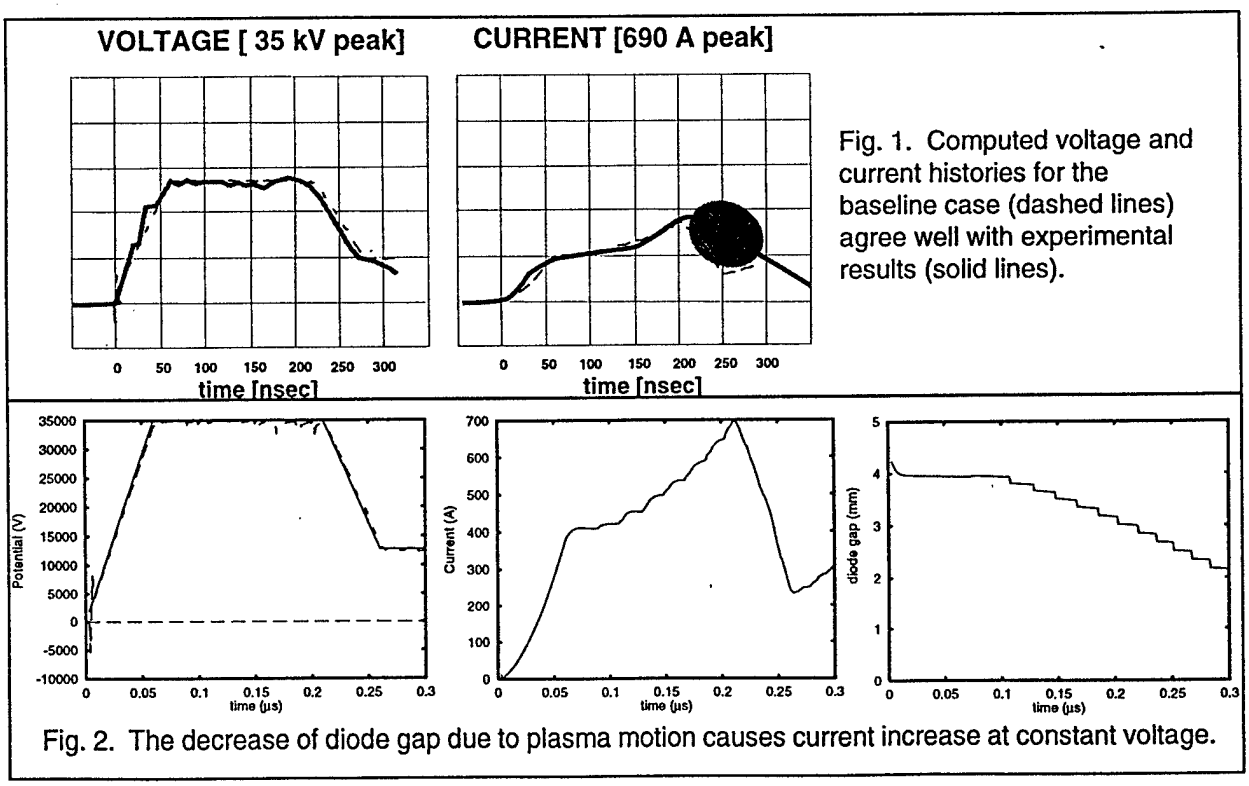

Fig. 1. Computed voltage and current histories for the baseline case (dashed lines) agree well with experimental results (solid lines).

Fig. 2. The decrease of diode gap due to plasma motion causes current increase at constant voltage.

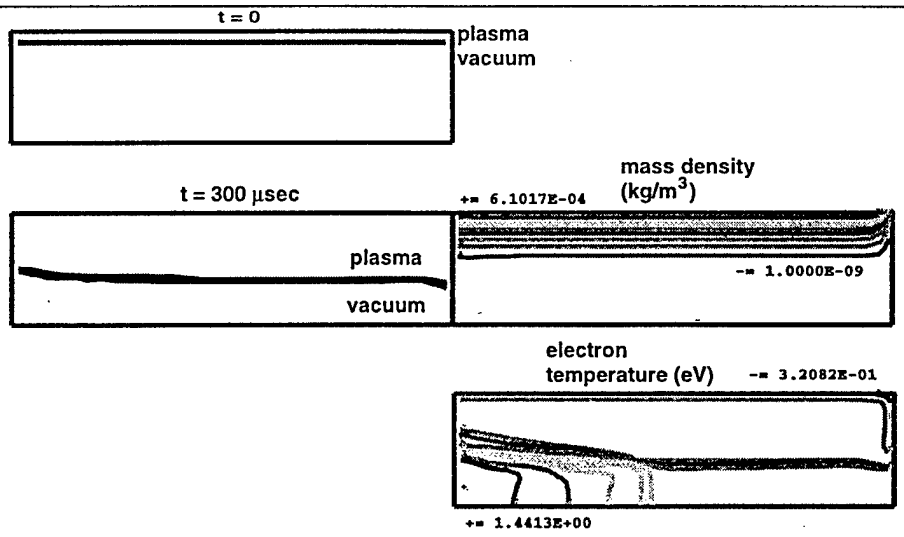

Fig. 3. MACH2 provides 2D distributions of plasma properties including plasma-vacuum interface.

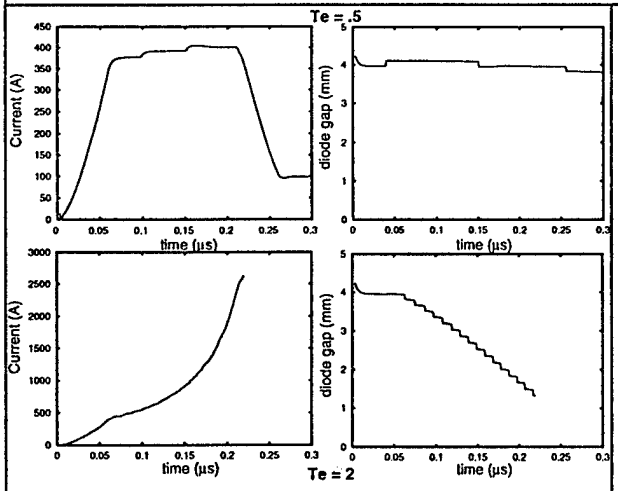

Fig. 4. Other initial electron temperatures (0.5 and 2.0 eV vs. 1.0 eV) predict plasma closure that is inconsistent with experiment.

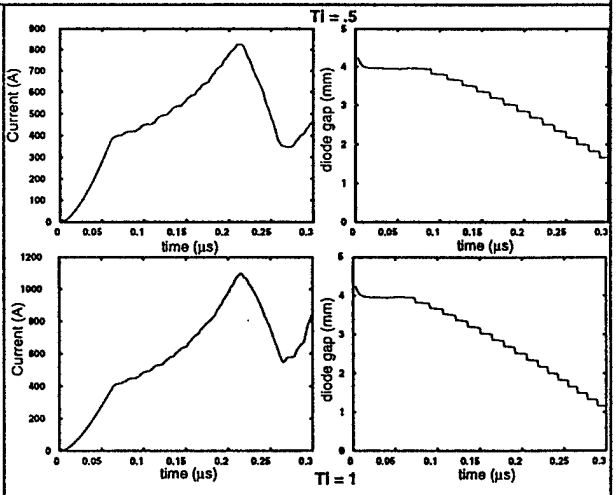

Fig. 5. Other initial ion temperatures (0.5 and 1.0 eV vs. 0.1 eV) also predict closure that is inconsistent with experiment.

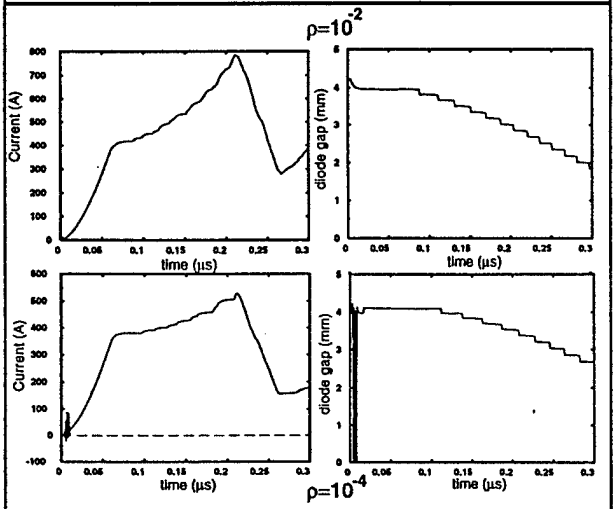

Fig. 6. Other initial mass densities at the surface (10^{-2} and 10^{-4} kg/m^3 vs. 10^{-3} kg/m^3) predict closure that is less consistent with experiment.

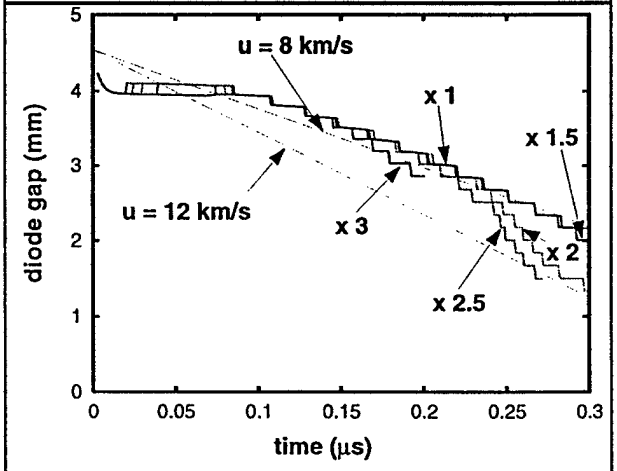

Fig. 7. The time dependent gap is computed for different applied voltages relative to the 35 kV baseline case. The average speed is between 8 and 12 km/s.